Synthesis of Eggshell-derived Nanoparticles and Bionanocomposites Thereof for Food Packaging

by

Punita Upadhyay

A thesis submitted in partial fulfillment of the requirements for the degree of

Master of Science

in

Bioresource Technology

Department of Agricultural, Food and Nutritional Science

University of Alberta

Abstract

Eggshells are widely considered an agricultural waste and hence they are generally disposed into landfills without any transformation into useful products. However, this waste can be valuable source material for fertilizer production, fodder, and the development of valuable high-performance nanostructured biomaterials. This waste has the potential of producing hydroxyapatite which is a major component present in bone and teeth. Hydroxyapatite nanoparticles (HANPs) are widely used in biomedical and other fields such as wastewater treatment, soil remediation, catalyst, and food packaging applications due to their excellent biocompatibility and bioactivity properties. In this study, HANPs were successfully synthesized from eggshell waste by microwave-assisted (MW) as well as conventional heating (CH) precipitation methods using the low temperature (40 ℃) and a green template i.e., Azadirachta Indica leaf (Neem) (AI). The synthesized HANPs were characterized by different analytical techniques such as Fourier Transformation Infrared spectroscopy (FTIR), Raman spectroscopy, Scanning Electron Microscopy (SEM), Transmission Electron Microscopy (TEM), X-ray Diffraction (XRD), and Thermogravimetric Analysis (TGA) for determining their functionality, shape, size, crystallinity, phase purity, and thermal stability. FTIR and Raman's spectroscopy confirmed the pure hydroxyapatite phase with no other impurities. SEM and TEM analyses confirmed that HANPs obtained uniform distribution with less agglomeration by the MW method in the presence of AI when compared to the CH method and without AI. TEM analyses revealed the average size of HANPs from both methods without AI was 30-31 nm in width and 53-55 nm in length while in the presence of AI was 27-28 nm in width and 44-46 nm in length. XRD analysis indicated the formation of the pure crystalline structure of nanoparticles. The synthesized HANPs were thermally very stable and had a lower Ca/P ratio (1.81) from the MW method compared to the conventional heating method which is 1.95. Thus, this study revealed that

HANPs synthesized by the MW method in presence of AI with smaller crystallite size and less agglomerated particles have a great potential to be used in the biomedical fields as well as food packaging applications.

Further, in this study, the synthesized HANPs were used to reinforce biopolymer to prepare bionanocomposites films without any cross-linking agent in the presence of glycerol as a plasticizer. The influence of HANPs in bionanocomposites was investigated by varying their concentrations (1wt%, 3wt%, 5wt%, and 10wt%). The effect of the addition of HANPs and their impact on the final film properties were evaluated by TGA, Differential Scanning Calorimetry (DSC), Dynamic Mechanical Analysis (DMA), Tensile Testing, and Water Vapor Permeability (WVP). The morphology of bionanocomposites and the dispersion of nanoparticles in the chitosan matrix were evaluated using SEM, TEM, and XRD. The structural changes in the films were investigated by FTIR and XPS techniques. Results indicated that the addition of HANPs exhibited improved thermal stability, delated melting point, and better viscoelastic properties (higher glass transition temperature) of bionanocomposites compared to chitosan control film. The tensile strengths of the bionanocomposites increased with low concentrations (1wt%, and 3wt%) and decreased with high concentration (5wt%, and 10wt%) of HANPs. The films with 3wt% HANPs, demonstrated the highest tensile strength i.e., 61.54 % increase compared to neat films. Furthermore, the WVP of the bionanocomposites significantly declined by the addition of nanoparticles e.g., the addition of 1wt% HANPs exhibited a decrease in WVP (52%) compared to the control films. The SEM, TEM, and XRD analyses, confirmed that the bionanocomposites with 1wt% and 3wt% HANPs had more uniform nano-dispersions leading to exfoliated to partially intercalated nanocomposites. Based on the attractive properties obtained, the egg-shell waste based bionanocomposites have a great potential to be used in food packaging applications.

Preface

This thesis holds the original work done by Punita Upadhyay and has been written according to the guidelines for a paper format thesis of the Faculty of Graduate Studies and Research at the University of Alberta. The concept of this thesis originated from my supervisor Dr. Aman Ullah. The thesis consisted of four chapters: Chapter 1 provides a general introduction to the food packaging system, chitosan biopolymer, hydroxyapatite nanoparticles, their synthesis methodologies, their potential applications, and the objectives of the thesis; Chapter 2 provides an in-depth literature review of bionanocomposites, hydroxyapatite and their application as a nanofiller in the biopolymer for food packaging application; Chapter 3 has been prepared as a manuscript for submission to a peer-reviewed journal: Punita Upadhyay, and Aman Ullah. "Facile synthesis of hydroxyapatite nanoparticles from eggshell biowaste via microwave-assisted precipitation using Azadirachta Indica extract as a green template" (submitted). I performed all laboratory work, data interpretation, and writing of the manuscript. Dr. Ullah greatly contributed to conceptualization, manuscript review, and editing.

Chapter 4 has been prepared as a manuscript for submission to a peer-reviewed journal: Punita Upadhyay, and Aman Ullah. "Enhanced mechanical and barrier properties of chitosan-based bionanocomposites films reinforced with eggshell-derived hydroxyapatite nanoparticles". I performed all laboratory work, data interpretation, and writing of the manuscript. Dr. Ullah greatly contributed to conceptualization, manuscript review, and editing.

Chapter 5 includes a conclusion with a future perspective of synthesized nanoparticles and bionanocomposites. I was responsible for the literature search relevant to the above studies, designing and performing laboratory experiments, data collection, and analysis, and drafting the thesis. Dr. Aman Ullah greatly contributed to conceptualization, manuscript review, and editing.

Dedication

This thesis is dedicated to my beautiful family, my two sweet sons Om and Ishaan, my loving husband Hemang, and my parents.

Acknowledgments

First and foremost, I would like to deeply express my sincere gratitude to my supervisor Dr. Aman Ullah for giving me this opportunity to be part of his research group and work on this project. I am sincerely thankful for his valuable guidance, incredible motivation, devoted time, and intellectual support throughout my degree.

I am sincerely thankful to Dr. Roopesh Syamaladevi for being my supervisory committee member and for providing valuable suggestions and discussions during the program. I am also thankful to Dr. Thava Vasanthan for serving as an examiner.

I would like to thank the AFNS staff, including Dr. Urmila Basu, Dr. Kelvin Lien, and Chris Kazala for their help during my whole program. I sincerely acknowledge the support served by Dr. Muhammad Arshad (former group member), and Ereddad Kharraz, for their help in using different pieces of equipment.

I would like to express my love and gratitude to my loving husband Hemang and my two lovely sons, Om and Ishaan for their endless support and encouragement during this journey. I am indebted to my dear parents, and my brother and sisters for their unconditional love, trust, and encouragement throughout my life.

Finally, I would like to extend my gratitude to my friends and group members, Muhammad Irfan, Irum Zahara, Dorra Gargouri, Muhammad Zubair, Huiqi Wang, Karen Lopez-Camas, Yanet Rodriguez Herrero, Siti Amirah, Frage Lhadi Abookleesh, Beenish Khanzada and Shifa Dinesh who encourage and help me throughout for accomplishing this undertaking.

Table of Contents

List of tables

List of figures

List of abbreviations

HA/HAp	Hydroxyapatite
MW	Microwave-assisted
HANPs	Hydroxyapatite nanoparticles
ATR-FTIR	Attenuated total reflectance-Fourier transform infrared spectroscopy
DMA	Dynamic mechanical analysis
DSC	Differential scanning calorimetry
DTG	Derivative thermogravimetric
E	Elongation at break
SEM	Scanning electron microscopy
TEM	Transmission electron microscopy
T_g	Glass transition temperature
TG	Thermogravimetric
TGA	Thermogravimetric analysis
T_m	Melting temperature
TS	Tensile strength
XPS	X-ray photoelectron spectroscopy
BE	Binding energy
XRD	X-ray diffraction
Wt	Weight
PHAs	Poly (hydroxyalkanoates)
PHB	Poly (β-hydroxybutyrate)
PHBV	Poly (3 hydroxybutyrate co 3-hydroxyvalerate)

PLA	Poly (lactide) acid
PCL	Poly (ε-caprolactone)
PVA	Poly (vinyl alcohol)
PGA	Polyglycolic acid

CHAPTER 1. INTRODUCTION AND OBJECTIVES

1.1 Overview of food packaging

Currently, the use of plastic and its production is growing every day. Annually, more than 358 million metric tons of petrochemical plastics are produced worldwide (Singh et al. 2022) and plastic production is estimated to be doubled in the next 20 years (Haghighi et al. 2020, Lebreton and Andrady 2019). The unavoidable use of plastic in different forms ends up discarded into the environment by being dumped into the land and ocean (Ghaffar et al. 2022). Due to their non-biodegradability, it has become a huge problem for the world. Plastics are mainly derived from non-renewable petroleum-based resources (crude oil) and thus, their production is totally dependent on those non-renewable resources and threats to the rapid depletion of fossil fuel.

Packaging is one of the bigger plastic use industries worldwide consuming 39.6 % of total plastic production (Huysman et al. 2017). Food packaging is the largest growing sector within the plastic-based packaging industry. The main aims of conventional food packaging are: (i) extension of shelf-life, (ii) maintenance of food quality, and (iii) the safety and security assurance of the food products. Food packaging technologies play an important role to protect food products from the outside environment and provide safe and secure transportation, delivery, and consumption of food (Han 2003).

Presently, plastic-based packaging materials such as polyethylene (PE), polystyrene (PS), polypropylene (PP), and polyethylene terephthalate (PET) and polyamide (PA) have been mainly used in the food packaging industries due to their low cost, and durability. However, the non-biodegradability of synthetic polymers and the accumulation of plastic waste create a serious problem for the environment. Approximately, 34 million tons of plastic waste is generated yearly

worldwide and 93 % of it is discarded into the land and ocean. Although, some of the organizations such as European Union (EU) have attempted to manage proper plastic waste disposal by banning landfilling application but still developing countries are depending on the conventional method of landfill. Approximately 50 % of plastic waste is still disposed of into landfills which creates carbon dioxide emission contributing to the global warming and led to the serious environmental pollution (Emadian et al. 2017).

Consequently, the food packaging industry is pushing towards the development of alternative environmental friendly, biobased, and biodegradable materials, such as bioplastics (Arikan and Ozsoy 2015). Bioplastics are plastics derived from renewable resources (biobased) either synthesized chemically or biologically (Goel et al. 2021), which can replace the fossil fuels, due to their high availability, biodegradability, and low carbon footprint (Reddy et al. 2013). Table 1.1 shows the comparison of features of bioplastics and petroleum-based plastics.

Table 1.1 Characteristic comparison of bioplastics and petroleum-based plastics {Adopted from (Harding et al. 2017)}.

Features	Bioplastic	Petroleum-based plastic
Renewable	Yes, or partially	No
Sustainable	Yes	No
Degradable	Biodegradable and/or compostable	Some degradable by polymer oxidation
Polymer range	Limited but growing	Extensive
Greenhouse gas emissions	Usually low	Relatively high
Fossil fuel usage	Usually low	Relatively high
Arable land use	Currently low	None

1.2 Overview of chitosan biopolymer as food packaging

Generally, biopolymers are biodegradable polymers, covalently bonded monomeric units to form chain like macromolecules. Most of the biopolymers can be degraded or broken down easily by the action of naturally occurring organism and converted into carbon dioxide (CO_2) and water. Mostly used biopolymers for food packaging applications are starch, cellulose, chitin, chitosan, agar, gelatin, collagen, alginate, gluten, and whey protein. Among these biopolymers, chitosan has been widely used in various field of applications such as food industry, food packaging, agriculture, biomedical science, cosmetics and waste water treatment due to its high availability, biodegradability, biocompatibility, non-toxicity, excellent film forming and antimicrobial properties (Ambaye et al. 2022, El-Aidie 2018). Table 1.2 presents the main general applications of chitosan.

Chitosan (CH) is a natural polysaccharide having β (1-4) linked D-glucosamine and N-acetylglucosamine units, derived from chitin by partially deacetylation which is the second most naturally occurring polymer after cellulose. The structure of chitin and chitosan are shown in Fig. 1.1.

The most popular and economical method for chitosan is its isolation from chitin by deacetylation. Crab and shrimp shell wastes are the main sources of chitosan production. However, it can be possible to extract chitosan from the some type of fungi as well (Rane and Hoover 1993).

Chitosan possesses a variety of physiochemical and biological properties (Table 1.3) Chitosan's properties and applications are highly dependent on the degree of deacetylation of chitosan and molecular weight of chitosan.

Table 1.2 General applications of chitosan {Adopted from (Rinaudo, 2006)}

Agriculture	Stimulation of plant growth, Seed coating, Frost protection, Time release of fertilizers and nutriments into the soil
Food and beverages	Preservative, Thickener and gelling agent, food stabilizer, Protective, fungistatic, antibacterial coating for fruit, animal food additive
Water and waste treatment	Flocculant/coagulant to clarify water, Removal of metal ions, Odor reducer
Medical/Biomedical	Blood cholesterol control, Skin burn, Artificial skin, Wound dressing, Dental implant, Bone reconstruction, Corneal contact lenses, Controlled drug release
Biotechnology	Enzyme Immobilization, Protein separation, antitumor agent, Hemostatic and anticoagulant, Cell recovery
Cosmetic	Creams and lotions maintaining skin moisture, Shampoos, hair colorants, hair sprays, Oral care (toothpaste, chewing gum)

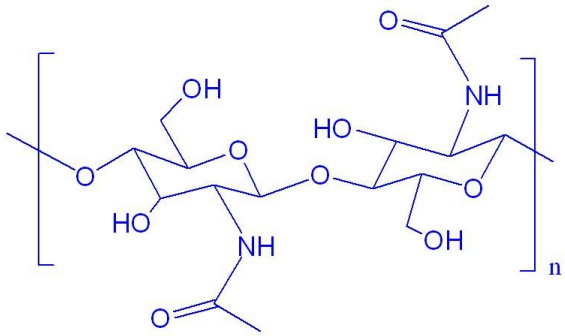

(Chitin)

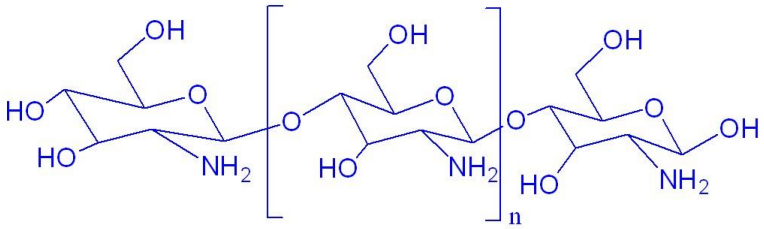

(Chitosan)

Figure 1.1 Structure of Chitin and Chitosan {Modified and adopted from (Sarode et al. 2019)}

Table 1.3 Chitosan general properties {Adopted from (Amar Cheba, 2020)}

Physiochemical properties	Degree of deacetylation, Molecular weight, Degree of polymerization, Facile derivatization crystallinity, Viscosity, Solubility, Stability, Chemical reactivity, Chelating activity, Ionic conductivity, Processability
Biological properties	Biocompatibility, Biodegradability, Bioactivity

However, the use of chitosan biopolymers as a food packaging material has some drawbacks such as poor mechanical, thermal, and low barrier properties which restrict their use in the industries. Recent advances in nanotechnology greatly contribute to overcome this problem.

1.3 Nanotechnology

Nanotechnology is the manipulation of materials on a nano scale size to fabricate new structure/material, ranging from 1-100 nm in length. All over the globe, several food packaging companies use nanotechnology in their manufacturing system to improve the physiochemical properties, and shelf lives of food products (Wesley et al. 2014). At nano scale, matter demonstrate better physical and chemical properties of materials compared to macro or micro scale (Kuswandi 2016). When polymer matrix combines with fillers, composites are formed, while nanocomposites fillers are in nano range. And in bionanocomposites, polymers are derived from biobased sources. Bionanocomposites are a special class of hybrid-materials which are composed of biopolymers (continuous phase/matrix) and inorganic/organic nanofillers (discontinuous phase) with at least one component is in nanometer range (1-100 nm). To enhance the biopolymer's properties many researchers studied bionanocomposites. The nanosized fillers play an important role to enhance mechanical and barrier properties of the biopolymer's matrix (Dong et al. 2022, Othman, 2014).

Currently, chitosan nanocomposites reinforced with inorganic nanoparticles are gaining much interest for the researchers due to organic-inorganic combination acquiring materials with unique properties (Spirescu et al. 2021).

Many studies have shown great enhancement in mechanical and barrier properties of the nanocomposites film using different inorganic nanoparticles such as silica, nano clays, metals and metal oxides (silver, gold, zinc oxide, copper oxides, titanium oxides etc.) (Dash et al. 2022,

Gasti et al. 2022, Li et al. 2022). However, some of the inorganic nanofillers are not the best for their use in food packaging due to their non-biodegradability, hidden bio-toxicity and poor biocompatibility (Zou et al. 2023). Hydroxyapatite nanoparticles (HANPs) are biocompatible, biodegradable, bioactive and non-toxic, thus HANPs is a good candidate as an inorganic nanofiller for the preparation of bionanocomposites.

1.4 Hydroxyapatite nanoparticles (HANPs)

Hydroxyapatite (HAp) is a main inorganic mineral component of calcium phosphate which belongs to apatite family with typical lattice structure ($Ca_{10}(PO_4)_6(OH)_2$) that is similar (in terms of morphology and composition) to human hard tissues such as bone and teeth (Li et al. 2018, Nazeer et al. 2017).

The applications of HANPs are significantly influenced by particle size, shape, phase purity, crystallinity, morphology, and composition of nano hydroxyapatite, which also depend on the synthesis precursors, synthesis route, and processing parameters (Dasgupta et al. 2013, Wu et al. 2016).

1.5 Synthesis methods of HANPs

There are different methods that have been used for the synthesis of HANPs (fig. 1.2) that include dry, wet, and other miscellaneous methods. Dry methods have two different methods like mechanochemical (Yeon et al. 2001) and solid-state (Guo et al. 2013) methods. On the other hand, wet methods are divided into several different methods such as chemical precipitation (Cengiz et al. 2008, Viswanath and Ravishankar 2008, Wang et al. 2010), hydrothermal (Lin et al. 2021, Zhang and Darvell 2010), sol-gel (Negrila et al. 2018, Phatai et al. 2019, Rajabi-Zamani et al. 2008), micro-emulsion (Bose and Saha 2003, Jemli et al. 2022, Ye et al. 2010), protein templated (Han et al. 2007), membrane-templated (Neelakandeswari et al. 2011) and microwave-

assisted (Goh et al. 2021, Han et al. 2006, Kumar et al. 2012, Yao et al. 2020). There are some other miscellaneous methods have also been reported which include sono-chemical synthesis (Brundavanam et al. 2011, Yan et al. 2018, Zhou et al. 2020), Biomimetic method, combustion method and plasma spray method.

1.5.1 HANPs synthesis by dry process

Synthesis of HANPs using dry method can be divided into two different methods, namely solid-state (Guo et al. 2013) and mechanochemical (Yeon et al. 2001) methods.

1.5.1.1 Solid-state method

The solid-state method is one of the simple methods for the synthesis of HAp. In which the chemical precursors, that contain calcium and phosphate are used in dry form and milled followed by calcination process to obtained HAp. This method required high temperature such as 1200-1300 ℃.

1.5.1.2 Mechanochemical method

Mechanochemical method is another dry method which is used for synthesis of HAp on a commercial scale. In a typical process, precursor materials are grounded on a planetary milling process. This technique is quite simple and reproducible. HAp powder obtained using this method, has much more defined structure as compared to the solid-state method (Fiume et al. 2021).

The final yield from both of these methods are usually in grain size with irregular shape (Sadat-Shojai et al. 2013), which is often obtained using low cost starting material. The particle size, most of the time is above the nano range with poor phase purity as compared to wet chemical method (Li and Webster 2018).

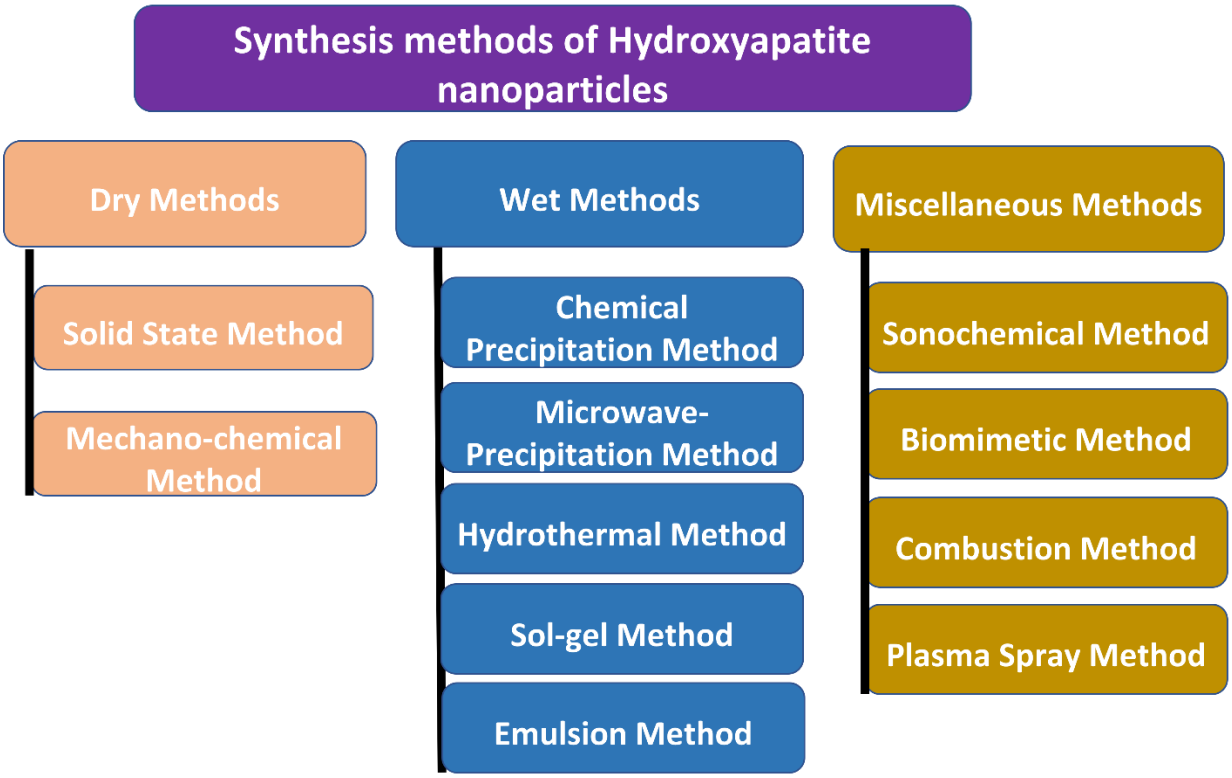

Figure 1.2 Different methods for the synthesis of hydroxyapatite nanoparticles {Modified and adopted from (Quadros et al. 2022)}

1.5.2 HANPs synthesis by wet process

HANPs obtained from wet chemical methods are usually with regular morphology. For this reason, this method is very popular and widely used by the researchers for the synthesis of nano hydroxyapatite powder (Zhan et al. 2005).

1.5.2.1 Chemical precipitation method

Chemical precipitation method is mostly used and the easiest method for synthesis of HANPs. In this method, precipitation reaction occurs between calcium and phosphorus precursors under mild conditions (low temperature and low pH) and continuous stirring to maintain Ca/P ratio (approximately 1.67). HANPs obtained by this process are poorly crystalline and non-

stoichiometric (Kumta et al. 2005). To improve phase purity of nano powder, precipitation reaction is needed to be conducted at higher temperature and higher pH.

1.5.2.2 Sol-gel method

Sol-gel method is used to obtain homogenous powder of HANPs more than two decades. Inorganic/organic acids, or alkoxides are the raw materials usually used for the preparation of sols. The reaction undergoes hydrolysis and polymerization to form a sol (colloidal suspension) that over the time with use of catalyst or temperature transform into the gel. The disadvantage of this method are high cost of raw materials, time consuming and risk of forming secondary phase (such as CaO) at the end of reaction (Fiume et al. 2021).

1.5.2.3 The hydrothermal method

The hydrothermal method is a popular procedure for the development of HANPs. This is the most popular method after chemical precipitation technique. This method is performed under high pressure and high temperature in an autoclave with the use of solution of calcium and phosphate precursor. In this method, organic solvent or water, or a mixture of aqueous organic solvents are used. By this method, use of high temperature results in higher phase purity with suitable Ca/P ratio compared to sol-gel methods. The major drawback of this method is the use of expensive equipment which is less affordable than other wet chemical methods.

1.5.2.4 Emulsion method

Emulsion method is known for achieving smaller particle size with controlled morphology and less agglomerated particles (Sadat-Shojai et al. 2013). The limitation of this method is the use of high cost of chemical or expensive surfactants such as polyoxyethylene, cetyltrimethyl

ammonium bromide and dioctyl sodium sulfosuccinate salt etc. (Fiume et al. 2021, Li et al. 2008).

Most of these methods require high temperatures and/or longer times to produce uniform sized, pure HANPs.

1.5.2.5 The microwave assisted precipitation method

Microwave assisted method has been found to be obtain higher purity HANPs with better yields in lesser reaction time. Microwave irradiation is proven to accelerate the reaction kinetics in a shorter time with lesser temperature when compared to conventional heating method (Goh et al. 2021, Herrero and Ullah 2021, Indira and Malathi 2022, Kumar et al. 2012, Ullah and Arshad 2017). Various approaches have been used for the microwave-based synthesis of HANPs as shown in fig.1.3. Microwave-assisted precipitation is popular in the researcher because of its simplicity, time sever, economical and high yield (Hassan et al. 2016b). Calcium and phosphate precursor mixed and treated in the microwave by setting up microwave parameters like temperature, exposure time, power etc.) to get precipitation.

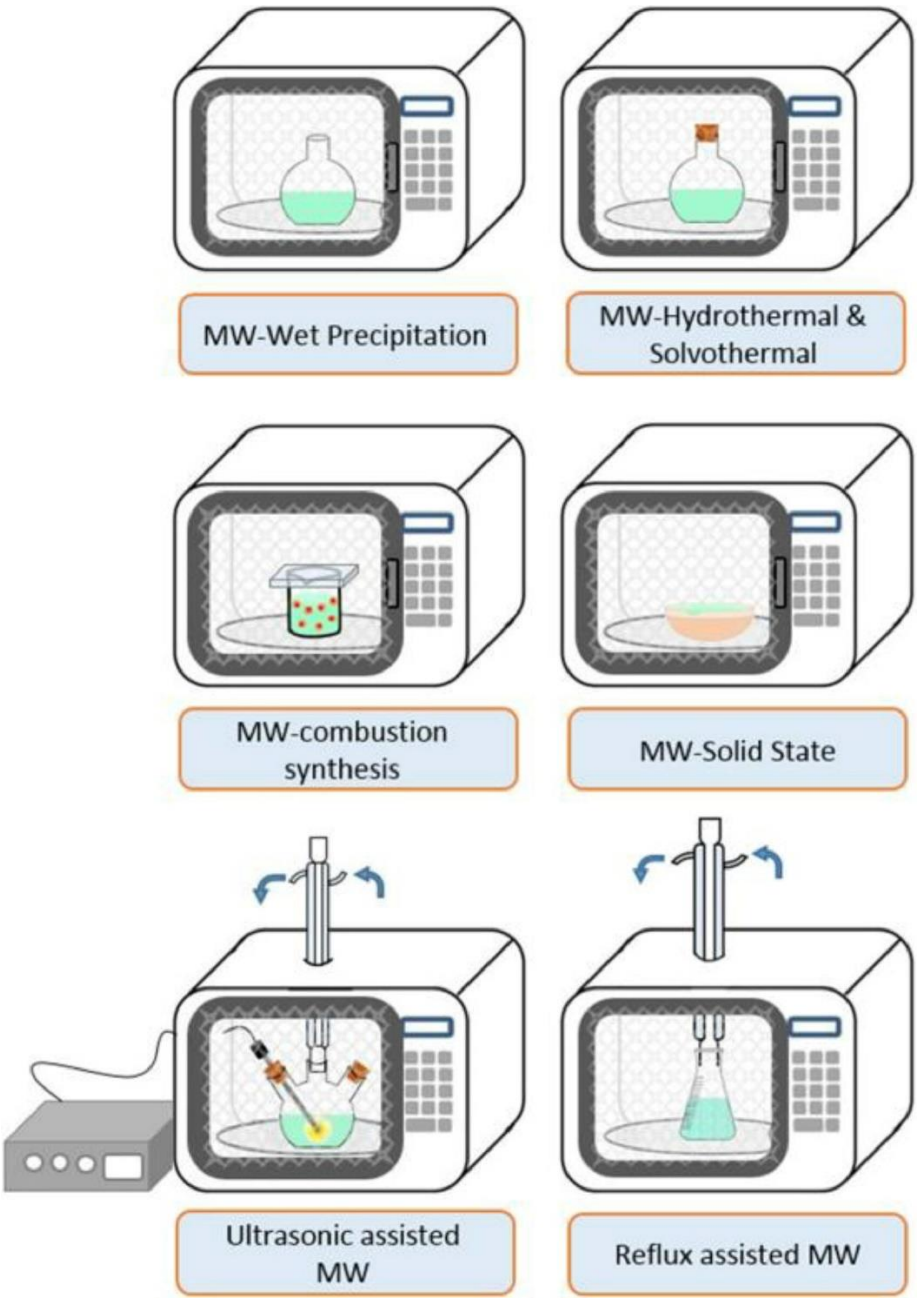

Figure 1.3 Different approaches used for the microwave-based synthesis of HANPs {Reproduced with permission from Elsevier: Microwave-assisted preparation of Nano-hydroxyapatite for bone substitutes (Hassan et al. 2016a)}

1.5.3 Miscellaneous methods

1.5.3.1 Sonochemical method

Sonochemical methods use powerful ultrasonic waves to accelerate heterogenous chemical reactions between calcium and phosphate precursors. HANPs form via this process obtained more uniform crystal lattice due to high speed and high kinetic energy stored during the synthesis (Fiume et al. 2021).

1.5.3.2 Combustion method

Combustion method used to quickly obtain highly pure HA powder with a single step operation. This method involves rapid exothermic redox reaction between an organic fuel (such as urea, glycine, citric acid, sucrose etc.), and oxidants (e.g., calcium nitrate or nitric acid) in an aqueous phase. In this, aqueous solutions of calcium and phosphate precursor mixed followed by adding nitric acid to dissolve obtained white precipitates. Then a single or a mixture of organic fuels are subsequently incorporated into the resultant solution mixture and followed by heating in furnace at low temperature (300 ℃). As a result of combustion, sudden increase in temperature to maximum noticed. Final step is rapid cooling of mixture that maximum nucleation induced and exothermic combustion provide enough heat to maintain temperature in the system while forming HA (Sadat-Shojai et al. 2013).

1.6 Synthesis of HANPs from bio-waste

HANPs can be synthesized through different methods using natural bio sources such as eggshells, snail shells, seashells, bovine bone, corals, and fish scales etc. as shown in fig. 1.4. However, eggshell derived HANPs are environment friendly and more desirable due to their properties such as renewability, biocompatibility, and bioactivity (Ummartyotin and

Tangnorawich 2015). Among all the natural biomaterial's eggshells are an excellent source of calcium for the synthesis of HANPs.

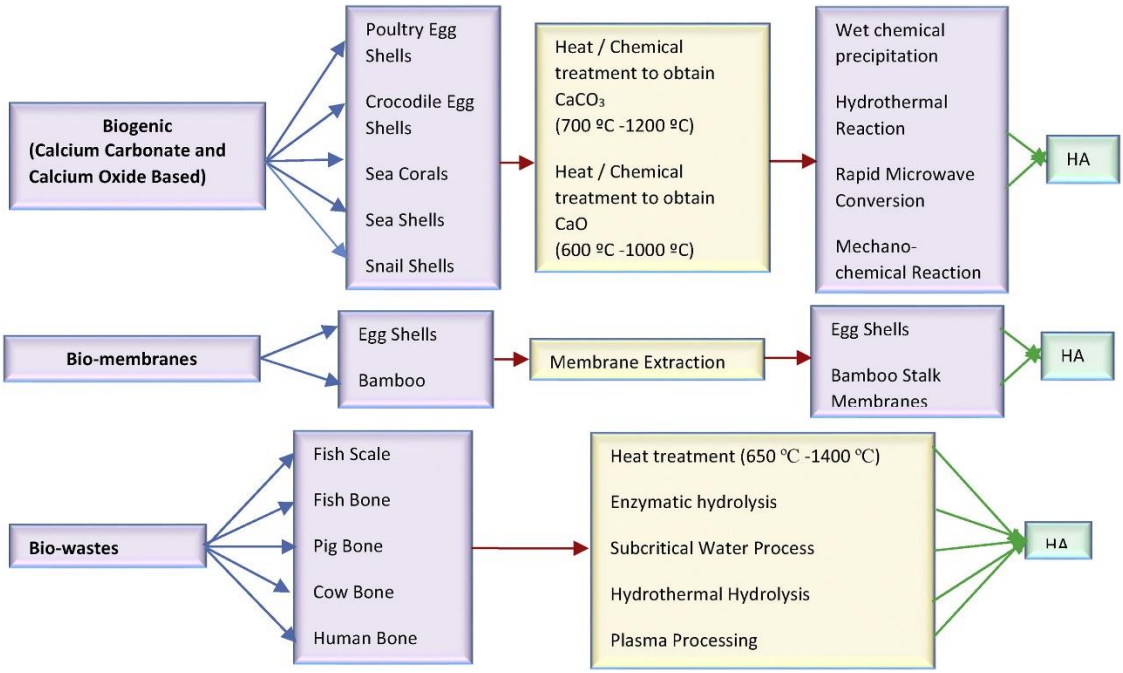

Figure 1.4 Non-synthetic bio sources for hydroxyapatite synthesis {Reproduced with permission from Elsevier: Environmentally sustainable processes for the synthesis of hydroxyapatite (Agbeboh et al. 2020)}

Several million tons of eggshells are generated as bio-waste from food industries worldwide on a daily basis. They are usually landfilled and hence creating huge environmental pollution (Kumar and Girija 2013, Wu et al. 2015). Eggshell is mainly composed of 94% calcium carbonate which represents about 11% of the total weight of the egg, along with some other components including 4% organic substances, 1% calcium phosphate, and 1% magnesium carbonate (Kamalanathan et al. 2014, Siva Rama Krishna et al. 2007). Eggshell is readily available, economical, and rich in calcium carbonate which makes it an excellent calcium source for deriving HANPs (Kumar and Girija 2013, Kumar et al. 2012).

1.7 Green template mediated synthesis of HANPs

Currently, green synthesis of nanoparticles using plant leaf extracts has become a very popular method because plant extracts act as a stabilizer and can be contributed to control the shape and size of the nanoparticles. Plant extracts are proven to be a good alternative to typical chemicals that are used to control the aggregation during the process. Plant extracts are rich in phytochemicals with antioxidant and anti-inflammatory properties. Therefore, it helps to regulate morphology and reduce the size due to the agglomeration (Alorku et al. 2020, Irwansyah et al. 2022). The plant mediated green synthesis of HAp falls under the wet chemical synthesis such as chemical precipitation, hydrothermal routes etc. It is easy to control aggregation, morphology, and size of HAp during these wet chemicals process. The mechanism of plant mediated synthesis of HAp mostly depends on the formation of chelates or complexes with calcium ions of HAp. The formation of precursors chelation/complexation is due to the functional group of the plant polyphenols. Flavonoids, terpenoids, alkaloids of amino, hydroxyl, carboxylic groups of plants play in important role in formation of Ca-complex/chelate during synthesis. And then formed Ca-complex reacts with the phosphate precursor to initiate the nucleation process under the suitable pH condition.

Recently, several researchers have reported the synthesis of uniformed size nano-hydroxyapatite using plant extract as a template such as licorice root, acacia falcata leaf, banana peel, tamarind, grape, coccinia grandis leaves, Azadirachta leaves, moringa oleifera flower etc. to obtained uniform size, shape and better crystallinity of HANPs (Ali et al. 2021, Ghate et al. 2022, Gopi et al. 2015, Gopi et al. 2014, Kalaiselvi et al. 2018, Kumar et al. 2018, Kumar et al. 2017, Umesh et al. 2021, Varadarajan et al. 2020).

1.8 Potential applications of HANPs

Due to excellent properties such as bioactivity, biocompatibility, biodegradability, and non-toxicity, HANPs are widely used in several biomedical applications (Goh et al. 2021, Trakoolwannachai et al. 2019) and other fields such as wastewater treatment (Zhou et al. 2021), cosmetics (Cunha et al. 2020, Morsy et al. 2017) soil remediation (Gan et al. 2021), catalyst (Usami and Okamoto 2017), column chromatography (Ashokan et al. 2021, Markov and Ivanov 1974), and food packaging applications (Malvano et al. 2021, Malvano et al. 2022).

However, their use as a nanofiller in nanocomposites in food packaging field is less explored. Recent scientific evidence indicates that the selection of nanofiller as well as their concentration have significant effects on nanocomposites to achieve desired properties for specific applications (Priyadarshi et al. 2021).

Therefore, this research aims to synthesize pure bioactive, biocompatible hydroxyapatite nanoparticles from the eggshell biowaste and their use to reinforce with chitosan biopolymer to develop bionanocomposites for food packaging applications. The prepared hydroxyapatite nanoparticles and chitosan-based bionanocomposites were widely studied in terms of morphological, structural, thermal, mechanical, and barrier properties.

1.9 Research Aim, Hypothesis and Objective

1.9.1 Aim of the study

This study aims to synthesize pure hydroxyapatite nanoparticles from eggshell waste and develop the bionanocomposites using this nanoparticle incorporated into chitosan biopolymer for food packaging applications.

1.9.2 Hypothesis

This study was undertaken with the hypothesis that,

- The microwave-assisted precipitation method using the green template Azadirachta Indica (AI) can improve the shape and size of hydroxyapatite nanoparticles.
- The use of HANPs as reinforcing material in chitosan matrix enhances chitosan biopolymer properties for food packaging applications.

1.9.3 Research Objective

The specific research objectives are,

1. Synthesis and characterization of hydroxyapatite nanoparticles from eggshell biowaste

(a) To successfully synthesize hydroxyapatite nanoparticles using the microwave-assisted and conventional heating method with and without green template Azadirachta Indica (AI)

(b) To evaluate the physicochemical, morphological, structural, and thermal properties of hydroxyapatite nanoparticles by using SEM, TEM, FTIR, XRD, XPS, and TGA

2. Preparation of chitosan biopolymer-based bionanocomposites films reinforced with hydroxyapatite nanoparticles from eggshell biowaste for food packaging applications.

(a) To prepare chitosan-based bionanocomposites film incorporating different concentrations of hydroxyapatite nanoparticles ranging from 1 to 10 %.

(b) To investigate the nano reinforcement effect on the chitosan matrix for material properties

(c) To characterize the bionanocomposites films using mechanical analysis (Tensile testing, DMA), water vapor permeability (WVP), thermal analysis (TGA, DSC), structural analysis (FTIR, XRD, XPS), and morphological observation (SEM, TEM)

Reference

Agbeboh, N.I., Oladele, I.O., Daramola, O.O., Adediran, A.A., Olasukanmi, O.O. and Tanimola, M.O. (2020) Environmentally sustainable processes for the synthesis of hydroxyapatite. Heliyon 6(4), e03765.

Ali, A.F., Alrowaili, Z.A., El-Giar, E.M., Ahmed, M.M. and El-Kady, A.M. (2021) Novel green synthesis of hydroxyapatite uniform nanorods via microwave-hydrothermal route using licorice root extract as template. Ceramics International 47(3), 3928-3937.

Alorku, K., Manoj, M. and Yuan, A. (2020) A plant-mediated synthesis of nanostructured hydroxyapatite for biomedical applications: a review. RSC Advances 10(67), 40923-40939.

amar Cheba, B. (2020) Chitosan: Properties, modifications and food nanobiotechnology. Procedia Manufacturing 46, 652-658.

Ambaye, T.G., Vaccari, M., Prasad, S., van Hullebusch, E.D. and Rtimi, S. (2022) Preparation and applications of chitosan and cellulose composite materials. Journal of Environmental Management 301, 113850.

Arikan, E.B. and Ozsoy, H.D. (2015) A review: investigation of bioplastics. Journal of Civil Engineering and Architecture 9(2), 188-192.

Ashokan, A., Rajendran, V., Sampath Kumar, T.S. and Jayaraman, G. (2021) Eggshell derived hydroxyapatite microspheres for chromatographic applications by a novel dissolution - precipitation method. Ceramics International 47(13), 18575-18583.

Cunha, C.S., Castro, P.J., Sousa, S.C., Pullar, R.C., Tobaldi, D.M., Piccirillo, C. and Pintado, M.M. (2020) Films of chitosan and natural modified hydroxyapatite as effective UV-protecting, biocompatible and antibacterial wound dressings. International Journal of Biological Macromolecules 159, 1177-1185.

Dasgupta, S., Tarafder, S., Bandyopadhyay, A. and Bose, S. (2013) Effect of grain size on mechanical, surface and biological properties of microwave sintered hydroxyapatite. Materials

Science and Engineering: C 33(5), 2846-2854.

Dash, K.K., Deka, P., Bangar, S.P., Chaudhary, V., Trif, M. and Rusu, A. (2022) Applications of Inorganic Nanoparticles in Food Packaging: A Comprehensive Review. Polymers 14(3), 521.

Dong, W., Su, J., Chen, Y., Xu, D., Cheng, L., Mao, L., Gao, Y. and Yuan, F. (2022) Characterization and antioxidant properties of chitosan film incorporated with modified silica nanoparticles as an active food packaging. Food Chem 373, 131414.

El-Aidie, S.A.-A.M. (2018) A review on chitosan: ecofriendly multiple potential applications in the food industry. International Journal of Advancement in Life Sciences Research, 1-14.

Emadian, S.M., Onay, T.T. and Demirel, B. (2017) Biodegradation of bioplastics in natural environments. Waste Management 59, 526-536.

Fiume, E., Magnaterra, G., Rahdar, A., Verné, E. and Baino, F. (2021) Hydroxyapatite for Biomedical Applications: A Short Overview. Ceramics 4(4), 542-563.

Gan, C.-d., Jia, Y.-b. and Yang, J.-y. (2021) Remediation of fluoride contaminated soil with nano-hydroxyapatite amendment: Response of soil fluoride bioavailability and microbial communities. Journal of Hazardous Materials 405, 124694.

Gasti, T., Dixit, S., Hiremani, V.D., Chougale, R.B., Masti, S.P., Vootla, S.K. and Mudigoudra, B.S. (2022) Chitosan/pullulan based films incorporated with clove essential oil loaded chitosan-ZnO hybrid nanoparticles for active food packaging. Carbohydrate Polymers 277, 118866.

Ghaffar, I., Rashid, M., Akmal, M. and Hussain, A. (2022) Plastics in the environment as potential threat to life: an overview. Environmental Science and Pollution Research 29(38), 56928-56947.

Ghate, P., Prabhu S, D., Murugesan, G., Goveas, L.C., Varadavenkatesan, T., Vinayagam, R., Lan Chi, N.T., Pugazhendhi, A. and Selvaraj, R. (2022) Synthesis of hydroxyapatite nanoparticles using Acacia falcata leaf extract and study of their anti-cancerous activity against cancerous mammalian cell lines. Environmental Research 214, 113917.

Goel, V., Luthra, P., Kapur, G.S. and Ramakumar, S.S.V. (2021) Biodegradable/Bio-plastics: Myths and Realities. Journal of Polymers and the Environment 29(10), 3079-3104.

Goh, K.W., Wong, Y.H., Ramesh, S., Chandran, H., Krishnasamy, S., Ramesh, S., Sidhu, A. and Teng, W.D. (2021) Effect of pH on the properties of eggshell-derived hydroxyapatite bioceramic synthesized by wet chemical method assisted by microwave irradiation. Ceramics International 47(7, Part A), 8879-8887.

Gopi, D., Bhuvaneshwari, N., Kavitha, L. and Ramya, S. (2015) Novel malic acid mediated green route for the synthesis of hydroxyapatite particles and their spectral characterization. Ceramics International 41(2, Part B), 3116-3127.

Gopi, D., Kanimozhi, K., Bhuvaneshwari, N., Indira, J. and Kavitha, L. (2014) Novel banana peel pectin mediated green route for the synthesis of hydroxyapatite nanoparticles and their spectral characterization. Spectrochimica Acta Part A: Molecular and Biomolecular Spectroscopy 118, 589-597.

Guo, X., Yan, H., Zhao, S., Li, Z., Li, Y. and Liang, X. (2013) Effect of calcining temperature on particle size of hydroxyapatite synthesized by solid-state reaction at room temperature. Advanced Powder Technology 24(6), 1034-1038.

Haghighi, H., Licciardello, F., Fava, P., Siesler, H.W. and Pulvirenti, A. (2020) Recent advances on chitosan-based films for sustainable food packaging applications. Food Packaging and Shelf Life 26, 100551.

Han, J.H. (2003) Novel Food Packaging Techniques. Ahvenainen, R. (ed), pp. 50-70, Woodhead Publishing.

Harding, K.G., Gounden, T. and Pretorius, S. (2017) “Biodegradable” Plastics: A Myth of Marketing? Procedia Manufacturing 7, 106-110.

Hassan, M.N., Mahmoud, M.M., Abd El-Fattah, A. and Kandil, S. (2016a) Microwave-assisted preparation of Nano-hydroxyapatite for bone substitutes. Ceramics International 42(3), 3725-3744.

Hassan, M.N., Mahmoud, M.M., El-Fattah, A.A. and Kandil, S. (2016b) Microwave-assisted preparation of Nano-hydroxyapatite for bone substitutes. Ceramics International 42(3), 3725-3744.

Herrero, Y.R. and Ullah, A. (2021) Rapid, Metal-Free, Catalytic Conversion of Glycerol to Allyl Monomers and Polymers. ACS Sustainable Chemistry & Engineering 9(28), 9474-9485.

Huysman, S., De Schaepmeester, J., Ragaert, K., Dewulf, J. and De Meester, S. (2017) Performance indicators for a circular economy: A case study on post-industrial plastic waste. Resources, conservation and recycling 120, 46-54.

Indira, J. and Malathi, K.S. (2022) Comparison of template mediated ultrasonic and microwave irradiation method on the synthesis of hydroxyapatite nanoparticles for biomedical applications. Materials Today: Proceedings 51, 1765-1769.

Irwansyah, F.S., Noviyanti, A.R., Eddy, D.R. and Risdiana, R. (2022) Green Template-Mediated Synthesis of Biowaste Nano-Hydroxyapatite: A Systematic Literature Review. Molecules 27(17), 5586.

Kalaiselvi, V., Mathammal, R., Vijayakumar, S. and Vaseeharan, B. (2018) Microwave assisted green synthesis of Hydroxyapatite nanorods using Moringa oleifera flower extract and its antimicrobial applications. International Journal of Veterinary Science and Medicine 6(2), 286-295.

Kamalanathan, P., Ramesh, S., Bang, L.T., Niakan, A., Tan, C.Y., Purbolaksono, J., Chandran, H. and Teng, W.D. (2014) Synthesis and sintering of hydroxyapatite derived from eggshells as a calcium precursor. Ceramics International 40(10, Part B), 16349-16359.

Kumar, G.S. and Girija, E.K. (2013) Flower-like hydroxyapatite nanostructure obtained from eggshell: A candidate for biomedical applications. Ceramics International 39(7), 8293-8299.

Kumar, G.S., Muthu, D., Karunakaran, G., Karthi, S., Girija, E.K. and Kuznetsov, D. (2018) Curcuma longa tuber extract mediated synthesis of hydroxyapatite nanorods using biowaste as a calcium source for the treatment of bone infections. Journal of Sol-Gel Science and Technology

86(3), 610-616.

Kumar, G.S., Rajendran, S., Karthi, S., Govindan, R., Girija, E.K., Karunakaran, G. and Kuznetsov, D. (2017) Green synthesis and antibacterial activity of hydroxyapatite nanorods for orthopedic applications. MRS Communications 7(2), 183-188.

Kumar, G.S., Thamizhavel, A. and Girija, E. (2012) Microwave conversion of eggshells into flower-like hydroxyapatite nanostructure for biomedical applications. Materials Letters 76, 198-200.

Kumta, P.N., Sfeir, C., Lee, D.-H., Olton, D. and Choi, D. (2005) Nanostructured calcium phosphates for biomedical applications: novel synthesis and characterization. Acta Biomaterialia 1(1), 65-83.

Kuswandi, B. (2016) Nanotechnology in food packaging. Nanoscience in food and agriculture 1, 151-183.

Lebreton, L. and Andrady, A. (2019) Future scenarios of global plastic waste generation and disposal. Palgrave Communications 5(1), 6.

Li, B. and Webster, T. (2018) Orthopedic Biomaterials, Springer.

Li, H., Zhu, M., Li, L. and Zhou, C. (2008) Processing of nanocrystalline hydroxyapatite particles via reverse microemulsions. Journal of materials science 43, 384-389.

Li, L., Iqbal, J., Zhu, Y., Zhang, P., Chen, W., Bhatnagar, A. and Du, Y. (2018) Chitosan/Ag-hydroxyapatite nanocomposite beads as a potential adsorbent for the efficient removal of toxic aquatic pollutants. International Journal of Biological Macromolecules 120, 1752-1759.

Li, S., Mu, B., Zhang, H., Kang, Y. and Wang, A. (2022) Incorporation of silver nanoparticles/curcumin/clay minerals into chitosan film for enhancing mechanical properties, antioxidant and antibacterial activity. International Journal of Biological Macromolecules 223, 779-789.

Malvano, F., Montone, A.M.I., Capparelli, R., Capuano, F. and Albanese, D. (2021) Development of a Novel Active Edible Coating Containing Hydroxyapatite for Food Shelf-life Extension. Chemical Engineering Transactions 87, 25-30.

Malvano, F., Montone, A.M.I., Capuano, F., Colletti, C., Roveri, N., Albanese, D. and Capparelli, R. (2022) Effects of active alginate edible coating enriched with hydroxyapatite-quercetin complexes during the cold storage of fresh chicken fillets. Food Packaging and Shelf Life 32, 100847.

Markov, G.G. and Ivanov, I.G. (1974) Hydroxyapatite column chromatography in procedures for isolation of purified DNA. Analytical Biochemistry 59(2), 555-563.

Morsy, R., Ali, S.S. and El-Shetehy, M. (2017) Development of hydroxyapatite-chitosan gel sunscreen combating clinical multidrug-resistant bacteria. Journal of Molecular Structure 1143, 251-258.

Nazeer, M.A., Yilgör, E. and Yilgör, I. (2017) Intercalated chitosan/hydroxyapatite nanocomposites: promising materials for bone tissue engineering applications. Carbohydrate Polymers 175, 38-46.

Othman, S.H. (2014) Bio-nanocomposite Materials for Food Packaging Applications: Types of Biopolymer and Nano-sized Filler. Agriculture and Agricultural Science Procedia 2, 296-303.

Priyadarshi, R., Roy, S., Ghosh, T., Biswas, D. and Rhim, J.-W. (2021) Antimicrobial nanofillers reinforced biopolymer composite films for active food packaging applications-a review. Sustainable Materials and Technologies, e00353.

Quadros, M., Momin, M. and Verma, G. (2022) Handbook on Synthesis Strategies for Advanced Materials: Volume-II: Processing and Functionalization of Materials. Tyagi, A.K. and Ningthoujam, R.S. (eds), pp. 617-658, Springer Nature Singapore, Singapore.

Rane, K.D. and Hoover, D.G. (1993) Production of chitosan by fungi. Food biotechnology 7(1), 11-33.

Reddy, M.M., Vivekanandhan, S., Misra, M., Bhatia, S.K. and Mohanty, A.K. (2013) Biobased plastics and bionanocomposites: Current status and future opportunities. Progress in Polymer Science 38(10), 1653-1689.

Rinaudo, M. (2006) Chitin and chitosan: Properties and applications. Progress in Polymer Science 31(7), 603-632.

Sadat-Shojai, M., Khorasani, M.-T., Dinpanah-Khoshdargi, E. and Jamshidi, A. (2013) Synthesis methods for nanosized hydroxyapatite with diverse structures. Acta Biomaterialia 9(8), 7591-7621.

Sarode, S., Upadhyay, P., Khosa, M.A., Mak, T., Shakir, A., Song, S. and Ullah, A. (2019) Overview of wastewater treatment methods with special focus on biopolymer chitin-chitosan. International Journal of Biological Macromolecules 121, 1086-1100.

Singh, N., Ogunseitan, O.A., Wong, M.H. and Tang, Y. (2022) Sustainable materials alternative to petrochemical plastics pollution: A review analysis. Sustainable Horizons 2, 100016.

Siva Rama Krishna, D., Siddharthan, A., Seshadri, S.K. and Sampath Kumar, T.S. (2007) A novel route for synthesis of nanocrystalline hydroxyapatite from eggshell waste. Journal of Materials Science: Materials in Medicine 18(9), 1735-1743.

Spirescu, V.A., Chircov, C., Grumezescu, A.M., Vasile, B.Ș. and Andronescu, E. (2021) Inorganic Nanoparticles and Composite Films for Antimicrobial Therapies. International journal of molecular sciences 22(9), 4595.

Trakoolwannachai, V., Kheolamai, P. and Ummartyotin, S. (2019) Development of hydroxyapatite from eggshell waste and a chitosan-based composite: In vitro behavior of human osteoblast-like cell (Saos-2) cultures. International Journal of Biological Macromolecules 134, 557-564.

Ullah, A. and Arshad, M. (2017) Remarkably Efficient Microwave-Assisted Cross-Metathesis of Lipids under Solvent-Free Conditions. ChemSusChem 10(10), 2167-2174.

Umesh, M., Choudhury, D.D., Shanmugam, S., Ganesan, S., Alsehli, M., Elfasakhany, A. and Pugazhendhi, A. (2021) Eggshells biowaste for hydroxyapatite green synthesis using extract piper betel leaf - Evaluation of antibacterial and antibiofilm activity. Environmental Research 200, 111493.

Ummartyotin, S. and Tangnorawich, B. (2015) Utilization of eggshell waste as raw material for synthesis of hydroxyapatite. Colloid and Polymer Science 293(9), 2477-2483.

Usami, K. and Okamoto, A. (2017) Hydroxyapatite: catalyst for a one-pot pentose formation. Organic & Biomolecular Chemistry 15(42), 8888-8893.

Varadarajan, V., Varsha, M., Vijayasekaran, K. and Shankar, S.V. (2020) Comparative studies of hydroxyapatite (HAp) nanoparticles synthesized by using different green templates. AIP Conference Proceedings 2240(1), 080002.

Wesley, S.J., Raja, P., Raj, A.A. and Tiroutchelvamae, D. (2014) Review on-nanotechnology applications in food packaging and safety. International Journal of Engineering Research 3(11), 645-651.

Wu, S.-C., Hsu, H.-C., Hsu, S.-K., Chang, Y.-C. and Ho, W.-F. (2015) Effects of heat treatment on the synthesis of hydroxyapatite from eggshell powders. Ceramics International 41(9), 10718-10724.

Wu, S.-C., Hsu, H.-C., Hsu, S.-K., Chang, Y.-C. and Ho, W.-F. (2016) Synthesis of hydroxyapatite from eggshell powders through ball milling and heat treatment. Journal of Asian Ceramic Societies 4(1), 85-90.

Yeon, K.C., Wang, J. and Ng, S.C. (2001) Mechanochemical synthesis of nanocrystalline hydroxyapatite from CaO and CaHPO4. Biomaterials 22(20), 2705-2712.

Zhan, J., Tseng, Y.H., Chan, J.C. and Mou, C.Y. (2005) Biomimetic formation of hydroxyapatite nanorods by a single-crystal-to-single-crystal transformation. Advanced Functional Materials 15(12), 2005-2010.

Zhou, C., Wang, X., Wang, Y., Song, X., Fang, D. and Ge, S. (2021) The sorption of single- and multi-heavy metals in aqueous solution using enhanced nano-hydroxyapatite assisted with ultrasonic. Journal of Environmental Chemical Engineering 9(3), 105240.

Zou, Z., Ismail, B.B., Zhang, X., Yang, Z., Liu, D. and Guo, M. (2023) Improving barrier and antibacterial properties of chitosan composite films by incorporating lignin nanoparticles and acylated soy protein isolate nanogel. Food Hydrocolloids 134, 108091.

CHAPTER 2. LITERATURE REVIEW

2.1 Bionanocomposites in food packaging

Bionanocomposite is a very popular and interesting subject among the world's researchers as they provide exciting platforms and serve as collaborators in nanotechnology, material science, and biology. Currently, it is proven to be a promising technique in the biomedical and food packaging application fields. Bionanocomposites are emerging hybrid materials of biodegradable biopolymers (including polysaccharides, protein, and polypeptides) and nanofillers organic/inorganic nanoparticles (such as clays, metal and metal oxide, and hydroxyapatite nanoparticles) (Ruiz-Hitzky et al. 2005). Bionanocomposites are also known as green composites or bio-based plastics also referred to as bioplastics. The bionanocomposites are the materials comprise of nanoparticles (at least one dimension in the nano range of 1 to 100 nm) and a main constitute matrix of the biopolymers or may be from the biological origin. Bionanocomposites are superior to composites and nanocomposites due to the use of biodegradable biobased materials with enhanced material mechanical properties. Figure 2.1 shows the major difference between composites, nanocomposites, and bionanocomposites.

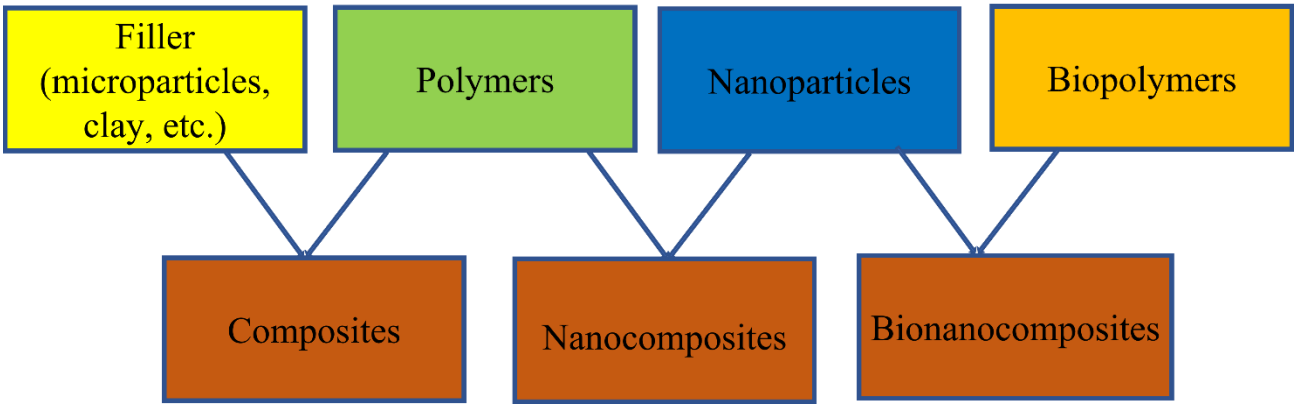

Figure 2.1. Constitutes of composites, nanocomposites and bionanocomposites {Modified and adopted from (Arora et al. 2018)}

Bionanocomposites display super beneficial properties like biocompatibility, biodegradability, antimicrobial activity, high mechanical, and barrier properties. Addition to that they are renewable and cost effective.

2.2 Biodegradable biopolymers and their categories

Biopolymers mainly consist of two or more monomers which are covalently bonded to form big molecules (polymer) and are usually derived from the living organisms, like plants, microbes, instead of traditional source of petroleum-based polymers. Biopolymers can be divided into different classes based on their origin and synthesis processes which shown are in fig. 2.2. Main categories include (1) natural biopolymers such as plant or animal origin carbohydrate including cellulose, starch, alginate, chitosan, agar, and carrageenan; and plant or animal-based proteins like corn zein, whey protein, wheat gluten, soy protein isolate (SPI), gelatin, collagen, casein etc., (2) synthetic biodegradable biopolymers like biomass derived, poly(lactide) (PLA) and petroleum-derived, poly (ε-caprolactone) (PCL), poly(vinyl alcohol) (PVA), polyglycolic acid (PGA), poly(butylene succinate) (PBS), etc., (3) biopolymers are produced or fermentation process by microorganism such as poly (hydroxyalkanoates) (PHAs) including poly(β-hydroxybutyrate) (PHB), poly (3 hydroxybutyrate co 3-hydroxyvalerate) (PHBV) etc. (Clarinval and Halleux 2005).

A variety of different biopolymers from natural sources such as starch, cellulose, and chitosan are widely used for food packaging applications. Among these biopolymers, chitosan has a great potential to use in food packaging applications due to its high availability, biodegradability, biocompatibility, non-toxicity, excellent film forming and antimicrobial properties.

However, the large-scale application of biopolymers in food packaging industries are limited due to their relatively poor mechanical and low barrier properties, and brittleness compared to non-renewable petroleum-based food packaging. The main problem correlated is in terms of processing, performance, and cost. Processing and performance are common problems in all biodegradable polymers regardless of their origin (Pandey et al. 2005, Rhim et al. 2013).

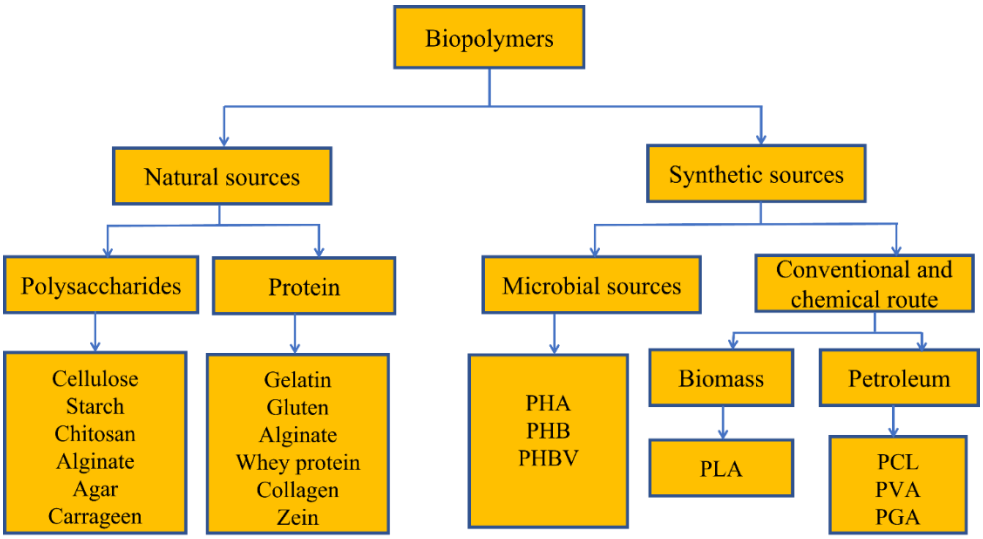

Figure 2.2 Biopolymers and their classification {Modified and adopted from (Rhim et al. 2013)}

(Abbreviations used in this figure described in the list of abbreviations)

Chitosan and chitosan derivatives nanocomposites have gained high interest due to their unique physical and chemical properties such as biocompatibility, biodegradability, antimicrobial, ionic conductivity, and high crystallinity. Nanoparticles can be easily embedded through amine ($-NH_2$) and hydroxyl (-OH) groups of chitosan structure which stimulate the formation of inter and intramolecular hydrogen bond between nanoparticles and chitosan matrix. Chitosan based nanocomposites has been earning more and more interest as a renewable, sustainable, eco-

friendly, and low-cost biomaterial nanocomposite.

2.3 Nanofillers

The utilization of nanotechnology in the food packaging industry has gained so much interest in the past few years due to the high reactivity, high surface area effect, improved bioactivity, and biocompatibility of the nanoparticles. Nanofillers for food packaging are classified based on their source of materials which includes organic and inorganic. The commonly used nanofillers in food packaging are shown in fig. 2.3.

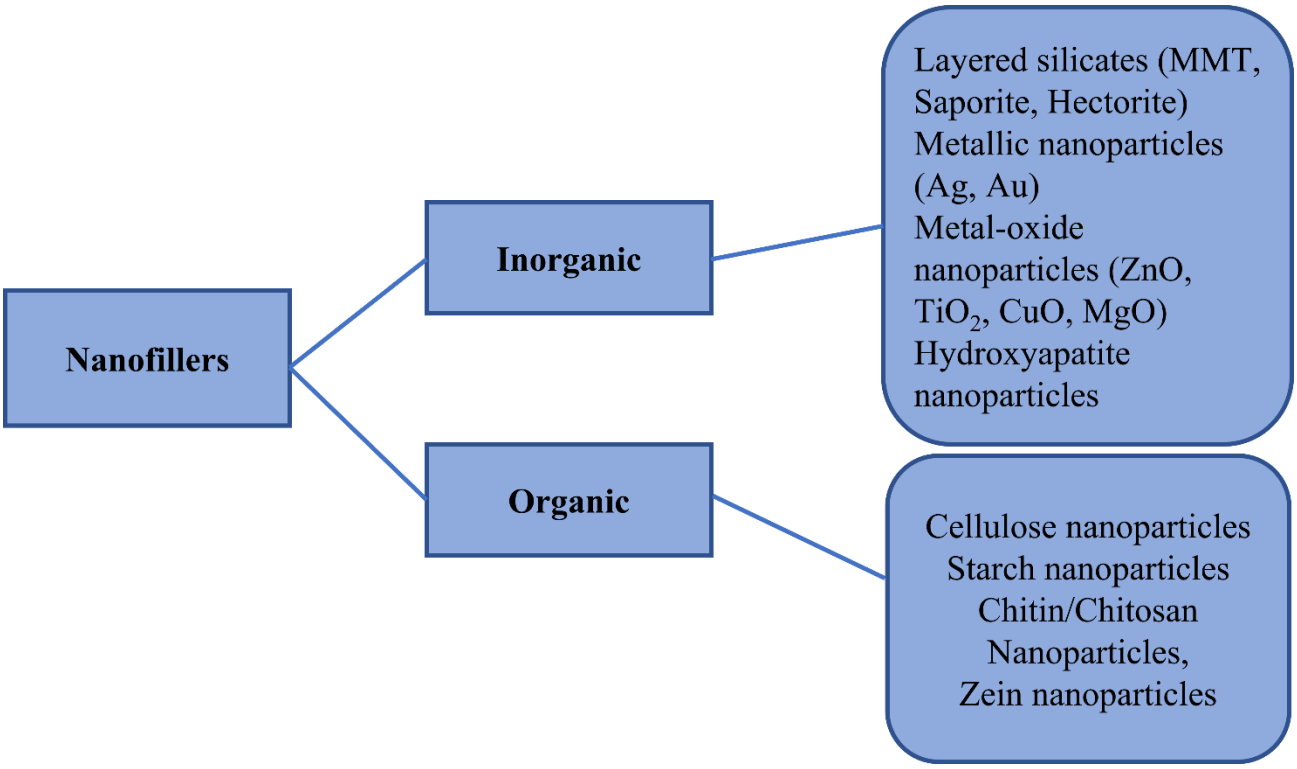

Figure 2.3 The commonly used nanofillers in the food packaging

Generally, chitosan based bionanocomposites produced by blending the inorganic/organic nanoparticles in acidic solution with dissolved chitosan, cast mixture slurry and let it dry at very

low temperature or room temperature (Priyadarshi and Rhim 2020). By using solvent casting method, it is possible to dispersed nanoparticles into chitosan matrix to enhance the mechanical, thermal and barrier properties of chitosan (Silva et al. 2021). Currently, chitosan biopolymer film reinforcing with inorganic nanofiller, organic-inorganic composites are gaining much attention due to organic and inorganic components combination acquiring materials with unique properties (Spirescu et al. 2021). Different inorganic metallic nanoparticles such as silica, silver, gold and metal oxide (zinc oxide, copper oxide, titanium oxide, and silicone oxide) and non-metallic, nano clays (e.g. montmorillonite (MMT)) have been used to prepared bionanocomposites film as an active food packaging materials (Dash et al. 2022). However, some of the inorganic nanoparticles are not exemplary nano addition/nanofiller for chitosan-based composites because of their non-biodegradability, hidden bio-toxicity, and mostly poor biocompatibility (Zou et al. 2023).

Hydroxyapatite nanoparticles are inorganic components having high biocompatibility, biodegradability and non-toxicity that make them a good choice as a nanofiller for the chitosan based bionanocomposites for food packaging applications.

2.4 Hydroxyapatite

Hydroxyapatite (HAp) ($Ca_{10}(PO_4)_6(OH)_2$) is a main inorganic mineral component of calcium phosphate apatite family found in the human hard tissues such as bone and teeth (Li et al. 2018, Nazeer et al. 2017). Typically, HAp contains Ca/P ratio of 1.67 has crystal structure of hexagonal unit cell with parameters space group of $P6_3/m$ with lattice parameters of a=b equal to 9.4225 Å, and c equal to 6.8850 Å having crystal growth direction along the c-axis (Fiume et al. 2021). Where a=b planes are mainly composed of positively charge calcium ions and c-plane is negatively charged phosphate ions. Fig. 2.4 displays crystal structure of HA. As it can be seen in

fig. 2.4, calcium ions (Ca^{2+}) occupy two different positions in the unit cell, Ca (I) has four Ca^{2+} ions which are vertically distributed along the c-axis and Ca (II) are surrounded by the six Ca^{2+} ion which are distributed in a triangle around the c-axis and they are coplanar with PO_4^{3-} tetrahedron, hence provide better stability in HAp structure. Among all the calcium phosphate family, HAp is the most stable phase, with a melting point of 1650 ℃ a density of 3.156 gm/cm^3 (Lu et al. 2019).

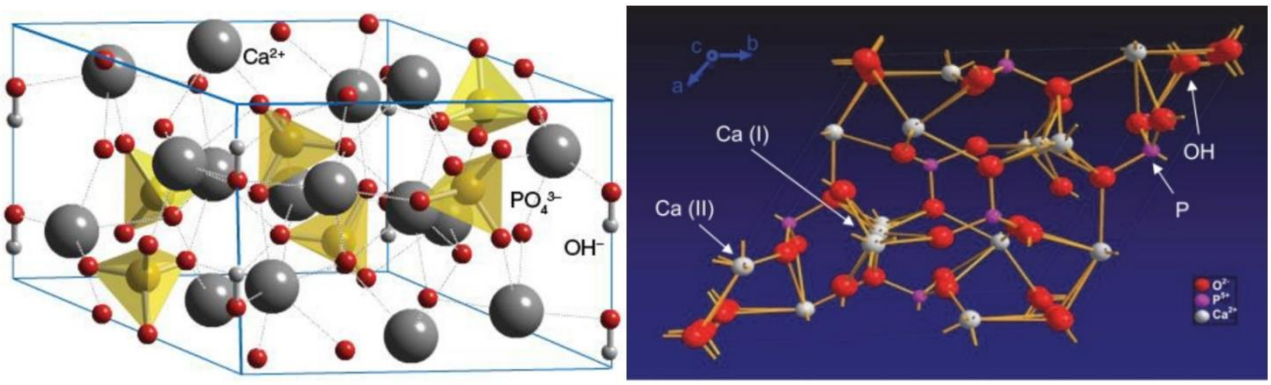

Figure 2.4 The crystal structure model of Hydroxyapatite {Reproduced with permission from MDPI: Hydroxyapatite for Biomedical Applications: A Short Overview (Fiume et al. 2021)}

Hydroxyapatites biomedical applications are well known due to their high biocompatibility, and bioactivity. Recently, hydroxyapatite nanoparticles have gained much interest in the perspective of food and food packaging applications.

The applications of HANPs are significantly influenced by their particle size, shape, phase purity, crystallinity, morphology, and composition of nano hydroxyapatite, which also depend on the synthesis precursors, synthesis route, and processing parameters (Dasgupta et al. 2013, Wu et al. 2016).

2.4.1 Preparation techniques for HANPs

Extensive literature data related to HANPs suggest that the preparation techniques and their parameters such as selection of precursors, temperature, pH, reaction time, Ca to P ratio and aging times play an important role to achieve pure HANPs with different morphology. Most relevant processes from synthetic as well as biogenic sources which are relevant to the current project objectives are discussed as follows:

Bouyer et al. prepared HANPs by wet chemical precipitation method using calcium hydroxide and phosphoric acid at different temperatures using various reactant (phosphoric acid) addition rate. They confirmed that the size, shape, and specific surface area of the nanoparticles were sensitive to the reaction temperature as well as addition rate of reactant. HANPs synthesized at low temperature (T= 60 ℃) are monocrystalline with needle shape hexagonal structure (Bouyer et al. 2000).

Kong et. al synthesized HANPs by chemical precipitation method using starting materials of calcium nitrate and phosphoric acid. They obtained single phase of HANPs with grain size of about 60 nm and surface area of 62 m^2/g (Kong et al. 2002).

Zanotto et al. studied the effect of thermal treatment, temperature range between 80 ℃ to 900 ℃ on particles size, morphology, and crystallinity of HA. They obtained HA using calcium nitrate and diammonium hydrogen phosphate by precipitation method. They observed two different morphologies, at 500 ℃, the prepared nano HA were irregular rod-shape with size of around 56 nm in width and around 220 nm in length. A pure nano HA with higher crystallinity obtained at 900 ℃ with hexagonal rod-shaped and size of around 65 nm in width and ~ 80 nm in length (Zanotto et al. 2012).

Li et al. prepared HA by precipitation method in the presence and absence of citric acid as a surfactant. They demonstrated the effect of surfactant on HA nanoparticles size when

coprecipitated calcium chloride and sodium phosphate precursors aging for 24 hours at pH range of 9-11. In the presence of surfactant (citric acid), HA showed rod-like morphology with the size of 10-20 nm in width and 50-70 nm in length. On the other hand, in the absence of surfactant, it showed an increased in size with particle size of 1 μm in width and 100 μm in length (Li et al. 2008).

Zhang and Lu prepared HANPs using wet chemical precipitation method at low temperature using two different precursors i.e., calcium nitrate and diammonium hydrogen phosphate. They observed that reaction temperature and mixing rate influences the crystallinity, phase, size, and shape of the HA nanoparticles. With rapid mixing mode at 40 ℃ develop spherical HANPs with an average size diameter of 20-50 nm (Zhang and Lu 2007).

Zhang and Darvell synthesized uniform highly crystalline HA whiskers by hydrothermal technique using calcium nitrate and diammonium hydrogen phosphate in the presence of acetamide that helps to increase pH during hydrolysis. The aspect ratio of hydroxyapatite whiskers depends on the concentration of acetamide. They obtained longer whiskers with higher concentration of acetamide with lower aspect ratio (Zhang and Darvell 2010).

Rodriguez-Lugo et al. synthesized HANPs by wet chemical synthesis method. They studied the effect of different pH (9-11) and sintering temperatures (300, 500, 700 and 900 ℃) on structural morphological properties. They observed at pH 9, spherical nanoparticles with size around 30-50 nm were formed. At pH 10, HA particles formed flask and at pH 11 combination of rod and flask were observed. Sintering temperature played an important role in the morphology (Rodríguez-Lugo et al. 2018) as well as shown in figure 2.5 where it is clear that with increase in temperature, morphology of HA completely changed from semi-spherical to flask like nanoparticles.

Han et al. produced nano HA by microwave hydrothermal method using initial precursors i.e., calcium hydroxide and phosphoric acid. The temperature and pressure were used 300 ℃ and 600 psi respectively. Mixed phases of HA and dicalcium phosphate anhydrous (DCPA) were observed at 450 W or less. However, at microwave energy of 550 W, pure phase, needle shaped HA in just 4 minutes of microwave radiation with size of dimensions of 4-15 nm by 20-50 nm were produced (Han et al. 2006).

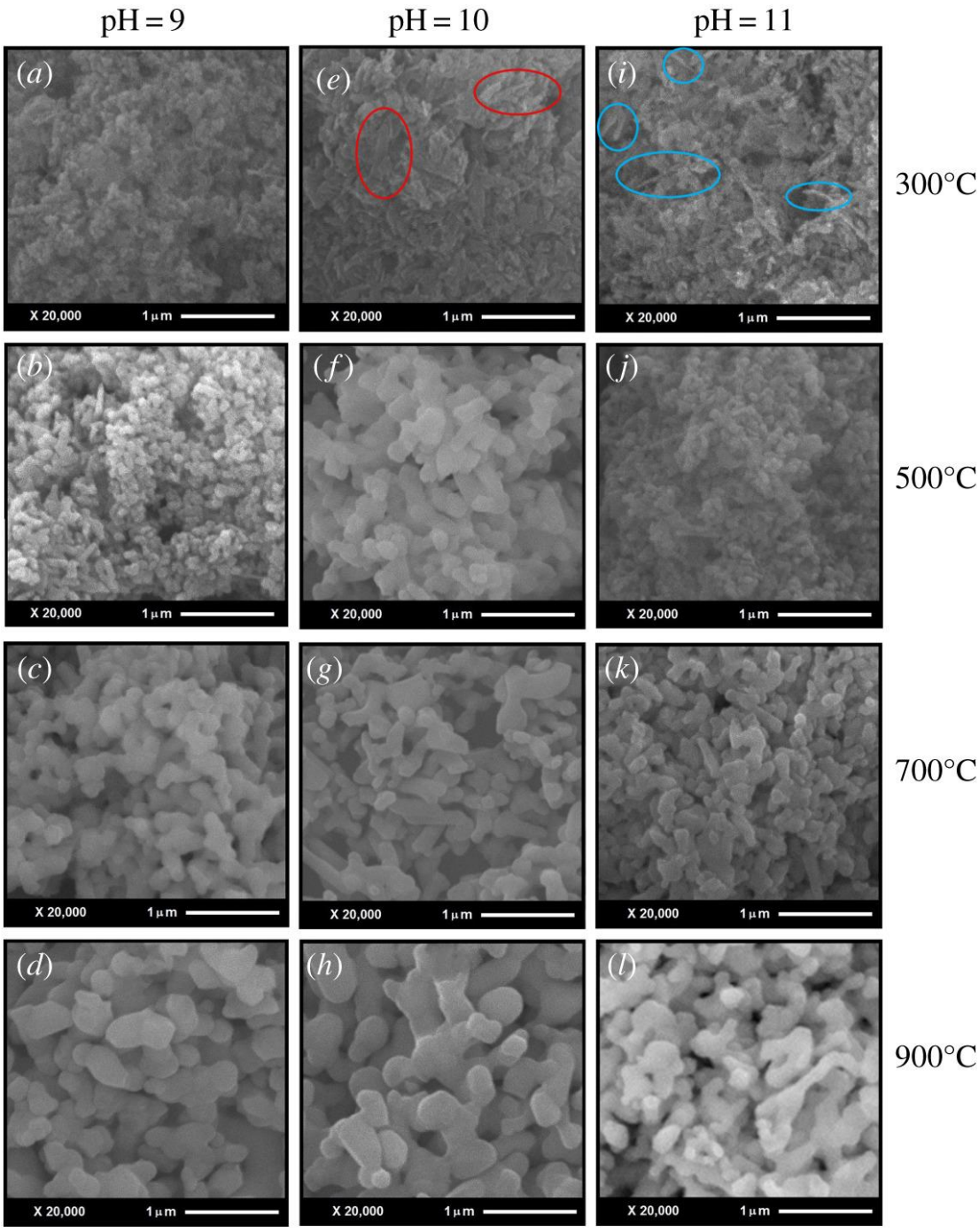

Figure 2.5 Scanning electron microscopy(SEM) of HAp nanoparticles at different temperatures and different pH { Reproduced with permission from The Royal Society: Wet chemical synthesis of nanocrystalline hydroxyapatite flakes (Rodríguez-Lugo et al. 2018)}

Kumar et al. synthesized magnesium substituted B-type HAp from eggshell waste by microwave assisted conversion. The chelating agent i.e., EDTA was used to form Ca-EDTA complex (fig.

2.6) and diammonium hydrogen phosphate used as a phosphate precursor. The reaction was carried out at 600 W microwave irradiation for 10 minutes at pH 13. Leaf like morphology was observed with size of 100-200 nm in width and 0.5 to 1 μm in length (Kumar et al. 2012).

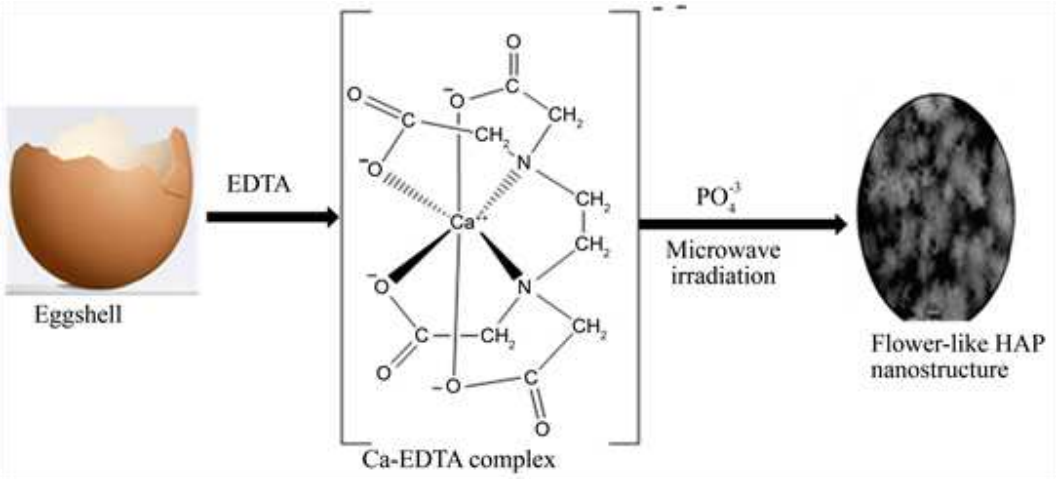

Figure 2.6 Hydroxyapatite nanoparticles from eggshell by microwave irradiation method { Modified and adopted from (Kumar et al. 2012)}

Gopi et al. synthesized the HA nanoparticles by banana peel pectin green template method. They used various concentrations of pectin extracted from banana peel to get pure HA. They obtained the pure, low crystalline, spherical, and smaller size HANPs in the presence of optimized concentration of pectin. And also the HANPs derived in the presence of pectin showed an enhanced antibacterial activity (Gopi et al. 2014).

Ali et al. successfully synthesized nanorod in the presence of an organic template licorice root extract (LE) using microwave-hydrothermal method without any synthetic surfactant. In the presence of LE, they observed HA nanorod was uniform size, very crystalline and well-defined in shape compared to control sample (without LE). This study proved that the plant extract as a template can contribute to regulate shape and size of nanoparticles (Ali et al. 2021).

A similar study by Kalaiselvi et al. was reported in 2018. They used moringa oleifera flower extract as a green template for the synthesis of HA nanorod by microwave assisted method. Synthesized HA nanorods in the presence of extract observed highly crystalline with a mean particle size of 41 nm with good antifungal properties (Kalaiselvi et al. 2018).

Kumar et al. prepared HA nanorods using curcuma longa tuber extract and eggshell waste as a calcium precursor. The prepared nanorods were magnesium and carbonate containing HA with strong antibacterial activity (Kumar et al. 2018). In their earlier study, they have reported the synthesis of pure HA nanorods with excellent antibacterial activity in the presence of Coccinia grandis and Azadirachta indica leaf extract as a solvent (Kumar et al. 2017).

Umesh et al. prepared HANPs using piper betel leaf extract by microwave conversion method with the help of chelating agent i.e., EDTA. The authors reported promising anti-bacterial and antibiofilm activity by green synthesized HA nanoparticles with crystallite size of 53-64 nm and cylindrical like shape (Umesh et al. 2021).

Ghate et al. reported the synthesis of HANPs using acacia falcata leaf extract. They observed aggregated needle shaped crystalline nanostructures with mean crystallite size of 55.04 nm from XRD and pore diameter of 25.7 nm from BET (Brunauer, Emmett, and Teller) analysis. This study reported the anti-cancerous potential of green plant based HANPs (Ghate et al. 2022).

2.4.2 Characterization techniques used for HANPs

For the characterization of HANPs, nanorods, and nano powder, various techniques has been used. These characterization techniques are mainly classified into sub-groups like spectroscopic and morphological behaviors (direct visualization) techniques. These techniques have their own advantages and limitations as given in table 2.1. X-ray diffraction (XRD), Fourier transform infrared (FTIR), and Raman spectroscopies have been regularly used to identify phase purity,

crystallinity, and chemical composition of HAp nanoparticles. XPS (X-ray photoelectron spectroscopy) is a surface sensitive quantitative analysis technique that provides elemental composition, and information about the chemical and electronic bond state and constitution within the material. EDX (Energy dispersive x-ray spectroscopy) is another very important technique which is used along with SEM (scanning electron microscopy) instrument. EDX technique provides peaks information appear due to the unique atomic structure such as Ca, P, and O of HAp which is appear at their characteristic positions. Morphological techniques (direct visualization) such as SEM, TEM (transmission electron microscopy), and atomic force microscopy (AFM) provide information about the morphology, size, shape, aggregation, and dispersion of the HAp nanoparticles.

Table 2.1. Advantages and limitations of the characterization techniques for hydroxyapatite nanoparticles (Haider et al. 2017).

Technique	Advantages	Limitations
Spectroscopy techniques		
XRD	Powerful and rapid technique, provide information like phase, crystallinity, data interpretation is relatively easy and straightforward	Homogeneous and single-phase materials are best for the identification, peak overlay may occur, worse for high angle reflections
EDS	This technique used in conjunction with SEM; provides chemical microanalysis of materials, unique peaks characteristic of the atomic structure of the atoms; quick and versatile technique	Comparatively lower precision
XPS	Provides unique information about the chemical composition of a material	Requires high vacuum, slow and poor spatial resolution
FTIR	Measures the intensity over a narrow range of wavelengths at a time; no external calibration is required; provides accurate results, and identifies even small concentrations of contaminants	Inorganic materials are not easily analyzed by FTIR spectroscopy
Raman Spectra	Highly specific technique	Very weak technique, requires

	provides a chemical fingerprint of the material; inorganic materials are easier to analyze	a sensitive and highly optimized instrument; fluorescence of the impurities can hide the Raman spectrum; intense laser radiation can destroy the sample
Morphological behavior (direct visualization technique)		
SEM	Direct visualization, high resolution	NP aggregation during the sample preparation
TEM	Direct visualization, high resolution	NP aggregation during the sample preparation, electron beam damage, preference for electron-dense atomic species
AFM	3D profile, high size resolution	Slow speed, limited scanning area

2.5 Main inorganic nanoparticles used as nano fillers in chitosan-based bionanocomposites

Mostly, metallic ions such as silver, copper, zinc, titanium, and their oxides have been added to chitosan matrix as a filler, dispersed inside the whole matrix to promote a desired physicochemical, mechanical and barrier and antimicrobial properties of chitosan for food packaging applications. Nano clay is another inorganic nanomaterial commonly used in food packaging.

Cao et al. studied biobased films, prepared using catechol- modified chitosan, silver nanoparticles, and gelatin. They reported that the addition of silver nanoparticles and gelatin significantly improved the tensile strength and water vapor properties of the films. The prepared films exhibited antibacterial activities against the *E. coli and S. aureus* (Cao et al. 2020).

Priyadarshi and Negi prepared nanocomposites using zinc oxide nanoparticles incorporated into the chitosan matrix. The resultant films showed substantial increase in mechanical properties as shown in fig. 2.7 and substantial decrease in water vapor transmission rate (WVTR) due to nanoparticles reinforcing effect. The films also showed strong antimicrobial properties against the *B. subtilis* and *E. coli* because of zinc oxide and chitosan (Priyadarshi and Negi 2017).

Similar, study has been reported by Rodrigues et al. They incorporated zinc oxide (ZnO) nanoparticles and modified clay nanoparticles into the chitosan matrix in different concentrations to evaluate mechanical and antimicrobial properties. They reported the best mechanical properties were achieved by the addition of 3 % clay and 8% ZnO nanoparticles into the chitosan. The synergistic effect of antibacterial activities was also observed between chitosan and ZnO (Rodrigues et al. 2020).

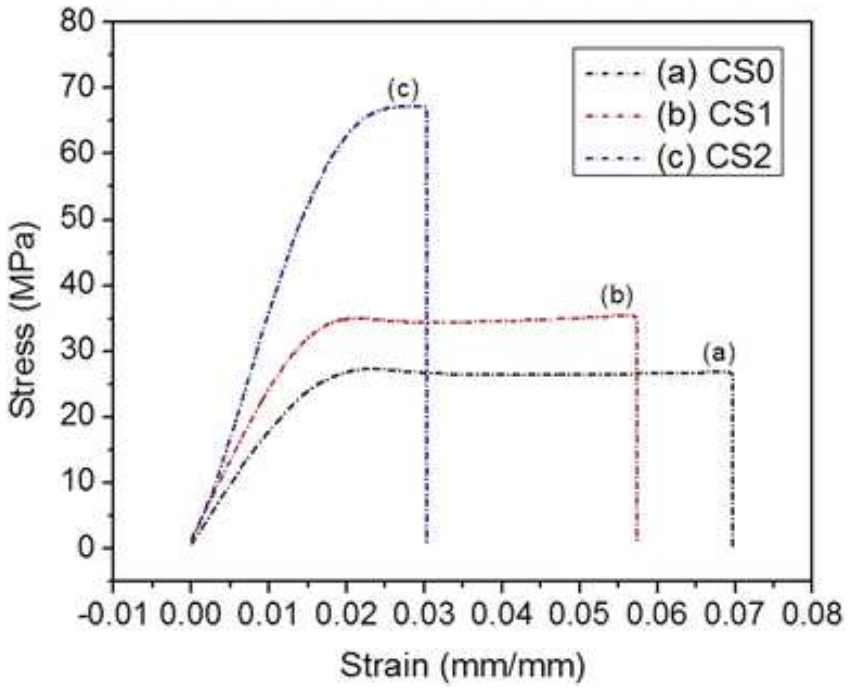

Figure 2.7 Stress Vs. Strain curve of neat chitosan (a), chitosan films with 1 % (b) and 2 % (c) zinc oxide nanoparticles concentration { Reproduced with permission by Springer Nature: Effect of Varying Filler Concentration on Zinc Oxide Nanoparticle Embedded Chitosan Films as Potential Food Packaging Material (Priyadarshi and Negi 2017)}

Mallakpour and Madani fabricated bio nanocomposite using modified titanium dioxide nanoparticles reinforced with chitosan biopolymer. The resultant bio nanocomposite films were substantially enhanced the thermal and mechanical properties compared to pure chitosan film (Mallakpour and Madani 2015).

Gasti et al. developed nanocomposite using chitosan-zinc oxide nanoparticle and obtained enhanced tensile strength and water vapor barrier properties approximately 39.82% and 84.64%, respectively (Gasti et al. 2022).

Li et al. prepared chitosan films incorporated by silver nanoparticles/curcumin/clay minerals. Compared to pure chitosan film, the tensile strength and elongation of nanocomposite films increased by 15.9 MPa and 27.27 % respectively. They also confirmed that the inactivation rate reached 100% of the nanocomposites against *Escherichia coli* and *Staphylococcus aureus* (Li et al. 2022).

2.6 HANPs used as nano fillers in bionanocomposites

Recent years, HANPs have attracted much attention as a nanofillers for the biopolymer matrix for food packaging applications. Several methods have been reported for the fabrication of bionanocomposites (refer to fig. 2.8).

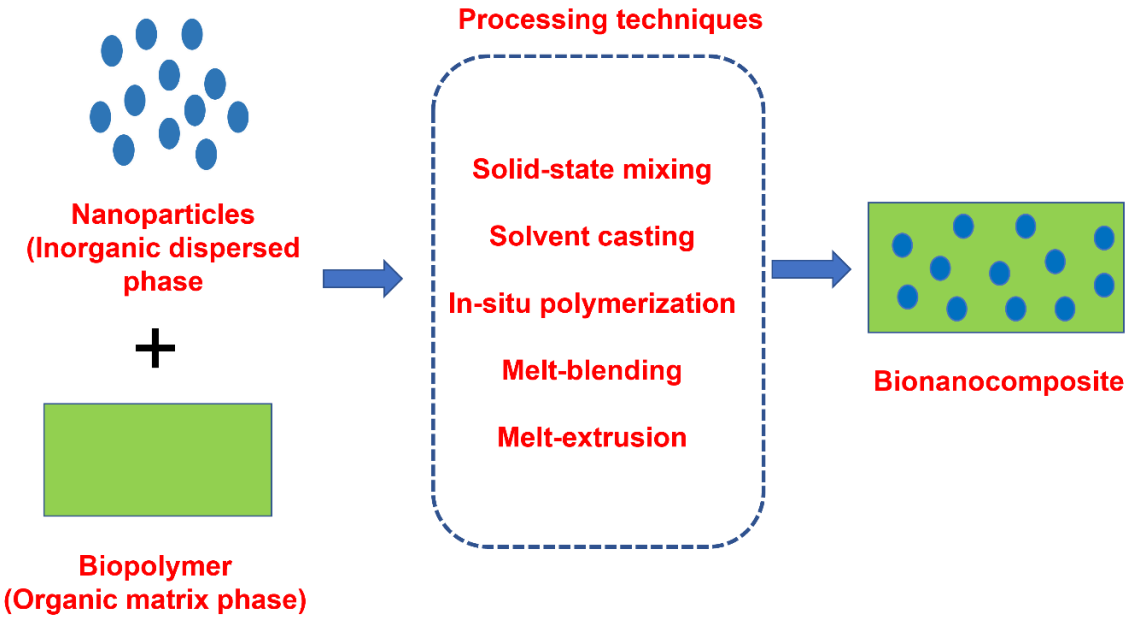

Figure 2.8 Common methods used for the fabrication of the bionanocomposites {Modified and adopted from (Sinha Ray 2012)}

Rahman et al. developed inexpensive green nanocomposite using soy protein isolate (SPI) incorporated HANPs derived from eggshell (nEHA) using different concentration (0 to 10%). They observed that increase in (nEHA) concentrations of 3% and 5% in SPI films showed an increased in tensile strength and young modulus as compared to pure SPI as shown in table 2.2 (Rahman et al. 2016).

Table 2.2 Tensile properties of SPI and SPI-nEHA nanocomposites films {Reproduced with permission by John Wiley and Sons: Bio-inspired "green" nanocomposite using hydroxyapatite synthesized from eggshell waste and soy protein (Rahman et al. 2016)}

Specimen films	Young's modulus (MPa)	Tensile strength (MPa)
SPI	923 ± 127^{a}	25 ± 2.5^{a}
SPI-nEHA3	1486 ± 135^{b}	35 ± 3.5^{b}
SPI-nEHA5	1737 ± 192^{b}	41 ± 3.5^{c}
SPI-nEHA10	2147 ± 207^{c}	38 ± 2.8^{bc}

Means not connected by same letter superscripts are significantly different at 95% confidence level through Tukey-Kramer HSD test.

Recently, Hadi et al. prepared starch-based nanocomposite films with addition of HANPs as a mineral filler. Various concentrations (0 to 20%) of HANPs were incorporated into the starch. The prepared films were labeled followed by concentration of HANPs (0 to 20%), i.e., FH0, FH3, FH5, FH15, FH20. They reported that the addition of 15% wt% addition of HANPs film could enhance the tensile strength and elongation at break of 3.03 MPa and 37.41%, respectively (Table 2.3) (Hadi et al. 2022).

Table 2.3 Effect of HANPs concentration on the mechanical properties of films {Modified and adopted from (Hadi et al. 2022)}

Sample	Thickness (mm)	Elongation at break (%)	Tensile strength (MPa)	Toughness ($MPa.m^{1/2}$)
FH0	0.40	31.57	1.21	21.78
FH3	0.41	28.50	1.49	22.25
FH5	0.41	23.37	1.54	28.54
FH15	0.43	37.41	3.03	65.09
FH20	0.45	28.83	2.50	45.99

2.7 Film properties

The surface morphology of the films is generally accessed by SEM, and TEM through particle size and its distribution in the matrix, surface smoothness and texture of films. Mechanical properties and water vapor permeability of bionanocomposites films are the main important parameters for the food packaging applications.

2.7.1 Mechanical properties

Mechanical properties are very important for food packaging application because of their use during storage, handling, transportation, processing, and distribution. Therefore, it is important to study mechanical properties of packaging films. Tensile strength (TS), elongation at break (ES) and elastic modulus are the essential mechanical properties of packaging films. For the food packaging films, it is crucial to maintain the mechanical handling during the transportation (Rhim and Lee 2004). Tensile strength is measured in MPa, and it is expressed by maximum

stress handled before film break. Elongation at break is measured in %, where film shows maximum stretch before break. The mechanical properties highly depend on the intra and inter molecular interaction between matrix and nanofillers. Chitosan based bionanocomposites films mechanical properties mostly results of hydrogen bonding/ ionic interaction/ van der Waals forces (Reddy and Rhim 2014). Many studies proved that nanoparticles dispersion and interaction with matrix play an important role in the enhancements of mechanical properties. Table 2.4 shows some of the chitosan-based bio nanocomposites reinforced with inorganic nanofillers.

Table 2.4 Mechanical properties of chitosan-based bionanocomposites

System/Formulation	Incorporation Method	Tensile Strength (Relatively to control)	Elongation at Break (Relatively to Control)	References
chitosan + TiO_2	Mechanical stirring and ultrasonic homogenizer	5%: Increased ~ 40% 10% TiO_2: Increased ~ 63% 15% TiO_2: Increased ~ 100%	5% TiO_2: Increased ~ 35% 10% TiO_2: Decreased ~ 6% 15% TiO_2: Decreased ~ 10%	(Mallakpour and Madani 2015)
chitosan + ZnO	Mechanical stirring	1% ZnO: Increased ~ 32% 2% ZnO: Increased ~ 67%	1% ZnO: Decreased ~ 18% 2% ZnO: Decreased ~ 57%	(Priyadarshi and Negi 2017)
Chitosan (Glycerol 30% (*w*/*w*) of chitosan + Clay nanoparticles (MMTNPs)	Mechanical stirring and ultrasonic homogenizer	0.5% MMTNPs: Decreased ~ 75% 1% MMTNPs: Decreased ~ 57%	0.5% MMTNPs: Increased ~ 20% 1%MMTNPs: Increased ~ 23%	(Llanos and Tadini 2018)

2.7.2 Water vapor permeability (WVP)

Barrier properties such as (moisture, carbon dioxide and oxygen) are another very important parameters affecting the food packaging materials properties. These are the parameters for maintaining food quality and extending the food shelf life. In the food packaging, preservation and safety of the food are the key elements. Moisture plays crucial role for microbial spoilage

and preservation of the texture of the food (Grossman and Nwabunma 2013). In general, chitosan based bionanocomposites, the hydrophilic group of chitosan favor moisture transportation than carbon dioxide and oxygen permeability. The barrier properties of chitosan based bionanocomposites depend on the number of factors such as degree of deacetylation of chitosan, plasticizer, and nanoparticles. Especially, nanoparticles size, shape and their distribution in the matrix are very important to get desired barrier properties. Therefore, a number of researchers studied using different nanoparticles and various concentrations to enhance chitosan barrier properties.

Sanuja et al. studied chitosan film incorporated with different concentration of zinc oxide nanoparticles (0.1, 0.3, and 0.5 %) to evaluate water vapor permeability (WVP) of the film. They observed the decreased of WVP with the increment of the concentration of nanoparticles which is up to 56 % lower than the control chitosan films (Sanuja et al. 2015).

Another similar study was reported by Motelica et al. where they observed that zinc oxide and silver nanoparticles enhanced the barrier properties of the chitosan films (Motelica et al. 2020).

References

Ali, A.F., Alrowaili, Z.A., El-Giar, E.M., Ahmed, M.M. and El-Kady, A.M. (2021) Novel green synthesis of hydroxyapatite uniform nanorods via microwave-hydrothermal route using licorice root extract as template. Ceramics International 47(3), 3928-3937.

Arora, B., Bhatia, R. and Attri, P. (2018) New Polymer Nanocomposites for Environmental Remediation. Hussain, C.M. and Mishra, A.K. (eds), pp. 699-712, Elsevier.

Bouyer, E., Gitzhofer, F. and Boulos, M. (2000) Morphological study of hydroxyapatite nanocrystal suspension. Journal of Materials Science: Materials in Medicine 11(8), 523-531.

Cao, W., Yan, J., Liu, C., Zhang, J., Wang, H., Gao, X., Yan, H., Niu, B. and Li, W. (2020) Preparation and characterization of catechol-grafted chitosan/gelatin/modified chitosan-AgNP blend films. Carbohydrate Polymers 247, 116643.

Clarinval, A.-M. and Halleux, J. (2005) Biodegradable polymers for industrial applications, pp. 3-31, Elsevier.

Dasgupta, S., Tarafder, S., Bandyopadhyay, A. and Bose, S. (2013) Effect of grain size on mechanical, surface and biological properties of microwave sintered hydroxyapatite. Materials Science and Engineering: C 33(5), 2846-2854.

Dash, K.K., Deka, P., Bangar, S.P., Chaudhary, V., Trif, M. and Rusu, A. (2022) Applications of Inorganic Nanoparticles in Food Packaging: A Comprehensive Review. Polymers 14(3), 521.

Fiume, E., Magnaterra, G., Rahdar, A., Verné, E. and Baino, F. (2021) Hydroxyapatite for Biomedical Applications: A Short Overview. Ceramics 4(4), 542-563.

Gasti, T., Dixit, S., Hiremani, V.D., Chougale, R.B., Masti, S.P., Vootla, S.K. and Mudigoudra, B.S. (2022) Chitosan/pullulan based films incorporated with clove essential oil loaded chitosan-ZnO hybrid nanoparticles for active food packaging. Carbohydrate Polymers 277, 118866.

Ghate, P., Prabhu S, D., Murugesan, G., Goveas, L.C., Varadavenkatesan, T., Vinayagam, R., Lan Chi, N.T., Pugazhendhi, A. and Selvaraj, R. (2022) Synthesis of hydroxyapatite

nanoparticles using Acacia falcata leaf extract and study of their anti-cancerous activity against cancerous mammalian cell lines. Environmental Research 214, 113917.

Gopi, D., Kanimozhi, K., Bhuvaneshwari, N., Indira, J. and Kavitha, L. (2014) Novel banana peel pectin mediated green route for the synthesis of hydroxyapatite nanoparticles and their spectral characterization. Spectrochimica Acta Part A: Molecular and Biomolecular Spectroscopy 118, 589-597.

Grossman, R.F. and Nwabunma, D. (2013) Biopolymer nanocomposites: processing, properties, and applications, John Wiley & Sons.

Hadi, Z., Hekmat, N. and Soltanolkottabi, F. (2022) Effect of hydroxyapatite on physical, mechanical, and morphological properties of starch-based bio-nanocomposite films. Composites and Advanced Materials 31, 26349833221087755.

Haider, A., Haider, S., Han, S.S. and Kang, I.-K. (2017) Recent advances in the synthesis, functionalization and biomedical applications of hydroxyapatite: a review. RSC Advances 7(13), 7442-7458.

Han, J.-K., Song, H.-Y., Saito, F. and Lee, B.-T. (2006) Synthesis of high purity nano-sized hydroxyapatite powder by microwave-hydrothermal method. Materials chemistry and physics 99(2-3), 235-239.

Kalaiselvi, V., Mathammal, R., Vijayakumar, S. and Vaseeharan, B. (2018) Microwave assisted green synthesis of Hydroxyapatite nanorods using Moringa oleifera flower extract and its antimicrobial applications. International Journal of Veterinary Science and Medicine 6(2), 286-295.

Kong, L., Ma, J. and Boey, F. (2002) Nanosized hydroxyapatite powders derived from coprecipitation process. Journal of materials science 37, 1131-1134.

Kumar, G.S., Muthu, D., Karunakaran, G., Karthi, S., Girija, E.K. and Kuznetsov, D. (2018) Curcuma longa tuber extract mediated synthesis of hydroxyapatite nanorods using biowaste as a calcium source for the treatment of bone infections. Journal of Sol-Gel Science and Technology

86(3), 610-616.

Kumar, G.S., Thamizhavel, A. and Girija, E. (2012) Microwave conversion of eggshells into flower-like hydroxyapatite nanostructure for biomedical applications. Materials Letters 76, 198-200.

Li, B., Guo, B., Fan, H. and Zhang, X. (2008) Preparation of nano-hydroxyapatite particles with different morphology and their response to highly malignant melanoma cells in vitro. Applied Surface Science 255(2), 357-360.

Li, L., Iqbal, J., Zhu, Y., Zhang, P., Chen, W., Bhatnagar, A. and Du, Y. (2018) Chitosan/Ag-hydroxyapatite nanocomposite beads as a potential adsorbent for the efficient removal of toxic aquatic pollutants. International Journal of Biological Macromolecules 120, 1752-1759.

Li, S., Mu, B., Zhang, H., Kang, Y. and Wang, A. (2022) Incorporation of silver nanoparticles/curcumin/clay minerals into chitosan film for enhancing mechanical properties, antioxidant and antibacterial activity. International Journal of Biological Macromolecules 223, 779-789.

Llanos, J.H. and Tadini, C.C. (2018) Preparation and characterization of bio-nanocomposite films based on cassava starch or chitosan, reinforced with montmorillonite or bamboo nanofibers. International Journal of Biological Macromolecules 107, 371-382.

Lu, Y., Dong, W., Ding, J., Wang, W. and Wang, A. (2019) Nanomaterials from Clay Minerals. Wang, A. and Wang, W. (eds), pp. 485-536, Elsevier.

Mallakpour, S. and Madani, M. (2015) Effect of Functionalized TiO2 on Mechanical, Thermal and Swelling Properties of Chitosan-Based Nanocomposite Films. Polymer-Plastics Technology and Engineering 54(10), 1035-1042.

Motelica, L., Ficai, D., Ficai, A., Truşcă, R.-D., Ilie, C.-I., Oprea, O.-C. and Andronescu, E. (2020) Innovative antimicrobial chitosan/ZnO/Ag NPs/citronella essential oil nanocomposite—Potential coating for grapes. Foods 9(12), 1801.

Nazeer, M.A., Yilgör, E. and Yilgör, I. (2017) Intercalated chitosan/hydroxyapatite nanocomposites: promising materials for bone tissue engineering applications. Carbohydrate Polymers 175, 38-46.

Pandey, J.K., Kumar, A.P., Misra, M., Mohanty, A.K., Drzal, L.T. and Palsingh, R. (2005) Recent advances in biodegradable nanocomposites. Journal of nanoscience and nanotechnology 5(4), 497-526.

Priyadarshi, R. and Negi, Y.S. (2017) Effect of varying filler concentration on zinc oxide nanoparticle embedded chitosan films as potential food packaging material. Journal of Polymers and the Environment 25, 1087-1098.

Priyadarshi, R. and Rhim, J.-W. (2020) Chitosan-based biodegradable functional films for food packaging applications. Innovative Food Science & Emerging Technologies 62, 102346.

Rahman, M.M., Netravali, A.N., Tiimob, B.J., Apalangya, V. and Rangari, V.K. (2016) Bio-inspired “green” nanocomposite using hydroxyapatite synthesized from eggshell waste and soy protein. Journal of Applied Polymer Science 133(22).

Reddy, J.P. and Rhim, J.-W. (2014) Characterization of bionanocomposite films prepared with agar and paper-mulberry pulp nanocellulose. Carbohydrate Polymers 110, 480-488.

Rhim, J.-W. and Lee, J.-H. (2004) Effect of $CaCl_2$ Treatment on Mechanical and Moisture Barrier Properties of Sodium Alginate and Soy Protein-based Films. Food Science and Biotechnology 13(6), 728-732.

Rhim, J.-W., Park, H.-M. and Ha, C.-S. (2013) Bio-nanocomposites for food packaging applications. Progress in Polymer Science 38(10), 1629-1652.

Rodrigues, C., de Mello, J.M.M., Dalcanton, F., Macuvele, D.L.P., Padoin, N., Fiori, M.A., Soares, C. and Riella, H.G. (2020) Mechanical, thermal and antimicrobial properties of chitosan-based-nanocomposite with potential applications for food packaging. Journal of Polymers and the Environment 28, 1216-1236.

Rodríguez-Lugo, V., Karthik, T., Mendoza-Anaya, D., Rubio-Rosas, E., Villaseñor Cerón, L., Reyes-Valderrama, M. and Salinas-Rodríguez, E. (2018) Wet chemical synthesis of nanocrystalline hydroxyapatite flakes: effect of pH and sintering temperature on structural and morphological properties. Royal Society open science 5(8), 180962.

Ruiz-Hitzky, E., Darder, M. and Aranda, P. (2005) Functional biopolymer nanocomposites based on layered solids. Journal of Materials Chemistry 15(35-36), 3650-3662.

Sanuja, S., Agalya, A. and Umapathy, M.J. (2015) Synthesis and characterization of zinc oxide–neem oil–chitosan bionanocomposite for food packaging application. International Journal of Biological Macromolecules 74, 76-84.

Silva, A.O., Cunha, R.S., Hotza, D. and Machado, R.A.F. (2021) Chitosan as a matrix of nanocomposites: A review on nanostructures, processes, properties, and applications. Carbohydrate Polymers 272, 118472.

Sinha Ray, S. (2012) Polylactide-Based Bionanocomposites: A Promising Class of Hybrid Materials. Accounts of Chemical Research 45(10), 1710-1720.

Spirescu, V.A., Chircov, C., Grumezescu, A.M., Vasile, B.Ș. and Andronescu, E. (2021) Inorganic Nanoparticles and Composite Films for Antimicrobial Therapies. International journal of molecular sciences 22(9), 4595.

Umesh, M., Choudhury, D.D., Shanmugam, S., Ganesan, S., Alsehli, M., Elfasakhany, A. and Pugazhendhi, A. (2021) Eggshells biowaste for hydroxyapatite green synthesis using extract piper betel leaf - Evaluation of antibacterial and antibiofilm activity. Environmental Research 200, 111493.

Wu, S.-C., Hsu, H.-C., Hsu, S.-K., Chang, Y.-C. and Ho, W.-F. (2016) Synthesis of hydroxyapatite from eggshell powders through ball milling and heat treatment. Journal of Asian Ceramic Societies 4(1), 85-90.

Zanotto, A., Saladino, M.L., Martino, D.C. and Caponetti, E. (2012) Influence of temperature on calcium hydroxyapatite nanopowders.

Zhang, H. and Darvell, B.W. (2010) Synthesis and characterization of hydroxyapatite whiskers by hydrothermal homogeneous precipitation using acetamide. Acta Biomaterialia 6(8), 3216-3222.

Zhang, Y. and Lu, J. (2007) A simple method to tailor spherical nanocrystal hydroxyapatite at low temperature. Journal of Nanoparticle Research 9(4), 589-594.

Zou, Z., Ismail, B.B., Zhang, X., Yang, Z., Liu, D. and Guo, M. (2023) Improving barrier and antibacterial properties of chitosan composite films by incorporating lignin nanoparticles and acylated soy protein isolate nanogel. Food Hydrocolloids 134, 108091.

CHAPTER 3. FACILE SYNTHESIS OF HYDROXYAPATITE NANOPARTICLES FROM EGGSHELL BIOWASTE VIA MICROWAVE-ASSISTED PRECIPITATION USING AZADIRACHTA INDICA EXTRACT AS A GREEN TEMPLATE

3.1 Introduction

Hydroxyapatite (HAp) is an inorganic mineral with the chemical formula $Ca_{10}(PO_4)_6(OH)_2$. It is one of the important family members of calcium phosphate (CaP) salt with Ca/P ratio of 1.67. HAp is chemically very similar to the naturally occurring main mineral component found in human bones, and teeth (Chesley et al. 2020, Fathi et al. 2008, Sawada et al. 2021, Teixeira et al. 2009, Wu et al. 2016).

In recent years, hydroxyapatite nanoparticles (HANPs) have gained a lot of interest because of their use in various biomedical and industrial applications due to their outstanding bioactivity, biocompatibility, and osteoconductive properties (Goh et al. 2021, Karakas et al. 2013, Karakas Aydınoğlu et al. 2012). Moreover, HANPs are also used for the removal of heavy metals from wastewater (Meski et al. 2010, Zhou et al. 2021), soil remediation (Gan et al. 2021), catalyst (Usami and Okamoto 2017), column chromatography (Ashokan et al. 2021, Markov and Ivanov 1974), and food packaging applications (Malvano et al. 2021, Malvano et al. 2022).

The applications of HANPs are significantly influenced by particle size, shape, phase purity, crystallinity, morphology, and composition of nano-hydroxyapatite, which also depend on the synthesis precursors, synthesis route, and processing parameters (Dasgupta et al. 2013, Wu et al. 2016). Therefore, there is still a great demand for developing simple, efficient, environmentally friendly, and rapid methods for the synthesis of HANPs.

Although numerous methods have been used for the synthesis of HANPs including wet precipitation (Cengiz et al. 2008, Viswanath and Ravishankar 2008, Wang et al. 2010),

hydrothermal (Lin et al. 2021, Zhang and Darvell 2010), sonochemical synthesis (Brundavanam et al. 2011, Yan et al. 2018, Zhou et al. 2020) sol-gel (Negrila et al. 2018, Phatai et al. 2019, Rajabi-Zamani et al. 2008), micro-emulsion (Bose and Saha 2003, Jemli et al. 2022, Ye et al. 2010), protein templated (Han et al. 2007b), membrane-templated (Neelakandeswari et al. 2011) and microwave-assisted (Goh et al. 2021, Han et al. 2006, Kumar et al. 2012, Yao et al. 2020). Most of these methods require high temperatures and/or longer times to produce uniform sized, pure HANPs. The microwave irradiation method is proven to accelerate the reaction kinetics in a shorter time with lesser temperature when compared to conventional heating method (Herrero and Ullah 2021, Ullah and Arshad 2017) (Goh et al. 2021, Indira and Malathi 2022, Kumar et al. 2012). Microwave-assisted precipitation is popular in the researcher because of its simplicity, time sever, economical and high yield (Hassan et al. 2016).

The materials used for synthesizing of HANPs can be obtained from synthetic or natural sources. Currently, naturally occurring bio sources are used for the synthesis of HAp with enhanced properties such as bioactivity and biocompatibility include eggshells, bovine bone, corals, seashells, snail shells, mussel shells, and fish scales (Agalya et al. 2021, Athinarayanan et al. 2020, Kumar et al. 2015, Ooi et al. 2007).

Among all these natural biomaterials, eggshells are an excellent source of calcium precursor for the synthesis of the HANPs. Several million tons of eggshells are generated as a bio-waste from food industry worldwide on daily basis. They are usually landfilled which creates huge environmental pollution (Kumar and Girija 2013, Wu et al. 2015). Eggshell, which is mainly composed of 94% calcium carbonate (calcite) which represents about 11% of the total weight of the egg, along with some other components including 4% organic substances, 1% calcium phosphate, and 1% magnesium carbonate (Kamalanathan et al. 2014, Siva Rama Krishna et al.

2007). Eggshell is readily available, economical, and rich in calcium carbonate which makes it an excellent calcium source for deriving HANPs (Kumar and Girija 2013, Kumar et al. 2012).

In recent years, nanotechnology has been largely utilized for the synthesis of nanomaterials with natural material sources. Currently, green synthesis of nanoparticles using plant leaf extracts has become a very popular method because plant extracts act as a stabilizers and reducers and greatly contribute to control the shape and size of the nanoparticles. Plant extracts are proven to be good alternative to typical chemicals used to control the aggregation during the process. Plant extracts are rich in phytochemicals with antioxidant and anti-inflammatory properties. Therefore, it helps to regulate morphology and reduce the size (Alorku et al. 2020, Irwansyah et al. 2022). Recently, several researchers have reported the synthesis of uniformed size nano-hydroxyapatite using plant extract as a template (Ali et al. 2021, Ghate et al. 2022, Gopi et al. 2015, Gopi et al. 2014, Kalaiselvi et al. 2018, Kumar et al. 2018, Kumar et al. 2017, Umesh et al. 2021, Varadarajan et al. 2020).

Azadirachta Indica (AI) is a tree that belongs to the Meliaceae family and is also known as the neem/nim tree, or Indian lilac. It is mostly found in the Indian subcontinent and some regions in Africa. Their leaf, fruit, and seeds are used for traditional medicine from ancient times against bacterial, viral, and fungal infections because it is a rich source of antioxidant (Alzohairy 2016).

To the best of our knowledge, there is no scientific report on the green synthesis of HANPs through the microwave-assisted precipitation method using AI leaf extract as a template from a biowaste eggshell.

The present work compared the synthesis of HANPs using microwave-assisted and conventional heating precipitation method with and without green AI template. Extensive characterization of the prepared HANPs in terms of structural, morphological, and thermal properties was carried

out.

3.2 Materials and methods

3.2.1 Materials

The analytical grade chemicals, orthophosphoric acid (H_3PO_4) (85%), nitric acid (HNO_3) (68%), sodium hydroxide (NaOH) (96%), and ethanol were purchased from Sigma-Aldrich and further used as received. Distilled water was used to make a stock solution of calcium and phosphate precursors.

3.2.2 Pre-treatment of waste eggshell

Chicken eggshells were collected from the local restaurant, in Edmonton, Canada. The collected eggshells were washed several times with distilled water and heated around 100 ℃ for 3 hours to remove the surface impurities and thin inner layer membrane from the eggshell. After that, the eggshells were dried at 80 °C overnight in the oven and were ground into a fine powder using a coffee grinder and finally stored in a glass bottle for further use. Then this pretreated eggshell powder was used for the synthesis of HANPs with the convectional heating method and microwave-assisted conversion method (Kumar et al. 2012).

3.2.3 Template preparation (Azadirachta Indica Extract)

Azadirachta Indica (AI) was purchased from the local supermarket store in Edmonton, AB and washed several times with distilled water, dried them at room temperature for two days, and then the separated leaves were ground using a coffee grinder. For the preparation of template leaf extract using crude method, 50 g fine powder of AI was taken into the beaker with 500 mL deionized water followed by heating at 60 ℃ for 2 hours. The solution was then cooled, filtered using Whatman No.1 filter paper and stored at 4 ℃ in the fridge for further use. This extract was used to prepare phosphorus precursor (orthophosphoric acid) solutions for further use as a

template for green synthesis.

3.2.4 Synthesis of HANPs from eggshell

Calcium precursor (calcium nitrate) was obtained by slowly adding concentrated HNO_3 (100 ml) into the eggshell powder (ES) (10 gm) with vigorous stirring using a magnetic stirrer at 1100 rpm for 30 minutes. And then pH was adjusted to 10 using 1M NaOH to form calcium hydroxide. Then resultant solution mixture, 50 ml was taken into the beaker and 50 ml of phosphate precursor, 0.6M orthophosphoric acid (50 ml) was added dropwise with continuous stirring at 700 rpm for 20 minutes. The pH of the resultant mixture was adjusted at 10 by adding 1M NaOH with continuous stirring. The white nano hydroxyapatite powders were separated from the reaction mixture by two different methods. First, the solution mixture was subjected to microwave irradiation using an open vessel reflux mode microwave reactor (CEM-Discover reactor unit, 120 V, Matthews, USA) for 15 minutes at 40 ℃ using 250 watts. The reaction mixture was centrifuged and washed three times with distilled water and ethanol. Settled powder was dried in the oven at 100 ℃ for 24 hours. The final dried powder was calcinated using a furnace at 600 ℃ for 3 hours with a heating rate of 10 ℃/minute (herein named as HAp 01).

In the second method, conventional heating was used. The reaction mixture was kept on stirring at 700 rpm on a hotplate at 40 ℃ for 3 hours and kept overnight to get white precipitation. The solution mixture was centrifuged, washed, dried, and calcined using same approaches as described above for microwave-assisted method. Herein, these HANPs precipitates were named HAp 02. The entire expected mechanism reaction is shown in the following equation (1-3).

$$CaCO_3 + 2HNO_3 \rightarrow Ca\,(NO_3)_2 + CO_2 + H_2O \quad (1)$$

$$Ca\,(NO_3)_2 + 2NaOH \rightarrow Ca\,(OH)_2 + 2NaNO_3 \quad (2)$$

$$10\ Ca\,(OH)_{2(aq)} + 6\ H_3PO_{4(aq)} \rightarrow Ca_{10}\,(PO_4)_6(OH)_{2(S)} + 18\ H_2O_{(aq)} \quad (3)$$

For the green template assisted synthesis of HANPs, phosphate precursor (0.6M H_3PO_4) was prepared using AI extract as a template and the synthesis was carried out using similar approaches as mentioned above for the synthesis of HAp 01 and HAp 02. The AI templated nanoparticles were described as HAp 03 by microwave method and HAp 04 using convectional heating method. The steps involved in the preparation of nanoparticles are shown in fig. 3.1. For the reaction method different parameters used in synthesis are shown in table 3.1.

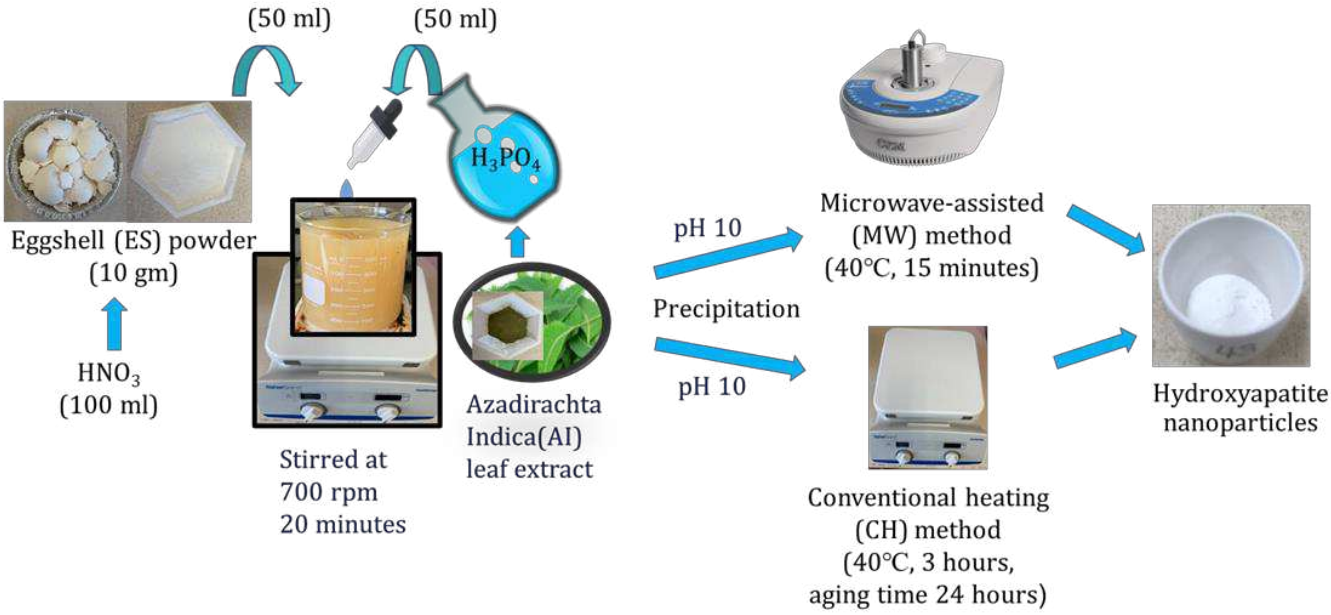

Figure 3.1 Synthesis of HANPs

Table 3.1. Reaction method parameters used for the synthesis of HANPs

Sample code	Method	Reaction Temperature (°C)	Time	Aging Time	Calcinate Temperature (°C)	Template
HAp-01	Microwave	40	15 minutes	0 minute	600	-
HAp-02	Convectional	40	3 hours	24 hours	600	-
HAp-03	Microwave	40	15 minutes	0 minute	600	Azadirachta Indica
HAp-04	Convectional	40	3 hours	24 hours	600	Azadirachta Indica

3.3 Characterization of synthesized HANPs

3.3.1 Crystallinity and phase composition: X-ray diffraction (XRD)

The phase purity, composition, and crystallinity of prepared hydroxyapatite nanoparticles were obtained by using the Rigaku Ultima IV X-Ray Diffractometer (XRD) using a Cobalt radiation source ($K\alpha_1$) λ= 1.78900 Å with an operating voltage of 38 kV and 38 mA current having a scanning range of 2θ was 5–90° with continuous scanning rate used of 2 degree per minute with a step size of 0.02. Phase identification was determined using DIFFRAC.EVA software with the 2020 ICDD PDF 4+ and PDF 4+/Organics databases.

The average crystallite size (τ) of the HANPs was calculated using the Debye-Sherrer equation from the XRD pattern (Gopi et al. 2013, Gopi et al. 2009, Pang and Bao 2003, Zhou et al. 2012).

$$\text{Crystallite size } (\tau) = K\lambda/B\tau\cos\theta$$

where, K is the Sherrer's constant, which is taken at 0.89, λ is the wavelength of the CoKα_1, B_τ is the full width at the half maximum and θ is the diffraction angle. The degree of crystallinity of all the HANPs samples were calculated based on the XRD data using JADE 9.6 software (Shi et al. 2021) using the following calculation:

$$\text{Degree of Crystallinity (\%)} = (\text{Area of the crystalline peaks/ Total ara of peaks}) \times 100$$

3.3.2 Functional Groups: Fourier transform infrared (FTIR) Spectroscopy

Structural analyses of HANPs were carried out using ATR-FTIR (Bruker Alpha Optics, Platinum ATR, Esslingen Germany) with a single bounce ATR crystal diamond. The FTIR spectra were performed within the wavelength range of 400-4000 cm^{-1}. A background spectrum of the clean diamond ATR crystal was taken before running the samples.

3.3.3 Vibrational modes: Raman Spectroscopy

Raman Spectroscopy analyses were perform using Renishaw inVia Qontor Confocal Raman Microscope with minimum stage step of 50 nm and 20X objective, spatial and axial resolution better than 300 nm and 2 μm respectively. Samples were taken in powder.

3.3.4 Morphology and topography: Scanning Electron Microscopy (SEM)

The morphology of the HANPs was determined by Scanning Electron Microscopy (SEM), Zeiss Sigma 300 VP FESEM operated at 20 kV with a resolution of 10 nm. All the samples were prepared by dispersing HANPs powder onto the adhesive surface of the stub. All the samples were coated with gold or carbon layer using Leica EM SCD005 (Anatech Ltd.) sputter coater before analyses.

3.3.5 Microstructure Morphology: Transmission Electron Microscopy (TEM)

TEM analysis was carried out using Philips/FEI Morgagni 268 (Hillsboro, USA) with Gatan digital CCD camera. TEM instrument was operated at accelerating voltage of 80 kV. HANPs were dispersed in ethanol, and then the droplet of sample placed on a TEM grid (Ted Pella

cat#01753-F) was then stained with 4% uranyl acetate before analyses.

3.3.6 Elemental Composition: Energy Dispersive X-Ray Spectroscopy (EDX)

Elemental composition and Ca/P ratio of HANPs was determined by Zeiss Sigma 300 VP-FESEM equipped with the Bruker EDX system containing drift dual silicon detectors with resolution of 123eV and area of 60 mm^2 for each detector. Samples were placed on the surface of stub followed by the carbon coating.

3.3.7 Surface elemental composition: X-ray Photoelectron Spectroscopy (XPS)

The surface elemental composition of the HANPs was analyzed using XPS. All the samples in powder form were analyzed by ultra spectrometer, Kratos Analytical (UK). X-ray source used was Al Kα. In the analytical chamber, basic pressure was less than 3×10^{-8} Pa and electron gun operated at 150W. The spectra for survey scans were recorded at 160eV pass-energy. For data processing the Vision-2 instrument software was used. The 284.8 eV binding energy for C 1S was set for the calibration of the spectrometer. Elemental compositions were achieved from the XPS spectra using the instrument database with the linear background and sensitivity factors.

3.3.8 Thermal Analysis: Thermogravimetric Analysis (TGA)

The thermal stability of Hydroxyapatite nanoparticles after synthesis were determined by thermogravimetric analysis TGA Q50 apparatus (TA Instruments, USA) with a heating rate of 10 ℃ /min under nitrogen flow and the temperature range between 25 and 700 ℃. Sample size was taken between 8-12 mg.

3.4 Results and discussion

3.4.1 X-Ray Diffraction (XRD) Spectroscopy

X-ray diffraction was used for the determination of the crystalline structure of the particular components in the material and to identify the structure and structural parameters such as crystalline phase, crystallite size and preferred orientation by using the intensity and diffraction

angle of the beam (Bunaciu et al. 2015).

Fig. 3.2 exhibited the x-ray diffraction pattern of all the synthesized HANPs derived from eggshells using microwave assisted and conventional precipitation methods with and without template AI. It was observed that the HANPs had a pure hexagonal crystalline phase (as shown in Fig. 3.2) that well matched with recorded data of the standard ICDD-PDF (International Centre for Diffraction Data powder diffraction File) # 00-009-0432 and no other impurities were detected such as other phases of calcium phosphate.

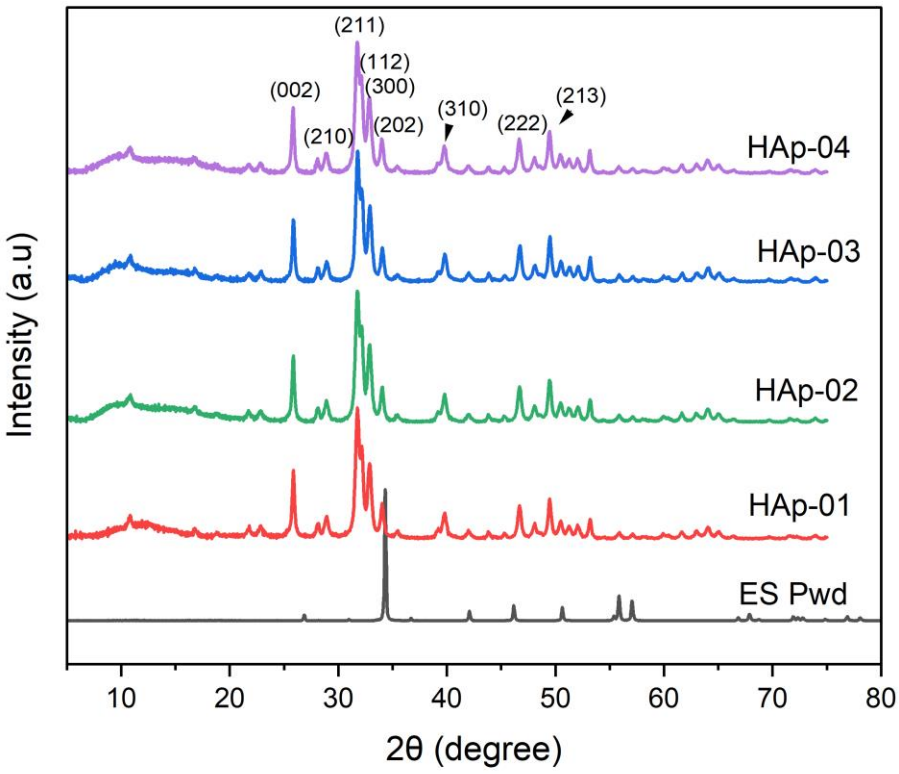

Figure 3.2. XRD spectrogram of HANPs

From the Fig. 3.2, the most relative reflection peaks at 2θ angle of 25.8°, 28.9°, 31.7°, 32.1°, 32.9°, 34.1°, 39.8°, 46.7°, and 49.5° correspond to the (002), (210), (211), (112), (300), (202), (310), (222) and (213) planes respectively of the pure hexagonal HAp. It is clearly observed from the XRD peaks that the synthesis using microwave assisted precipitation method (HAp-01) shows slight decrease in the intensities compared to the conventional synthesis method (HAp-02). Similarly, a slight decrease in intensities was observed when AI used as templet in microwave assisted method (HAp-03) compared to conventional method (HAp-04). This decrease in intensity of the XRD peaks suggests decrease in the crystallite size and degree of crystallinity of the samples (Gopi et al. 2013, Gopi et al. 2010, Gopi et al. 2009, Gopi et al. 2014). It was observed that the addition of the AI in both methods did not substantially impact the degree of crystallinity and crystallite size. This is also evident from the calculated crystallite size using the Sherrer equation as shown in table 3.2. In this work, all the main peaks of HANPs were used to calculate the average crystallite size. From the XRD results, it is shown that all the samples of HANPs have a pure single phase and HANPs synthesized using microwave precipitation method give small particles over the conventional method with or without template. The microwave method provides rapid homogenous heating for the synthesis of nanoparticles. Due to homogenous nucleation and rapid crystal growth, microwave method contributes to regulate morphology and size compared with other methods (Han et al. 2007a, Jayaprakash et al. 2017).

Table 3.2. Data acquired from XRD analysis of synthesized HANPs

Sample	Wavelength (Å)	Average Crystallite Size (nm)	Degree of Crystallinity (%)
HAp-01	1.78899	23.83 ± 9.5	77.15 ± 1.2
HAp-02	1.78899	25.15 ± 7.6	81.29 ± 9.2
HAp-03	1.78899	23.50 ± 9.4	71.09 ± 5.4
HAp-04	1.78899	24.25 ± 16.3	77.67 ± 7.1

3.4.2 ATR-Fourier transform infrared (FT-IR) Spectroscopy

ATR-FTIR investigation was done to determine the structural changes in HANPs. The FTIR spectra of eggshell powder and synthesized HANPs samples, HAp-01, HAp-02, HAp-03 and HAp-04 are shown in fig. 3.3. The appearance of peaks at 632 cm^{-1} and 3570 cm^{-1}, confirmed the presence of the hydroxyl group (OH^-) in HANPs. Characteristic peaks of phosphate appeared at 472, 565, 599, 963, 1026 and 1089 cm^{-1} in all the synthesized samples, as can be clearly seen in fig. 3.3. The band at 565 and 599 cm^{-1} are ν4 (vibration of O-P-O mode), the strong band at 1026 and 1089 cm^{-1} are the asymmetric ν3 (P-O stretching), and band at 963 cm^{-1} symmetric ν1 (P-O stretching) of phosphate group. The symmetric vibration band ν2 (P-O) appeared at 472 cm^{-1}. The FTIR spectra obtained from all the methods clearly indicate the formation of pure HANPs without any impurities such as calcium carbonate and other calcium phosphate salts. No additional peaks in the AI templated samples (HAp-03 & HAp-04) were noticed indicating that AI acted only as template and no AI residues were left after washing purification and calcination. The results from FTIR corelate with the results from XRD and matched with earlier reported data (Gopi et al. 2013, Gopi et al. 2010, Indira and Malathi 2022).

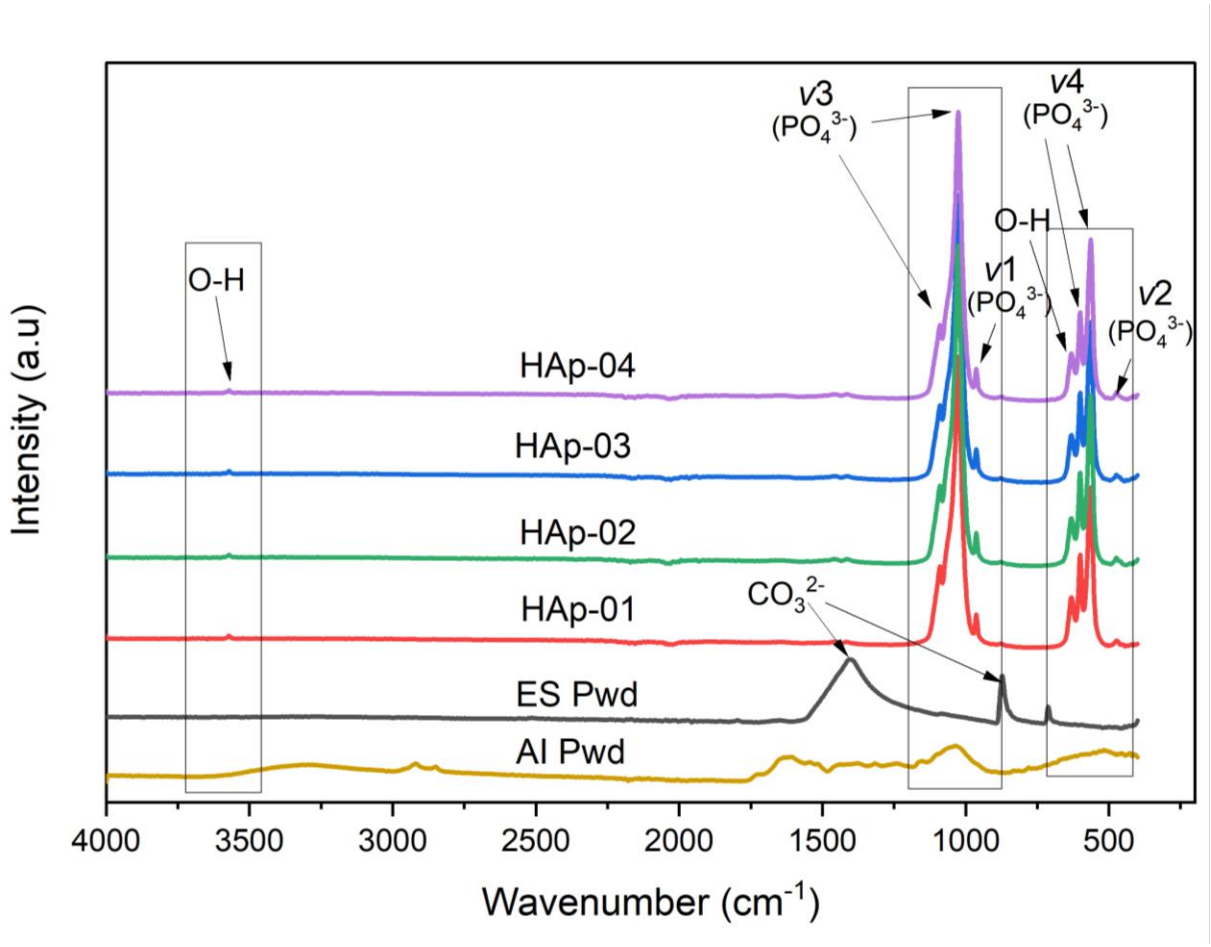

Figure 3.3. FTIR spectra of synthesized HANPs

3.4.3 Raman Spectroscopy

Raman spectroscopy is an excellent characterization tool to determine both amorphous and crystalline phases of the samples. This technique is more sensitive to detect impurities and any other phases present in the sample. Raman spectra of the all the HANPs samples are shown in Fig. 3.4. The main peaks in the graph are observed at 431, 592, 962, 1048 and 1078 cm^{-1} which confirms the pure phase of HANPs. The main sharp characteristic peak at 962 cm^{-1} corresponds to ν1 stretching vibration of the phosphate group in the HANPs structure. The peaks appeared at 1048 and 1078 cm^{-1} are the ν3 vibration bending mode of the phosphate group and the peaks at

431 and 592 cm^{-1} confirm the vibration stretching modes *v*2 and *v*4 respectively in the phosphate group. Both the samples from microwave method (HAp-01) and convectional method (HAp-02) show pure and single phase of hydroxyapatite with no other impurities (Karunakaran et al. 2019).

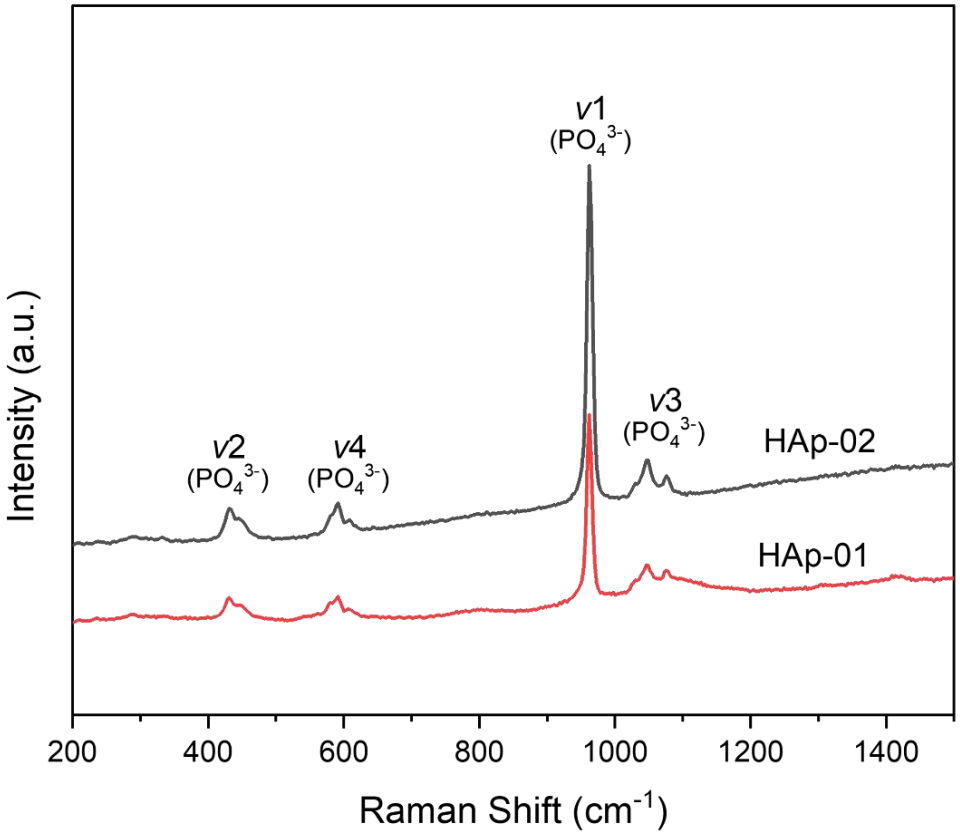

Figure 3.4. Raman spectra of synthesized HANPs

3.4.4 Scanning Electron Microscopy (SEM)

The surface morphology, shape, size, and distribution of HANPs synthesized by both methods microwave and conventional method with and without template were investigated by SEM and the resulted images are shown in Fig. 3.5. The SEM images of HANPs confirmed the formation

of the nanorod in all the samples. However, addition of template shows great change in uniformity, and distribution of the nanoparticles. The micrographs of HAp-01 and HAp-02 synthesized from both methods without AI template represents the formation of nanorods with irregular distribution of nanorod and shows agglomerated nanoparticles throughout the surface, while using AI template in both methods, more uniform distribution without agglomeration found in the micrograph of HAp-03 and HAp-04. Many researchers claim that use of green plant extracts in the synthesis of nanoparticles as a template for natural precursor can prevent agglomeration and it greatly contributes to regulate the shape and size of the nanoparticles (Alorku et al. 2020, Irwansyah et al. 2022). The average size of nanorods was investigated from SEM micrograph using Image J software. It is ranging from 40-60 nm in length and 25-35 nm in diameter which was further confirmed with TEM analysis. From the SEM results, it is confirmed that AI template played an important role in the distribution and to prevent the agglomeration of nanorods.

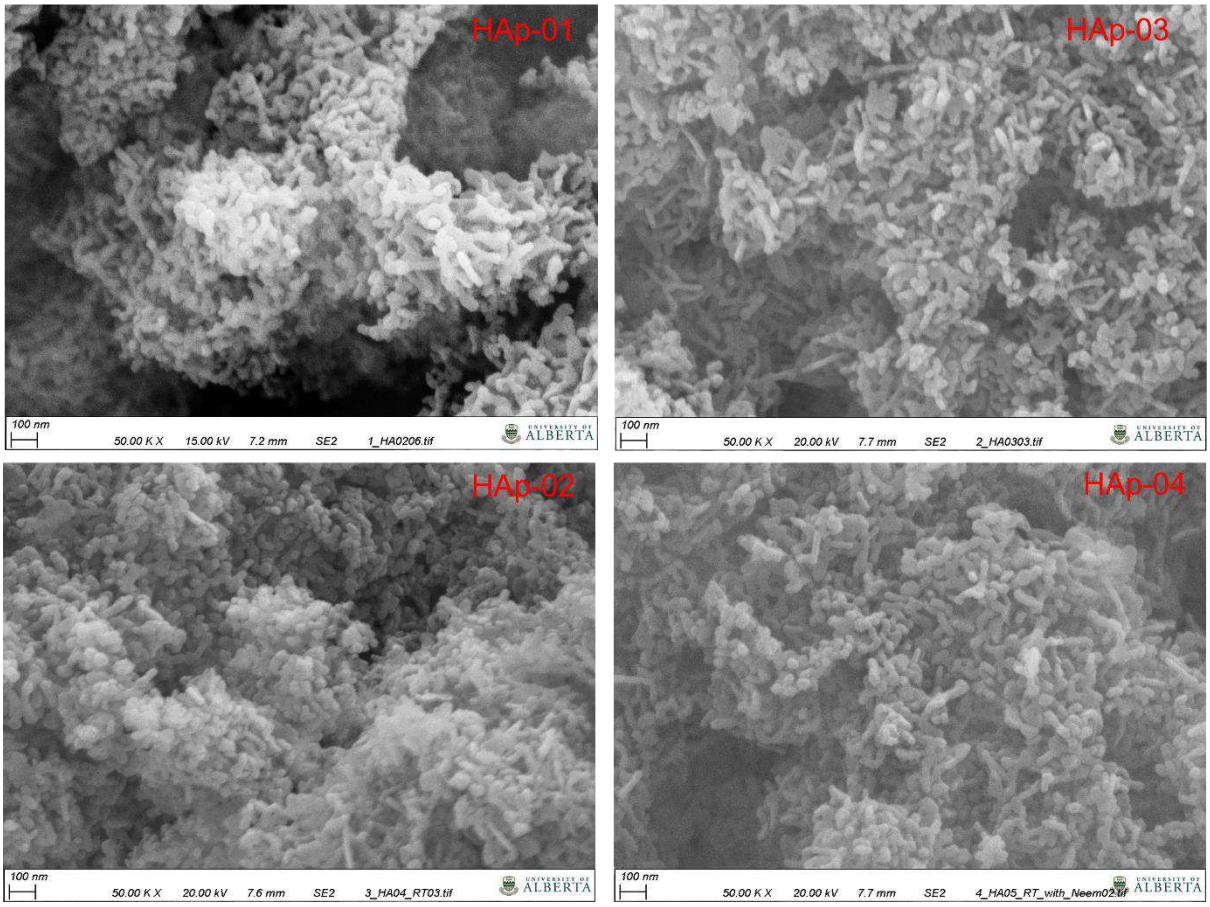

Figure 3.5. SEM images of synthesized HANPs

3.4.5 Transmission Electron Microscopy (TEM)

The TEM images of HANPs synthesized by microwave method without and with AI template (HAp-01 and HAp-03) and convectional method with and without AI template (HAp-02 and HAp-04) shown in Fig. 3.6. From fig. 3.6, it is clearly confirmed that samples HAp-01 and HAp-02 without template reveals the formation of imperfect shape nanorod interconnected to each other with agglomeration. While samples, synthesized with template AI (HAp-03 and HAp-04) had improved nanorod shapes and their size was slightly reduced compared to the samples without template (HAp-01 and HAp-02). Less agglomerated nanorods were shown in samples

HAp-03 and HAp-04, which validated the SEM results. The average particle size of the nanoparticles of HAp-01, HAp-02, HAp-03 and HAp-04 consisted of 53, 55,44, 46 nm length and 30, 31, 27, 28 nm diameter respectively. The TEM results depicted that the size of nanoparticles was slightly reduced when AI template was used. From the TEM analysis, it was confirmed that AI played an important role to regulate shape (nucleation and growth) of synthesized HANPs. Average size of nanoparticles from all the synthesis methods were shown in between 25-30 nm (diameter) and 40-60 nm in length.

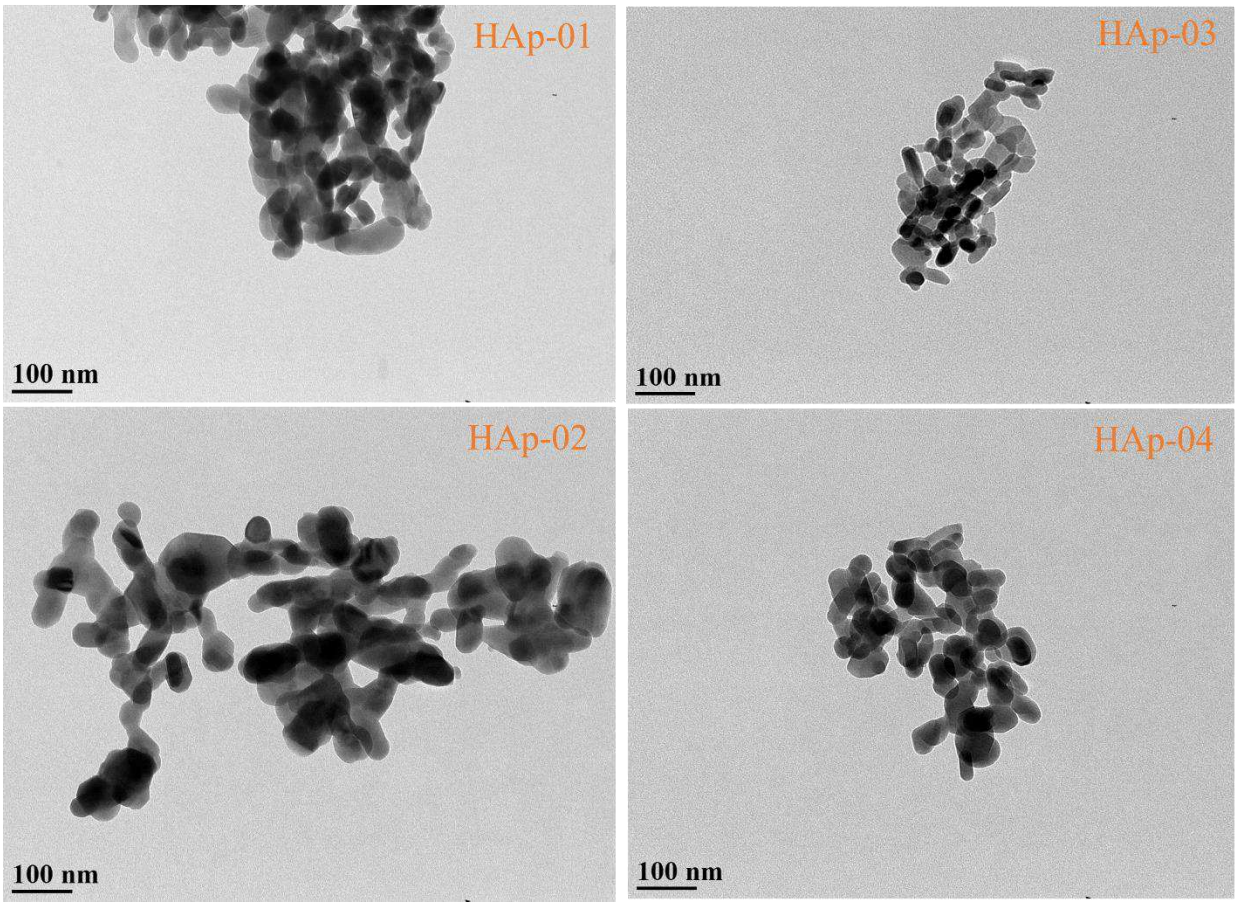

Figure 3.6. TEM images of synthesized HANPs

3.4.6 Energy Dispersive X-Ray Spectroscopy (EDX)

Analytical technique, EDX is widely used for the quantitative elemental analysis of HANPs. Fig.

3.7 shows the EDX patterns of the synthesized HANPs with and without AI template. The EDX spectra confirmed the formation of pure HANPs in the presence of main constitutes, Ca (calcium), P (phosphorus), and O (oxygen). EDX spectra also show that the carbon peak appeared at 0.5 KeV that is due to sample coating with carbon before analysis. Chemical composition and Ca/P ratio of all the samples found from EDX were shown in Table 3.3.

Table 3.3. Chemical composition of synthesized HANPs by using EDX

Element Content (wt %)	Eggshell	HANPs Samples			
		HAp-01	HAp-02	HAp-03	HAp-04
Ca	41.6	14.5	12.3	9.4	10.5
P	-	8.0	6.3	5.2	5.4
O	57.8	59.5	51.4	45.9	52.9
Ca/P ratio	-	1.81	1.95	1.81	1.94

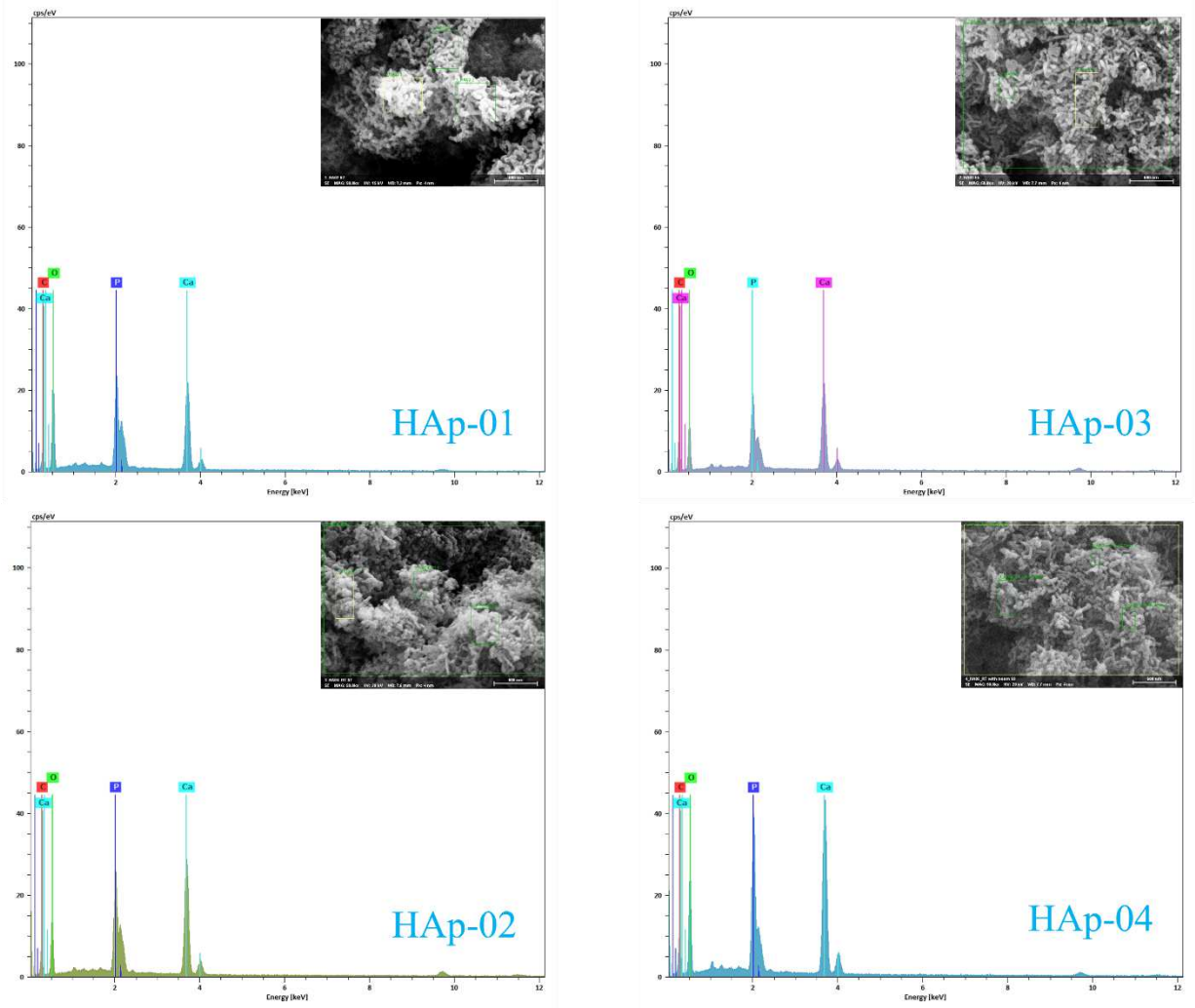

Figure 3.7. EDX spectra of synthesized HANPs

3.4.7 X-ray Photoelectron Spectroscopy (XPS)

XPS is an important technique to identify and estimate elemental composition on the surface of the materials. Fig. 3.8 shows XPS survey spectrum of HANPs synthesized using microwave and conventional methods. The major component of the HANPs (Ca, P, and oxygen) are present in the survey spectrum and no other elements were present ruling out the presence of any impurities which is consistent with the finding of EDX and XRD.

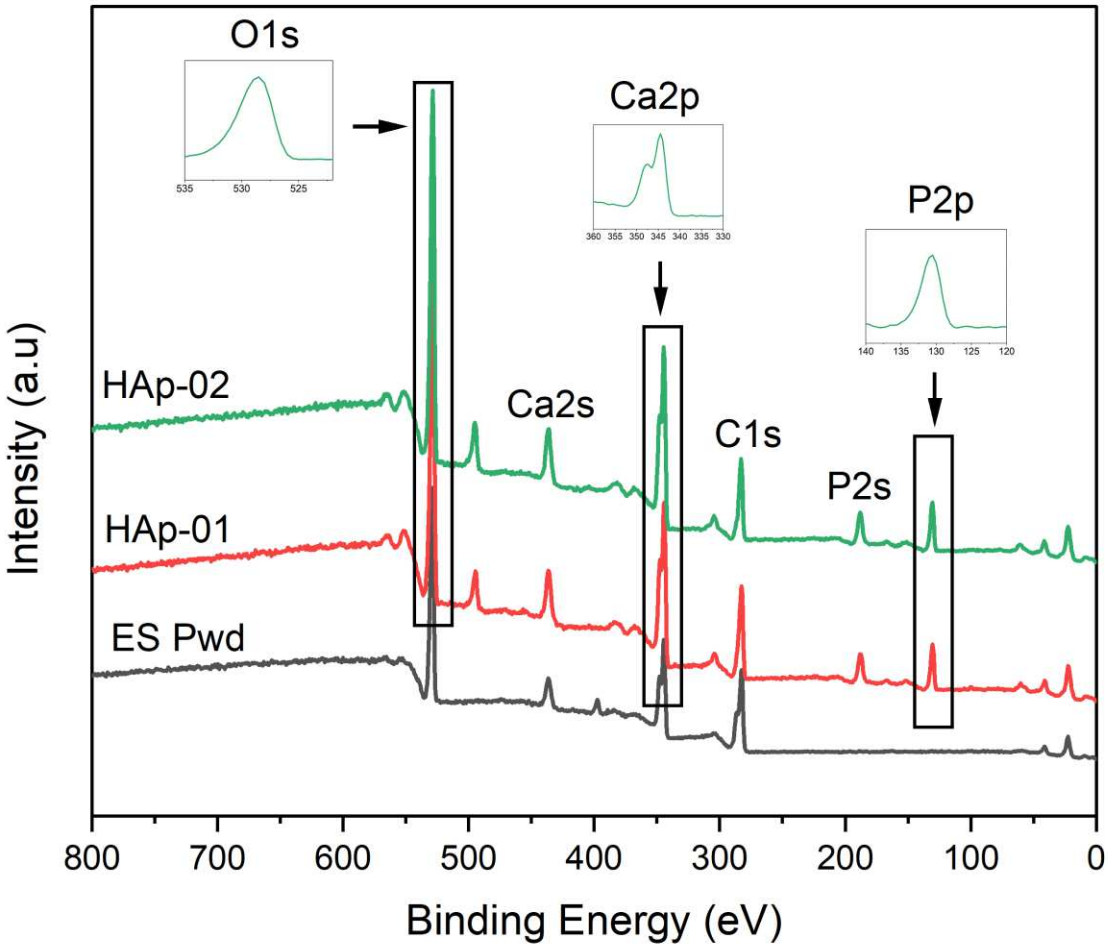

Figure 3.8. XPS spectra of synthesized HANPs

Fig. 3.8, represents XPS spectra of synthesized HANPs samples HAp-01 and HAp-02 shows the typical characteristic peaks of Ca_{2p}, P_{2p}, and O_{1s}, that form the HANPs stoichiometry (Ghate et al. 2022, Gomes et al. 2017, Ofudje et al. 2019). From the XPS spectrum, prominent peaks at high resolution, the binding energies of Ca_{2p}, P_{2p}, and O_{1s} corresponded to 346.5, 131.5, and 529.9 eV respectively. The peak was found at 283.5 eV corresponding to C_{1s}, was believed to be from surface organic contamination, as no coating or sputtering was done before analysis. In the

insert section of Fig. 8 (Ca_{2p}), there is a spin doublet at 344.5 and 347.5 eV binding energy corresponding to $Ca_{2p3/2}$ and $Ca_{2p1/2}$ respectively, which confirmed the presence of calcium in the sample. The intense peak at 130.5 belonged to the P_{2p} phosphate constitutes and notable peak at 529.5 eV shows the presence of O_{1s} and P-O moieties.

3.4.8 Thermogravimetric Analysis (TGA)

Hydroxyapatite nanoparticles synthesized by microwave assisted precipitation method and conventional method. Eggshell powder (ES Pwd) and after the synthesis and before the calcination, HANPs from both methods were analyzed using TGA to determine the thermal stability of the material (Fig. 3.9). There were two main stages of mass loss in both methods. The first is of 0.5% around 100 $^{\circ}$C due to the water and ethanol evaporation. The dominating weight loss is the second one which is 0.5% in between temperature of 100 ℃ to 500 ℃ that correspond to the evaporation of ethanol residues (Costescu et al. 2010). Beyond 500 ℃, the graph shown from both methods were steady. Based on this reason, calcination of all the synthesized HANPs samples were done at 600 ℃.

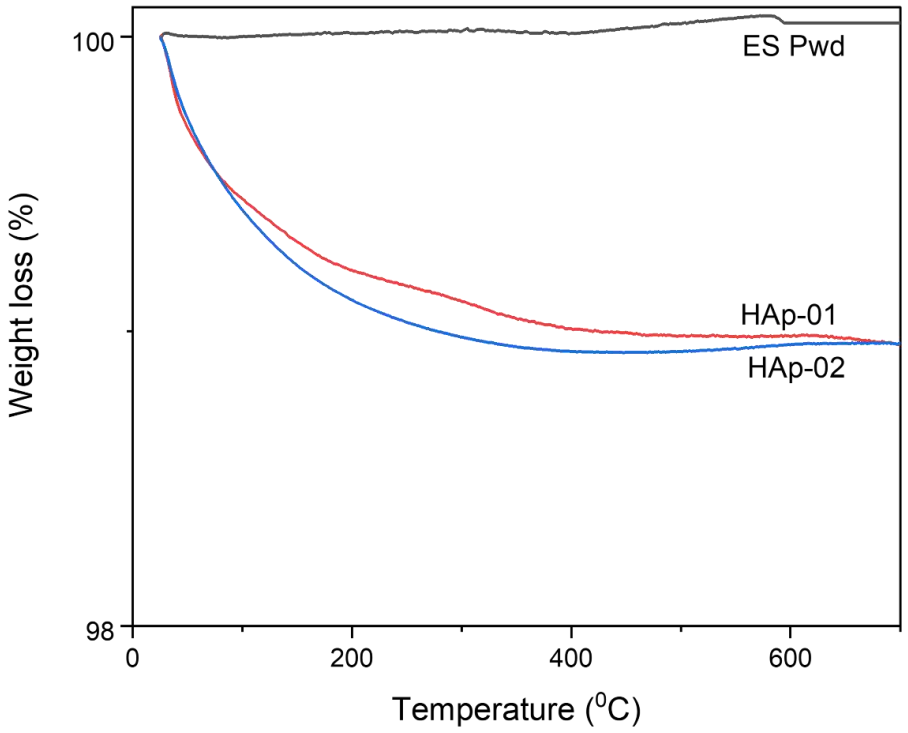

Figure 3.9. TGA profiles of synthesized HANPs before calcination

The crystallite size and shape of the HANPs synthesized using plant extract used in this study and by other methods recently reported in the literature are given in table 3.4 for the comparison purpose. As seen from table 3.4, several green methods reported synthesis of HANPs and synthesis time varied from few to several hours. While, in the present work, HANPs synthesized using microwave reactor in very short time (15 minutes) with lowered temp. (40 °C) without use of chemical/chelating agent (e.g. EDTA) achieved smallest crystallite size so far with Ca/P ratio 1.81, which is suitable for many biomedical application and potential to use in food packaging applications as a nanofiller.

Table 3.4. Results of HANPs synthesized in presence of green plant extracts by various studies

Calcium source/ chemicals	Plant extract	Synthesis method and condition	Total time (hours)	pH	Crystallite size (nm)	Shape	Ca/P ratio	Ref.
Calcium chloride	Acacia falcata leaf	Chemical precipitation	27	12	55.04	Niddle-like rod	-	(Ghate et al. 2022)
Calcium chloride	Curcurma longa	Sol-gel	24	10	-	Rod	1.62	(Kumar et al. 2018)
Calcium hydroxide	Euclea-natalensis roots	Chemical precipitation	24	10	<100	Rod	-	(Aguilar et al. 2021)
Calcium chloride	A. indica and C. grandis leaf	Chemical precipitation	25	10	53 64	Rod	-	(Kumar et al. 2017)
Calcium nitrate tetrahydrate	Banana peel Tamarind leaf Prickly pear Grapes	Chemical precipitation	24	10-12	422.1 319.8 291.3 292	Spherical Flower-like Flower-like Rod	-	(Varadarajan et al. 2020)
Calcium hydroxide	Moringa oleifera flower	Chemical precipitation	25 +	12	12.4-18.6	Rod	1.82	(Kalaiselvi et al. 2018)

		plus microwave	10 minutes					
Calcium nitrate tetrahydrate	Licorice root	Microwave-hydrothermal 400 W 125 ℃	7.1/2	6.1	36	Rod	1.69	(Ali et al. 2021)
Eggshells and EDTA	Piper betel leaf	Microwave 600 W	12 minutes	13	53-64	Cylindrical-like rod	-	(Umesh et al. 2021)
Eggshells	Azadirachta Indica	Microwave 250 W, 40 ℃	15 minutes	10	23.5	Rod	1.81	Present work

3.5 Conclusion

In summary, HANPs have been successfully synthesized from eggshell waste by two different methods, rapid microwave assisted precipitation and convectional heating method using with and without AI extract as a green template. All the synthesized HANPs were pure single phase without any impurities as confirmed by XRD, FTIR and Raman spectroscopy. The crystallinity and crystalline size of the hydroxyapatite nanorods obtained by microwave method was slightly lower compared to conventional heating method with and without AI template. SEM images clearly indicate that AI template played an important role in improving size and shape of HANPs and obtaining uniform distribution without agglomeration. TEM confirmed the average size of the synthesized nanorods from all the synthesis methods had a diameter of 25-30 nm and length of 40-60 nm. EDS and XPS confirmed the main elements of the HANPs. From the EDX spectra Ca/P ratio of 1.81 was observed when microwave assisted precipitation method was used which is close to the Ca/P ratio found in human bone and teeth. This study revealed that the HANPs can be effectively and efficiently synthesized using microwaves and/or conventional heating in the presence of AI template. Microwave assisted synthesis promotes formation of nanorods with smaller length and diameter compared to conventional heating. The synthesized HANPs are biocompatible, biodegradable, and eggshells being a cheap starting material makes them potentially economically more viable compared to HANPs synthesized using synthetic chemicals. The synthesis is facile and could be easily scaled up indicating that these materials may be used for many applications including biomedical such as bone repair, bone regeneration, drug delivery and other applications like cosmetics, wastewater treatment. Because of small crystallite size, it has a great potential for use as an inorganic nanofiller in the preparation of bionanocomposites films for their use in food packaging.

References

Agalya, P., Suresh Kumar, G., Srinivasan, R., Prabu, K.M., Karunakaran, G., Cholan, S., Kolesnikov, E. and Kim, M. (2021) Hydroxyapatite-based antibacterial bio-nanomaterials: an insight into the synthesis using mussel shell as a calcium source, physicochemical properties, and nanoindentation characteristics. Applied Physics A 127(8), 589.

Aguilar, A.E.M., Fagundes, A.P., Macuvele, D.L.P., Cesca, K., Porto, L., Padoin, N., Soares, C. and Riella, H.G. (2021) Green synthesis of nano hydroxyapatite: morphology variation and its effect on cytotoxicity against fibroblast. Materials Letters 284, 129013.

Ali, A.F., Alrowaili, Z.A., El-Giar, E.M., Ahmed, M.M. and El-Kady, A.M. (2021) Novel green synthesis of hydroxyapatite uniform nanorods via microwave-hydrothermal route using licorice root extract as template. Ceramics International 47(3), 3928-3937.

Alorku, K., Manoj, M. and Yuan, A. (2020) A plant-mediated synthesis of nanostructured hydroxyapatite for biomedical applications: a review. RSC Advances 10(67), 40923-40939.

Alzohairy, M.A. (2016) Therapeutics Role of Azadirachta indica (Neem) and Their Active Constituents in Diseases Prevention and Treatment. Evid Based Complement Alternat Med 2016, 7382506.

Ashokan, A., Rajendran, V., Sampath Kumar, T.S. and Jayaraman, G. (2021) Eggshell derived hydroxyapatite microspheres for chromatographic applications by a novel dissolution - precipitation method. Ceramics International 47(13), 18575-18583.

Athinarayanan, J., Periasamy, V.S. and Alshatwi, A.A. (2020) Simultaneous fabrication of carbon nanodots and hydroxyapatite nanoparticles from fish scale for biomedical applications. Materials Science and Engineering: C 117, 111313.

Bose, S. and Saha, S.K. (2003) Synthesis and Characterization of Hydroxyapatite Nanopowders by Emulsion Technique. Chemistry of Materials 15(23), 4464-4469.

Brundavanam, R.K., Jiang, Z.-T., Chapman, P., Le, X.-T., Mondinos, N., Fawcett, D. and

Poinern, G.E.J. (2011) Effect of dilute gelatine on the ultrasonic thermally assisted synthesis of nano hydroxyapatite. Ultrasonics sonochemistry 18(3), 697-703.

Bunaciu, A.A., Udriştioiu, E.g. and Aboul-Enein, H.Y. (2015) X-Ray Diffraction: Instrumentation and Applications. Critical Reviews in Analytical Chemistry 45(4), 289-299.

Cengiz, B., Gokce, Y., Yildiz, N., Aktas, Z. and Calimli, A. (2008) Synthesis and characterization of hydroxyapatite nanoparticles. Colloids and Surfaces A: Physicochemical and Engineering Aspects 322(1), 29-33.

Chesley, M., Kennard, R., Roozbahani, S., Kim, S.M., Kukk, K. and Mason, M. (2020) One-step hydrothermal synthesis with in situ milling of biologically relevant hydroxyapatite. Materials Science and Engineering: C 113, 110962.

Costescu, A., Pasuk, I., Ungureanu, F., Dinischiotu, A., Costache, M., Huneau, F., Galaup, S., Coustumer, P.L. and Predoi, D. (2010) PHYSICO-CHEMICAL PROPERTIES OF NANO-SIZED HEXAGONAL HYDROXYAPATITE POWDER SYNTHESIZED BY SOL-GEL. Digest Journal of Nanomaterials & Biostructures (DJNB) 5(4).

Dasgupta, S., Tarafder, S., Bandyopadhyay, A. and Bose, S. (2013) Effect of grain size on mechanical, surface and biological properties of microwave sintered hydroxyapatite. Materials Science and Engineering: C 33(5), 2846-2854.

Fathi, M., Hanifi, A. and Mortazavi, V. (2008) Preparation and bioactivity evaluation of bone-like hydroxyapatite nanopowder. Journal of materials processing technology 202(1-3), 536-542.

Gan, C.-d., Jia, Y.-b. and Yang, J.-y. (2021) Remediation of fluoride contaminated soil with nano-hydroxyapatite amendment: Response of soil fluoride bioavailability and microbial communities. Journal of Hazardous Materials 405, 124694.

Ghate, P., Prabhu S, D., Murugesan, G., Goveas, L.C., Varadavenkatesan, T., Vinayagam, R., Lan Chi, N.T., Pugazhendhi, A. and Selvaraj, R. (2022) Synthesis of hydroxyapatite nanoparticles using Acacia falcata leaf extract and study of their anti-cancerous activity against cancerous mammalian cell lines. Environmental Research 214, 113917.

Goh, K.W., Wong, Y.H., Ramesh, S., Chandran, H., Krishnasamy, S., Ramesh, S., Sidhu, A. and Teng, W.D. (2021) Effect of pH on the properties of eggshell-derived hydroxyapatite bioceramic synthesized by wet chemical method assisted by microwave irradiation. Ceramics International 47(7, Part A), 8879-8887.

Gomes, G.C., Borghi, F.F., Ospina, R.O., López, E.O., Borges, F.O. and Mello, A. (2017) Nd:YAG (532nm) pulsed laser deposition produces crystalline hydroxyapatite thin coatings at room temperature. Surface and Coatings Technology 329, 174-183.

Gopi, D., Bhuvaneshwari, N., Indira, J. and Kavitha, L. (2013) Synthesis and spectroscopic investigations of hydroxyapatite using a green chelating agent as template. Spectrochimica Acta Part A: Molecular and Biomolecular Spectroscopy 104, 292-299.

Gopi, D., Bhuvaneshwari, N., Kavitha, L. and Ramya, S. (2015) Novel malic acid mediated green route for the synthesis of hydroxyapatite particles and their spectral characterization. Ceramics International 41(2, Part B), 3116-3127.

Gopi, D., Indira, J., Kavitha, L., Kannan, S. and Ferreira, J.M.F. (2010) Spectroscopic characterization of nanohydroxyapatite synthesized by molten salt method. Spectrochimica Acta Part A: Molecular and Biomolecular Spectroscopy 77(2), 545-547.

Gopi, D., Indira, J., Prakash, V.C.A. and Kavitha, L. (2009) Spectroscopic characterization of porous nanohydroxyapatite synthesized by a novel amino acid soft solution freezing method. Spectrochimica Acta Part A: Molecular and Biomolecular Spectroscopy 74(1), 282-284.

Gopi, D., Kanimozhi, K., Bhuvaneshwari, N., Indira, J. and Kavitha, L. (2014) Novel banana peel pectin mediated green route for the synthesis of hydroxyapatite nanoparticles and their spectral characterization. Spectrochimica Acta Part A: Molecular and Biomolecular Spectroscopy 118, 589-597.

Han, J.-K., Song, H.-Y., Saito, F. and Lee, B.-T. (2006) Synthesis of high purity nano-sized hydroxyapatite powder by microwave-hydrothermal method. Materials chemistry and physics 99(2-3), 235-239.

Han, S.-C., Jiang, N., Sujandi, Burri, D.R., Choi, K.-M., Lee, S.-C. and Park, S.-E. (2007a) Studies in Surface Science and Catalysis. Zhao, D., Qiu, S., Tang, Y. and Yu, C. (eds), pp. 25-28, Elsevier.

Han, Y., Li, S., Wang, X., Jia, L. and He, J. (2007b) Preparation of hydroxyapatite rod-like crystals by protein precursor method. Materials research bulletin 42(6), 1169-1177.

Hassan, M.N., Mahmoud, M.M., El-Fattah, A.A. and Kandil, S. (2016) Microwave-assisted preparation of Nano-hydroxyapatite for bone substitutes. Ceramics International 42(3), 3725-3744.

Herrero, Y.R. and Ullah, A. (2021) Rapid, Metal-Free, Catalytic Conversion of Glycerol to Allyl Monomers and Polymers. ACS Sustainable Chemistry & Engineering 9(28), 9474-9485.

Indira, J. and Malathi, K.S. (2022) Comparison of template mediated ultrasonic and microwave irradiation method on the synthesis of hydroxyapatite nanoparticles for biomedical applications. Materials Today: Proceedings 51, 1765-1769.

Irwansyah, F.S., Noviyanti, A.R., Eddy, D.R. and Risdiana, R. (2022) Green Template-Mediated Synthesis of Biowaste Nano-Hydroxyapatite: A Systematic Literature Review. Molecules 27(17), 5586.

Jayaprakash, N., Vijaya, J.J., Kaviyarasu, K., Kombaiah, K., Kennedy, L.J., Ramalingam, R.J., Munusamy, M.A. and Al-Lohedan, H.A. (2017) Green synthesis of Ag nanoparticles using Tamarind fruit extract for the antibacterial studies. Journal of Photochemistry and Photobiology B: Biology 169, 178-185.

Jemli, Y.E., Abdelouahdi, K., Minh, D.P., Barakat, A. and Solhy, A. (2022) Design and Applications of Hydroxyapatite-Based Catalysts, pp. 19-72.

Kalaiselvi, V., Mathammal, R., Vijayakumar, S. and Vaseeharan, B. (2018) Microwave assisted green synthesis of Hydroxyapatite nanorods using Moringa oleifera flower extract and its antimicrobial applications. International Journal of Veterinary Science and Medicine 6(2), 286-295.

Kamalanathan, P., Ramesh, S., Bang, L.T., Niakan, A., Tan, C.Y., Purbolaksono, J., Chandran, H. and Teng, W.D. (2014) Synthesis and sintering of hydroxyapatite derived from eggshells as a calcium precursor. Ceramics International 40(10, Part B), 16349-16359.

Karakas, A., Yoruc, A., Gokce, H., Karabulut, A. and Erdogan, D. (2013) Effect of different phosphorus precursors on biomimetic hydroxyapatite powder properties. Acta Physica Polonica A 123(2).

Karakas Aydınoğlu, A., Yoruc, A., Erdogan, D. and Doğan, M. (2012) Effect of different calcium precursors on biomimetic hydroxyapatite powder properties. Acta Physica Polonica A 121(1).

Karunakaran, G., Cho, E.-B., Kumar, G.S., Kolesnikov, E., Karpenkov, D.Y., Gopinathan, J., Pillai, M.M., Selvakumar, R., Boobalan, S. and Gorshenkov, M.V. (2019) Sodium dodecyl sulfate mediated microwave synthesis of biocompatible superparamagnetic mesoporous hydroxyapatite nanoparticles using black Chlamys varia seashell as a calcium source for biomedical applications. Ceramics International 45(12), 15143-15155.

Kumar, G.S. and Girija, E.K. (2013) Flower-like hydroxyapatite nanostructure obtained from eggshell: A candidate for biomedical applications. Ceramics International 39(7), 8293-8299.

Kumar, G.S., Muthu, D., Karunakaran, G., Karthi, S., Girija, E.K. and Kuznetsov, D. (2018) Curcuma longa tuber extract mediated synthesis of hydroxyapatite nanorods using biowaste as a calcium source for the treatment of bone infections. Journal of Sol-Gel Science and Technology 86(3), 610-616.

Kumar, G.S., Rajendran, S., Karthi, S., Govindan, R., Girija, E.K., Karunakaran, G. and Kuznetsov, D. (2017) Green synthesis and antibacterial activity of hydroxyapatite nanorods for orthopedic applications. MRS Communications 7(2), 183-188.

Kumar, G.S., Sathish, L., Govindan, R. and Girija, E. (2015) Utilization of snail shells to synthesise hydroxyapatite nanorods for orthopedic applications. RSC Advances 5(49), 39544-39548.

Kumar, G.S., Thamizhavel, A. and Girija, E. (2012) Microwave conversion of eggshells into flower-like hydroxyapatite nanostructure for biomedical applications. Materials Letters 76, 198-200.

Lin, D.-J., Lin, H.-L., Haung, S.-M., Liu, S.-M. and Chen, W.-C. (2021) Effect of pH on the In Vitro Biocompatibility of Surfactant-Assisted Synthesis and Hydrothermal Precipitation of Rod-Shaped Nano-Hydroxyapatite. Polymers 13(17), 2994.

Malvano, F., Montone, A.M.I., Capparelli, R., Capuano, F. and Albanese, D. (2021) Development of a Novel Active Edible Coating Containing Hydroxyapatite for Food Shelf-life Extension. Chemical Engineering Transactions 87, 25-30.

Malvano, F., Montone, A.M.I., Capuano, F., Colletti, C., Roveri, N., Albanese, D. and Capparelli, R. (2022) Effects of active alginate edible coating enriched with hydroxyapatite-quercetin complexes during the cold storage of fresh chicken fillets. Food Packaging and Shelf Life 32, 100847.

Markov, G.G. and Ivanov, I.G. (1974) Hydroxyapatite column chromatography in procedures for isolation of purified DNA. Analytical Biochemistry 59(2), 555-563.

Meski, S., Ziani, S. and Khireddine, H. (2010) Removal of Lead Ions by Hydroxyapatite Prepared from the Egg Shell. Journal of Chemical & Engineering Data 55(9), 3923-3928.

Neelakandeswari, N., Sangami, G. and Dharmaraj, N. (2011) Preparation and characterization of nanostructured hydroxyapatite using a biomaterial. Synthesis and Reactivity in Inorganic, Metal-Organic, and Nano-Metal Chemistry 41(5), 513-516.

Negrila, C.C., Predoi, M.V., Iconaru, S.L. and Predoi, D. (2018) Development of Zinc-Doped Hydroxyapatite by Sol-Gel Method for Medical Applications. Molecules 23(11), 2986.

Ofudje, E.A., Adeogun, A.I., Idowu, M.A. and Kareem, S.O. (2019) Synthesis and characterization of Zn-Doped hydroxyapatite: scaffold application, antibacterial and bioactivity studies. Heliyon 5(5).

Ooi, C.Y., Hamdi, M. and Ramesh, S. (2007) Properties of hydroxyapatite produced by annealing of bovine bone. Ceramics International 33(7), 1171-1177.

Pang, Y.X. and Bao, X. (2003) Influence of temperature, ripening time and calcination on the morphology and crystallinity of hydroxyapatite nanoparticles. Journal of the European Ceramic Society 23(10), 1697-1704.

Phatai, P., Futalan, C.M., Kamonwannasit, S. and Khemthong, P. (2019) Structural characterization and antibacterial activity of hydroxyapatite synthesized via sol-gel method using glutinous rice as a template. Journal of Sol-Gel Science and Technology 89(3), 764-775.

Rajabi-Zamani, A.H., Behnamghader, A. and Kazemzadeh, A. (2008) Synthesis of nanocrystalline carbonated hydroxyapatite powder via nonalkoxide sol–gel method. Materials Science and Engineering: C 28(8), 1326-1329.

Sawada, M., Sridhar, K., Kanda, Y. and Yamanaka, S. (2021) Pure hydroxyapatite synthesis originating from amorphous calcium carbonate. Scientific Reports 11(1), 11546.

Shi, D., Tong, H., Lv, M., Luo, D., Wang, P., Xu, X. and Han, Z. (2021) Optimization of hydrothermal synthesis of hydroxyapatite from chicken eggshell waste for effective adsorption of aqueous Pb(II). Environmental Science and Pollution Research 28(41), 58189-58205.

Siva Rama Krishna, D., Siddharthan, A., Seshadri, S.K. and Sampath Kumar, T.S. (2007) A novel route for synthesis of nanocrystalline hydroxyapatite from eggshell waste. Journal of Materials Science: Materials in Medicine 18(9), 1735-1743.

Teixeira, S., Rodriguez, M., Pena, P., De Aza, A., De Aza, S., Ferraz, M. and Monteiro, F. (2009) Physical characterization of hydroxyapatite porous scaffolds for tissue engineering. Materials Science and Engineering: C 29(5), 1510-1514.

Ullah, A. and Arshad, M. (2017) Remarkably Efficient Microwave-Assisted Cross-Metathesis of Lipids under Solvent-Free Conditions. ChemSusChem 10(10), 2167-2174.

Umesh, M., Choudhury, D.D., Shanmugam, S., Ganesan, S., Alsehli, M., Elfasakhany, A. and

Pugazhendhi, A. (2021) Eggshells biowaste for hydroxyapatite green synthesis using extract piper betel leaf - Evaluation of antibacterial and antibiofilm activity. Environmental Research 200, 111493.

Usami, K. and Okamoto, A. (2017) Hydroxyapatite: catalyst for a one-pot pentose formation. Organic & Biomolecular Chemistry 15(42), 8888-8893.

Varadarajan, V., Varsha, M., Vijayasekaran, K. and Shankar, S.V. (2020) Comparative studies of hydroxyapatite (HAp) nanoparticles synthesized by using different green templates. AIP Conference Proceedings 2240(1), 080002.

Viswanath, B. and Ravishankar, N. (2008) Controlled synthesis of plate-shaped hydroxyapatite and implications for the morphology of the apatite phase in bone. Biomaterials 29(36), 4855-4863.

Wang, P., Li, C., Gong, H., Jiang, X., Wang, H. and Li, K. (2010) Effects of synthesis conditions on the morphology of hydroxyapatite nanoparticles produced by wet chemical process. Powder Technology 203, 315-321.

Wu, S.-C., Hsu, H.-C., Hsu, S.-K., Chang, Y.-C. and Ho, W.-F. (2015) Effects of heat treatment on the synthesis of hydroxyapatite from eggshell powders. Ceramics International 41(9), 10718-10724.

Wu, S.-C., Hsu, H.-C., Hsu, S.-K., Chang, Y.-C. and Ho, W.-F. (2016) Synthesis of hydroxyapatite from eggshell powders through ball milling and heat treatment. Journal of Asian Ceramic Societies 4(1), 85-90.

Yan, D., Lou, Y., Han, Y., Wickramaratne, M.N., Dai, H. and Wang, X. (2018) Controllable synthesis of poly(acrylic acid)-stabilized nano-hydroxyapatite suspension by an ultrasound-assisted precipitation method. Materials Letters 227, 9-12.

Yao, H.-L., Yang, C., Yang, Q., Hu, X.-Z., Zhang, M.-X., Bai, X.-B., Wang, H.-T. and Chen, Q.-Y. (2020) Structure, mechanical and bioactive properties of nanostructured hydroxyapatite/titania composites prepared by microwave sintering. Materials chemistry and

physics 241, 122340.

Ye, F., Guo, H., Zhang, H. and He, X. (2010) Polymeric micelle-templated synthesis of hydroxyapatite hollow nanoparticles for a drug delivery system. Acta Biomater 6(6), 2212-2218.

Zhang, H. and Darvell, B.W. (2010) Synthesis and characterization of hydroxyapatite whiskers by hydrothermal homogeneous precipitation using acetamide. Acta Biomaterialia 6(8), 3216-3222.

Zhou, C., Wang, X., Song, X., Wang, Y., Fang, D., Ge, S. and Zhang, R. (2020) Insights into dynamic adsorption of lead by nano-hydroxyapatite prepared with two-stage ultrasound. Chemosphere 253, 126661.

Zhou, C., Wang, X., Wang, Y., Song, X., Fang, D. and Ge, S. (2021) The sorption of single- and multi-heavy metals in aqueous solution using enhanced nano-hydroxyapatite assisted with ultrasonic. Journal of Environmental Chemical Engineering 9(3), 105240.

Zhou, R., Si, S. and Zhang, Q. (2012) Water-dispersible hydroxyapatite nanoparticles synthesized in aqueous solution containing grape seed extract. Applied Surface Science 258(8), 3578-3583.

CHAPTER 4. ENHANCED MECHANICAL AND BARRIER PROPERTIES OF CHITOSAN-BASED BIONANOCOMPOSITES FILMS REINFORCED WITH EGGSHELL-DERIVED HYDROXYAPATITE NANOPARTICLES

4.1 Introduction

To date, plastic use and production are increasing every day. Annually, approximately more than 350 million metric tons of plastic are produced worldwide, and it is estimated to double in the next twenty years. (Haghighi et al. 2020, Lebreton and Andrady 2019). Currently, plastic-based packaging materials have been widely used in the food packaging industries such as polyethylene (PE), polystyrene (PS), polypropylene (PP), and polyethylene terephthalate (PET). Food packaging is a medium for safe handling through transportation, and distribution and protects the foods from any exterior contamination. Food packaging is probably one of the biggest applications of plastic owing to its low cost, easy formation, high strength modulus, and excellent physiochemical properties (Cui et al. 2020). Non-biodegradability of synthetic plastics, the accumulation of plastic in the environment is huge and creates a serious problem for the environment. Consequently, the food packaging industry is pushing toward environmentally friendly, biobased, and biodegradable materials, such as bioplastic. (Arikan and Ozsoy 2015). Bioplastics are plastics derived from renewable resources (biobased) either synthesized chemically or through a biological process (Goel et al. 2021). In this context, poly-lactic acid (PLA), polycaprolactone (PCL), starch, cellulose, and chitosan are examples of commonly used biodegradable bioplastic over synthetic plastic (Mohammadi sadati et al. 2022).

Among various biopolymers, chitosan has been considered the most suitable candidate for food packaging applications due to its high availability, biodegradability, biocompatibility, non-toxicity, excellent film forming, and antimicrobial properties (Cunha et al. 2020, Khanzada et al.

2023). Chitosan (CH) is a natural cationic polysaccharide form of β (1-4) linked to D-glucosamine and N- acetylglucosamine unit and it is derived from chitin by de-acetylation (Jakubowska et al. 2020, Rinaudo 2006). Due to its unique properties, chitosan has been used as a coating and main base material (as a matrix) in food packaging applications (Ghosh et al. 2021, Zhang et al. 2021). However, low mechanical and thermal properties, poor barrier properties, and brittleness of pure form of chitosan limit their use in larger scale in food packaging industries (Khanzada et al. 2023, Shikinaka et al. 2020). In this context, recently, bionanocomposites are gaining much attention. Bionanocomposites are made of hybrid materials of biopolymers and organic/inorganic nanofiller (at least one dimension is in 1-100 nm range). The addition of nanofillers has been already proven to enhanced biopolymers properties, thanks to nanomaterials unique properties such as high surface area to volume ratio, high reactivity, small size, and high mechanical strength (Dong et al. 2022).

Currently, chitosan films reinforcing with inorganic nanofiller (organic-inorganic composites) are gaining increasing attention due to organic and inorganic components combination acquiring materials with unique properties (Spirescu et al. 2021). Different inorganic nanoparticles such as nanoclays, silica, silver, gold and metal oxide (Zinc oxide, copper oxide, titanium oxide, and silicone oxide) have been used to prepared nanocomposite film as an active food packaging materials (Dash et al. 2022). Recently, for example, Gasti et al. developed nanocomposite using chitosan-zinc oxide nanoparticle and obtained enhanced tensile strength and water vapor barrier properties approximately 39.82% and 84.64% respectively (Gasti et al. 2022). Shue Li et al. prepared chitosan films incorporated by silver nanoparticles/curcumin/clay minerals and reported enhanced mechanical properties (Li et al. 2022). V. Ramji and M. Vishnuvarthanan developed chitosan ternary bionanocomposites film incorporated with MMT K10 nano clay and spirulina,

they exhibited highest tensile strength 46.3 MPa compared to pure chitosan film (24.6 MPa) (Ramji and Vishnuvarthanan 2022) . However, some of the inorganic nanoparticles are not exemplary nano addition/nanofiller for chitosan-based composites because of their non-biodegradability, hidden bio-toxicity, and mostly poor biocompatibility (Zou et al. 2023).

Hydroxyapatite (HA) ($Ca_{10}(PO_4)_6(OH)_2$) is a main inorganic mineral component of calcium phosphate family found in the human hard tissues in terms of morphology and composition (Li et al. 2018, Nazeer et al. 2017). Various methods are used for synthesis of HANPs using synthetic or natural sources. However, eggshell derived HANPs are environment friendly and enhanced their properties such as renewability, biocompatibility, and bioactivity (Ummartyotin and Tangnorawich 2015). In our previous work (submitted) we synthesized HANPs using microwave-assisted (MW) and conventional heating method using waste eggshell as a calcium source. MW method provided pure HANPs with excellent homogeneity.

Due to excellent properties such as biocompatibility, biodegradability, bioactivity and non-toxic of hydroxyapatite nanoparticles (HANPs) are widely used in several biomedical applications (Goh et al. 2021, Trakoolwannachai et al. 2019) and other fields such as wastewater treatment (Zhou et al. 2021) and cosmetics (Cunha et al. 2020, Morsy et al. 2017). However, their use as a nanofiller in food packaging field is less explored. Recent scientific evidence indicates that selection of nanofiller as well as their concentration have significant effects on nanocomposites to achieve desired properties for specific applications (Priyadarshi et al. 2021).

Therefore, the main objective of our work is the development of chitosan based bionanocomposites reinforced with HANPs with different concentration for food packaging applications. The developed bionanocomposites were prepared by simple physical evaporation/solvent casting method. The impact of various concentration of HANPs nanofillers

on the prepared chitosan-based bionanocomposites were widely studied in terms of morphological, structural, thermal, mechanical, barrier properties. To the best of our knowledge, there is no report on the chitosan-based bionanocomposites incorporated with eggshell derived HANPs for food packaging application.

4.2 Experimental

4.2.1 Materials

Low molecular weight Chitosan (CS) (MW 50-190 kDa) with a degree of deacetylation of about 75-85% was purchased from Sigma-Aldrich. Chicken eggshells were obtained from the local restaurant (Edmonton, Canada). They were washed with water and then boiled at 100 ℃ for 3 hours to remove any impurities. Eggshells were dried in the oven at 80 ℃ overnight. Then they were ground to a fine powder using a coffee grinder.

Orthophosphoric acid (ACS reagent, ≥85 wt. % in H_2O), nitric acid (ACS reagent, 70 %), sodium hydroxide (reagent grade ≥98%, pellets anhydrous), ethanol (≥95%), glacial acetic acid (≥95%), and glycerol (99.6%), were acquired from Sigma-Aldrich and further used as received.

4.2.2 Preparation of HANPs from eggshell

Calcium precursor (calcium nitrate) was obtained by slowly adding concentrated HNO_3 (100 ml) into the eggshell powder (ES) (10 gm) with vigorous stirring using a magnetic stirrer at 1100 rpm for 30 minutes. And then pH was adjusted to 10 using 1M NaOH to form calcium hydroxide. Then resultant solution mixture, 50 ml was taken into the beaker and 50 ml of phosphate precursor, 0.6M orthophosphoric acid (50 ml) was added dropwise with continuous stirring at 700 rpm for 20 minutes. The pH of the resultant mixture was adjusted at 10 by adding 1M NaOH with continuous stirring. The white nano-hydroxyapatite powders were obtained by using the microwave method. The resultant solution mixture was subjected to microwave

irradiation using an open vessel reflux mode microwave reactor (CEM-Discover reactor unit, 120 V, Matthews, USA) for 15 minutes. The temperature and power used for this reaction were 40 ℃ and 250 watts respectively. The precipitated mixture was centrifuged and washed three times with distilled water and ethanol. The settled powder was dried in the oven at 100 ℃ for 24 hours. The final dried powder, hydroxyapatite nanoparticles (HANPs) were calcinated using a furnace at 600 ℃ for 3 hours with a heating rate of 10 ℃/minute.

4.2.3 Preparation of chitosan-hydroxyapatite (CH-HA) film

The physical evaporation/solvent casting method was implemented to obtain chitosan-hydroxyapatite (CH-HA) bionanocomposites films. First, CS powder (2 % w/v) was taken into a 250 ml flask then added 1%(v/v) acetic acid. The solution mixture was under continuous magnetic stirring for 4 hours at 80 ℃ to allow the complete dissolution of CS powder. After that solution mixture was cooled down to room temperature. Then glycerol (20% w/v to CS) was added to the solution mixture which acted as a plasticizer for all the film. The different concentrations of HANPs (0 %, 1%, 3%, 5%, and 10% w/v) were added to the resultant solution mixture of CS and subsequently stirred at 60 ℃ for 2 hours at 250 rpm speed. Further, for better dispersion of nanoparticles, the solution mixture was sonicated using the ultrasonic processor (Crest Ultrasonics, CP360D 115 volts, Trenton, NJ, USA) for 30 minutes and again stirred at 60 ℃ for 1 hour at the same speed. The obtained liquidly gel-like solution mixture was poured into the aluminum petri dish, and oven dried for 24 hours at 40 ℃. All the films were subjected to conditioning before use by keeping them for one day at 25 ℃ and relative humidity (50%) before peeling them from the dish. Films were noted as CH-HA 0%, CH-HA 1%, CH-HA 3% CH-HA 5%, and CH-HA 10%. Figure 4.1 shows the synthesis step involved in the preparation of CH-HA bionanocomposites film.

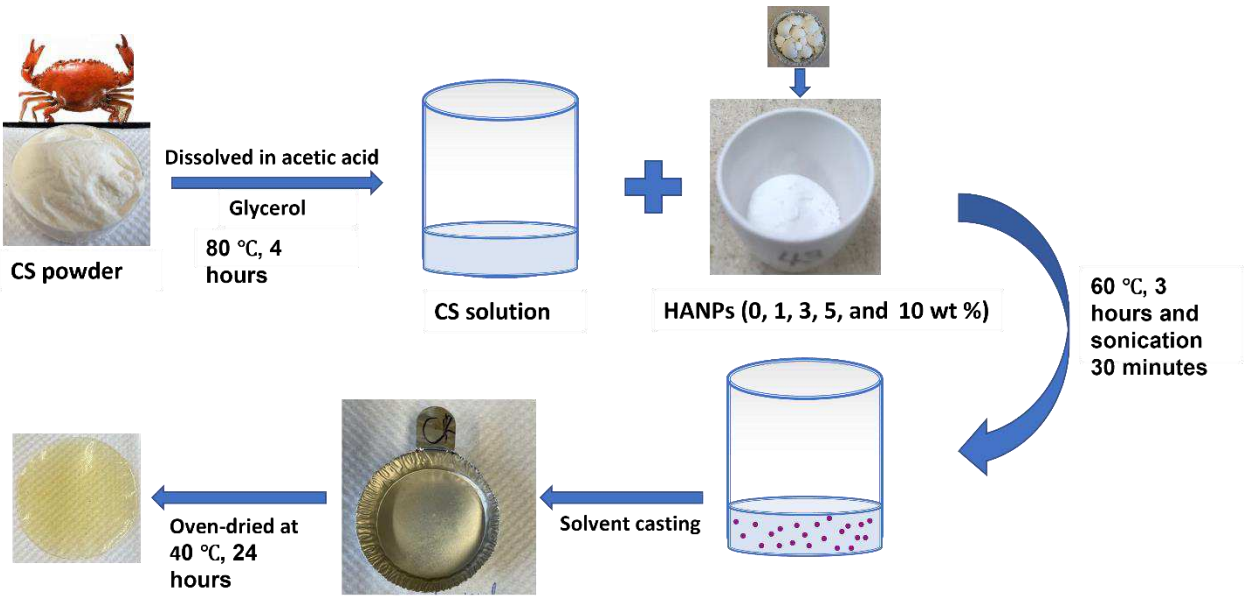

Figure 4.1. Schematic illustration of synthesis of CH-HA bionamocomposites films

4.2.4 Film Thickness

The thickness and width of the films were measured using a digital-Max vernier caliper (USA, Sigma Aldrich). Three different readings of the sample film were taken to calculate the average thickness and used for the determination of the mechanical properties, dynamic mechanical properties, and water vapor properties.

4.2.5 Mechanical properties

Tensile properties of bionanocomposite were measured using the universal tensile testing machine (An Autograph AGS-X, Shimadzu, Canada). Rectangle pieces of the films (50 × 5 mm) were taken for analysis of the films. 50 N static load cell was used according to ASTM standard method D822 to get tensile strength (TS) and percentage of elongation (% E). The initial grid separation (2.5 cm) and crossed-head speed (50 cm/min.) were kept fixed. The peak load was divided by the initial cross-sectional area of the sample to calculate the tensile strength of the

film. (% E) at break was determined by observing the percentage changes between the grip in the length of specimens. Each sample was evaluated in triplicate for accuracy.

4.2.6 Barrier properties

4.2.6.1 Water vapor permeability (WVP)

CH-HA bionamocomposites' water vapor permeability was determined using the previously reported method with minor modifications (Zubair et al. 2019). The film samples were placed in a permeation cell with an exposed film area of $1.95x10^{-3}$ m^2 containing anhydrous calcium hydride with relative humidity (RH) of 0 %. The permeation cell was placed in the desiccator which contained saturated sodium chloride (RH, 75%) solution. The changes in the cell weight were noted every 24 h for 6 days.

4.2.6.2 Water solubility and moisture content

The water solubility and moisture content of the films were evaluated using the gravimetric method (Müller et al. 2011, Yang et al. 2018). First, the film samples were cut in 1× 4 cm^2 and weighed as m_1. After that samples were placed in the oven for drying at 105 ℃ for 1 day to get constant dry weight (m_2). Then dried samples were soaked in the distilled water for 24 hours at room temperature. After that film samples were removed, and air dried for few minutes until achieved constant mass (m_3). Again, after that film samples were oven dried at 105 ℃ until to get constant mass (m_4). Water solubility, moisture content, and swelling degree were calculated using the following equations.

$$\text{Water solubility (\%)} = m_2 - m_4 / m_4 \times 100 \quad (1)$$

$$\text{Moisture content (\%)} = m_1 - m_2 / m_2 \times 100 \quad (2)$$

$$\text{Swelling degree (\%)} = m_3 - m_2 / m_2 \times 100 \quad (3)$$

4.2.7 Structural characterization

4.2.7.1 X-Ray Diffraction (XRD)

XRD of CH-HA films were obtained by using the Rigaku Ultima IV X-Ray Diffractometer (XRD) unit using a copper radiation source (Kα) λ= 1.540 Å with an operating voltage of 38 kV and 38 mA current having a scanning range of 2θ was 5–45° with continuous scanning rate used of 2 degrees per minute with a step size of 0.02. A sample (1.5×1.5 cm) of all the bionanocomposites films was used for scanning the XRD pattern.

4.2.7.2 Fourier Transform Infrared (FTIR) Spectroscopy

Structural analyses (change in the functional group) of Bionanocomposites films were carried out using ATR-FTIR (Bruker Alpha Optics, Platinum ATR, Esslingen Germany) with a single bounce ATR crystal diamond. The FTIR spectra were performed within the wavelength range of 400-4000 cm^{-1} and OPUS software, version 6.5 was used. As a background spectrum, the clean diamond ATR crystal spectrum was taken before running the film samples. OMNIC (Nicolet) software used for processing the data.

4.2.7.3 X-Ray Photoelectron Spectroscopy (XPS)

High resolution C1s spectra and elemental composition survey spectra of bionanocomposites were carried out using XPS. Powder samples of bionanocomposites were used and analyzed by ULTRA-spectrometer, Kratos Analytical, UK with a source of Al Kα X-ray. The base pressure used in the analytical chamber and kept lower than 3×10^{-8} Pa. The charge compensation and aperture slot used in the electron flood gun were 150 W and 400×700 μm^2 respectively. For Ag 3d peak resolution of the instrument was set at 0.55 eV and for Au 4f was at 0.70 eV. For the survey scan, 160 eV (pass energy) and high resolution at 40 eV were used for recording the spectrum. The instrument was calibrated for the binding energy position of C 1s at 284.8 eV. For data processing the Vision-2 instrument software was used.

4.2.8 Morphology and topography

4.2.8.1 Scanning Electron Microscopy (SEM)

The morphology of the CH-HA bionanocomposites were determined by Scanning Electron Microscopy (SEM), Zeiss Sigma 300 VP FESEM operated at 20 kV with a resolution of 10 nm. The small film specimen was put on to the adhesive surface of the stub. All the samples were coated with gold or carbon layer using Leica EM SCD005 (Anatech Ltd.) sputter coater before analyses.

4.2.8.2 Transmission Electron Microscopy (TEM)

Transmission electron microscopic analysis of bionanocomposites were carried out using Philips/FEI Morgagni 268 (Hillsboro, USA) with Gatan digital CCD camera. TEM instrument was operated at accelerating voltage of 80 kV. The films were embedded in SPURR resin, sectioned at ~80nm and mounted on a TEM grid (Ted Pella cat #01802-F), then stained with uranyl acetate and lead citrate before analysis.

4.2.9 Thermal properties

4.2.9.1 Thermogravimetric Analysis (TGA)

The thermal behavior of the CH-HA bionanocomposites was determined by a thermos gravimetric analyzer, TGA Q50 (USA, TA Instruments) under the nitrogen atmospheric flow. The temperature range was kept at 25 ℃ to 600 ℃ for all the films with a heating rate of 10 ℃ per minute. The sample size was taken between 8-12 mg for all the samples.

4.2.9.2 Differential Scanning Colorimetry (DSC)

Thermal properties of CH-HA films were measured by DSC, TA instrument (Q 100, USA) under the continuous flow of nitrogen. All the film samples were measured at the temperature range between 0-350 ℃ using a heating rate of 5 ℃/min. Pure indium was for the calibration of the

instrument for heat flow and temperature aspects.

4.2.9.3 Dynamic Mechanical Analysis (DMA)

The viscoelastic behavior analysis was carried out by a dynamic analyzer (TA Instrument, Q 800) under nitrogen flow at 1 Hz of an oscillatory frequency and amplitude of 15 μm. The sample's length, width, and thickness were measured, and the film was analyzed from -50 to 200 ℃, with a heating rate of 3 ℃/min. The tan δ/loss tangent, loss modulus (E"), and storage modulus (E') were calculated in terms of temperature.

4.2.10 Statistical Analysis

Triplicates of all the synthesized film were used to determine measurement of all the properties and mean values were reported. ANOVA (one-way analysis of Variance) with Tukey's subsequent test was performed to evaluate mechanical and barrier properties data. Statistix 10 statistical analysis software was used to determine significant differences ($p < 0.05$).

4.3 Results and discussion

4.3.1 Mechanical properties of CH-HA bionanocomposites films

Mechanical properties of CH-HA bionanocomposites films are shown in Table 4.1. Several researchers reported that the addition of nanoparticles has significant impact on tensile strength (TS) and percentage elongation (% E) (Kaur et al. 2018) . The reinforcement effect of chitosan with HANPs greatly influence on tensile properties of CH-HA bionanocomposites. CH-HA bionanocomposites blended with HANPs (0, 1, 3, 5, and 10%) showed significant improvement in tensile strength compared to neat chitosan film (without HANPs). TS of chitosan film reinforced with HANPs remarkably increased with increasing HANPs concentration 1 to 3% then further it was noticed slight decreased in 5 % and significant decreased with a 10% addition. Normally, the mechanical properties of polymer nanocomposite reinforced with nano fillers

significantly depends on nano particles dispersion in polymer matrix (Vaia and Giannelis 2001). CH-HA films reinforced with 3% HA noticed the highest TS (73.71 MPa) among all the CH-HA films which is 61.54 % increase compared to neat chitosan film. This is attributed to strong interaction of positive charge amino group (cation) of chitosan with the negative charge hydroxyl group (anion) of hydroxyapatite nanoparticles via hydrogen bonding/ ionic interaction/ Van der Waals forces (Reddy and Rhim 2014). Furthermore, TS significantly decreased with addition of 10 % HANPs (56.72 MPa) but still higher than pure chitosan (CH-HA 0%) (45.36 MPa). This drastic change probably connection of weak interaction between HANPs and chitosan matrix, owing to the formation of HANPs agglomerates, which could lead to poor dispersion in the chitosan matrix. This is also evident as results observed in the SEM. Similar finding reported by other researchers (Deng et al. 2020, Gholizadeh et al. 2018, Jemli et al. 2022).

Flexibility/ductility of chitosan films measured through the % elongation at break (% E) which is also depending on the varied content of HANPs. % Elongation of bionanocomposites film was decreased with increase of HANPs content from 1 to 10%. This decreasing demonstrated the addition of HANPs decreased the deformability of bionanocomposites due to imparted stiffening effect into the chitosan composites (Husseinsyah et al. 2011, Rong et al. 2017).

Table 4.1. Effect of contents of hydroxyapatite nanoparticles (HANPs) on the Tensile Properties of CH-HA bionanocomposites films

Bionanocomposites Film	Thickness (nm)	Tensile Strength (MPa)	Elongation at break (%)
CH-HA 0%	0.09 ± 0.002 [A]	45.36 ± 1.97 [D]	38.58 ± 3.93 [A]
CH-HA 1%	0.09 ± 0.005 [A]	66.64 ± 0.13 [B]	29.13 ± 2.28 [AB]
CH-HA 3%	0.093 ± 0.01 [A]	73.71 ± 3.13 [A]	27.13 ± 0.80 [B]
CH-HA 5%	0.095 ± 0.005 [A]	72.359±0.99 [AB]	22.312±3.11 [B]
CH-HA 10%	0.10 ± 0.02 [A]	56.72 ± 2.98 [C]	22.20 ± 6.41 [B]

[A] Mean value of three replicates ± standard deviation. Average means in the same column observed by the same letter are not significantly different (P > 0.05).

4.3.2 Barrier properties

4.3.2.1 Water Vapor Permeability (WVP)

WVP is an important parameter to measure in food packaging film because it can determine the transmission rate of vapor, speed and amount of water passes through the packing material. Low WVP is desired to enhance the food shelf life and protect the food from direct contact with moisture (Ahari et al. 2022, Aldana et al. 2014, Fakhreddin Hosseini et al. 2013). WVP of CH-HA bionanocomposite is shown in Table 4.2 ranging from 4.65 to 8.85 (gmm/m^2 d k Pa × 10^2). The WVP of neat chitosan film (CH-HA 0%) was 8.85 × 10^2 gmm/m^2 d k Pa and it greatly

decreased after addition of HANPs. Although, the decrease in the WVP of the chitosan bionanocomposite film was depended on dispersion and concentration of the nanofiller. WVP was significantly decreased with an increase in the content of 1 % HANPs down to 4.65×10^2 gmm/m^2 d k Pa (decrease in 52 %), then it increased with increased the HANPs nano filler content but still lower than the neat chitosan film. Mostly, barrier properties of nanocomposite film are better when less permeable nanofillers are dispersed well in the polymer matrix (Rhim et al. 2011). The impermeable HANPs that dispersed in the chitosan polymer matrix which created a tortuous path for water diffusion and led to increase path length for water molecules diffusion thus it is resulting in decrease the water vapor permeability of the nanocomposite (Rhim et al. 2009, Rhim et al. 2006). The results are fairly supported by SEM and TEM analysis.

Table 4.2. Berrier properties of CH-HA bionanocomposites films

Bionanocomposites Film	WVP (gmm/m^2 d k Pa) x10^2	Moisture content (%)	Water solubility (%)
CH-HA 0%	8.85 ± 0.049 ^{A}	14.90 ± 0.07 ^{AB}	26.62 ± 0.01 ^{A}
CH-HA 1%	4.65 ± 0.071 ^{B}	13.06 ± 0.04 ^{B}	16.96 ± 0.07 ^{D}
CH-HA 3%	6.47 ± 0.016 ^{C}	13.14 ± 0.43 ^{B}	17.68 ± 0.19 ^{CD}
CH-HA 5%	6.73 ± 0.016 ^{D}	14.59 ± 1.79 ^{B}	17.93 ± 0.09 ^{C}
CH-HA 10%	7.08 ± 0.029 ^{E}	18.28 ± 0.83 ^{A}	21.26 ± 0.35 ^{B}

^{A}Mean value of three replicates ± standard deviation. Average means in the same column observed by the same letter are not significantly different (P > 0.05).

4.3.2.2 Moisture Content (MC), and Water Solubility (WS) of the films

The results on MC and WS of CH-HA bionanocomposites are shown in table 4.2. The MC and WS of films were affected by the addition of HANPs. Moisture content of bionanocomposites films were decreased by increasing HANPs content probably because of the hydrophobic properties of hydroxyapatite nanoparticles in the films. Due to the increase in HANPs content increased the hydrophilicity, led to surface water adsorption. The WS of bionanocomposites film decreased from 26.62 % of the pure chitosan film (CH-HA 0%) down to 16.96 % of CH-HA film with 1 % inclusion of HANPs, and it increased with further addition of the HANPs but still the lower than pure chitosan film (CH-HA 0%). Based on the diffusion phenomena, HANPs may act as a barrier, and it interfered with water to penetrate the film structure by generating strong hydrogen bond interactions with chitosan. Similar finding reported in 2009, W.W. Thein-Han and R.D.K Misra were studied water adsorption phenomena of chitosan-nano hydroxyapatite scaffold (Thein-Han and Misra 2009). In their finding, they reported that the amount of moisture adsorption increased with increasing nanocrystals, which acted as a barrier. In this process scaffolds, reduced pores numbers on the surface and led to the moisture content decreased.

4.3.3 Structural characterization of the bionanocomposites

4.3.3.1 X-Ray Diffraction (XRD)

X-ray diffractogram of HANPs, neat chitosan powder and CH-HA bionanocomposites are given in Figure 4.2. Synthesized HANPs exhibited most relative reflection peaks at 2θ angle of 25.8°, 28.9°, 31.7°, 32.1°, 32.9°, 34.1°, 39.8°, 46.7°, and 49.5° respectively which are well matched with standard hydroxyapatite (International Centre for Diffraction Data powder diffraction File # 00-009-0432) (Apalangya et al. 2018). The characteristic peaks of HANPs were seen at 2θ of 25.8, 31.7, 32.1, and 32.9° correspond to the (002), (211), (32.1) and (300) reflections of crystallographic plane respectively. The acquired crystal structure of the HANPs is agreement

with earlier reported highly pure crystalline phase of HANPs (Ali et al. 2021, Indira and Malathi 2022). From the XRD graph (figure 2), it can be observed that most of the crystallinity characteristic peaks of HANPs have vanished in 1 % and 3 % CH-HA bionanocomposites. Although, in case of concentration of 5% and 10% CH-HA bionanocomposites film the crystallinity peaks were detained at 2θ° of 25.8, 31.7, 32.1, and 32.9°. However, a significant decrease in intensity of peaks was noticed. These crystallinity peaks of HANPs observed in 5% and 10 % CH-HA bionanocomposites are due to the higher concentration of HANPs, which confirmed that higher concentration of HANPs retained crystallinity in biopolymer structure (Abdollahi et al. 2013, Kaur et al. 2018). The accordance with these results, it was clear that 1% and 3% nanoparticles in CH-HA bionanocomposites films were well dispersed than 5% and 10% CH-HA bionanocomposites film, which were further validated by their SEM and TEM analysis. The XRD results are in agreement with TGA and DSC analysis.

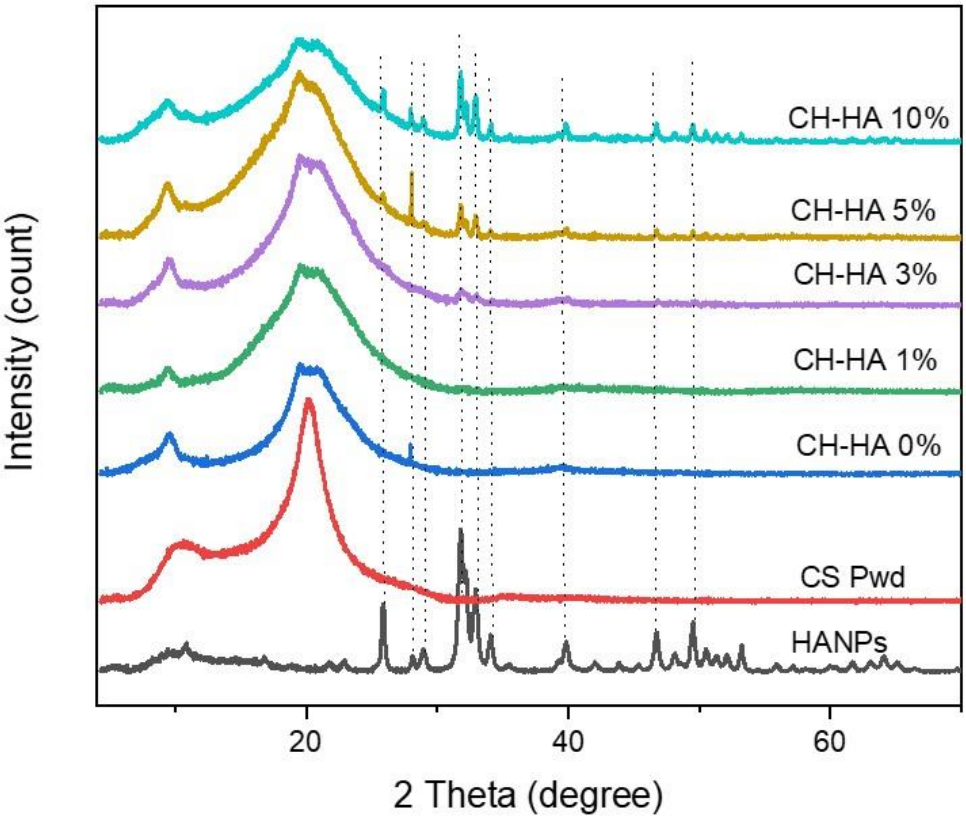

Figure 4.2. X-ray diffractograms of neat chitosan powder (CS Pwd), HANPs, and CH-HA bionanocomposites films

4.3.3.2 Fourier Transform Infrared (FTIR) Spectroscopy

The FTIR spectrum is a useful tool to examine the interaction between biopolymer and nanoparticles. FTIR was used to understand the change in chemical structure of pure chitosan, HANPs, and all the prepared CH-HA bionanocomposites are shown in figure 4.3. All the bionanocomposites showed the characteristic peaks of chitosan at 650.8, 1024.2, 1152, 1377.2, 1405.8, 1548.6, 1656.7, 2854, 2921, and 3289 cm^{-1}. The peaks at 3289 cm^{-1} is attributed to the saccharide vibrational mode corresponding to O-H (intra molecular hydrogen bonding) and N-H stretching vibrational mode, while peaks at 1654.7, 1548.6, and 1309.9 cm^{-1} ascribed to the

presence of amide I (C=O), amide II (N-H) and amide III (C-N) respectively (Ji et al. 2020). The peak at 2860.5 (symmetric) and 2921.7 cm $^{-1}$ (asymmetric) attributed to the C-H vibrational stretching mode. Furthermore, sharp peak at 1152, 1026.3 cm $^{-1}$ are associated with combined effect of C-O and C-N vibrational stretching from the alcohol group in the chitosan (Flauzino Neto et al. 2013, Mincke et al. 2019). In comparison with CH-HA 0% bionanocomposites, 1, 3, 5 and 10 % CH-HA bionanocomposites showed additional peaks at 559.04 and 603 cm $^{-1}$ (O-P-O mode), 469.2 cm $^{-1}$ (P-O stretching) from phosphate group confirmed the incorporation of HANPs in the films (Teixeira et al. 2009). The major change observed in peak intensity and peak broadening change at 3289 cm $^{-1}$, the bionanocomposites with nanoparticles shown much higher intensity than neat chitosan film without nanoparticles it may be because of intra molecular hydrogen bonding. Moreover, other peaks represented for amide I, II and III also exhibited sharp increase in peaks intensity compared to neat chitosan film. Hence, FTIR results confirmed addition of nanoparticles increased interaction between the chitosan matrix and nanofiller. The FTIR results are consistent with XRD and tensile strength analysis results.

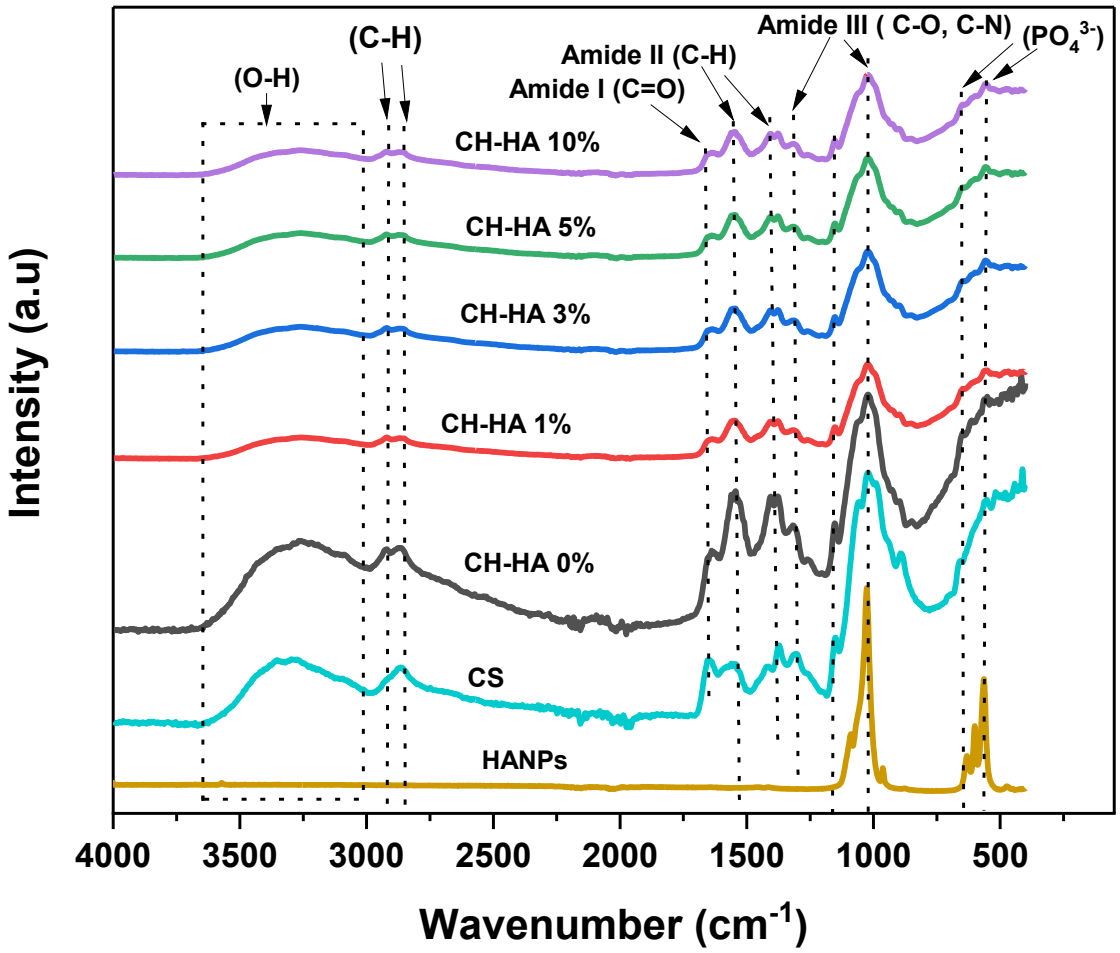

Figure 4.3. FTIR Spectra of neat chitosan powder (CS), HANPs, and CH-HA bionanocomposites films

4.3.3.3 X-Ray Photoelectron Spectroscopy (XPS)

X-ray photoelectron spectroscopy is an important accurate technique to identify and obtained the elemental composition on the surface of the bionanocomposites. Figure 4.4 presents the XPS full-scan survey spectrum of synthesized HANPs and CH-HA bionanocomposites films with and without nanoparticles. The survey scan of all the CH-HA bionanocomposites and HANPs were exposed major key photoelectron peaks, oxygen (O1s) at 530.5 eV, carbon (C1s) at 284 eV and nitrogen (N1s) at 397.5 eV. The additional peak for calcium (Ca 2p) is shown in case of CH-HA

5% and CH-HA 10%, indicating exposure of chitosan and HANPs both on the surface. While, calcium peak not seen by the CH-HA 1% and CH-HA 3 % bionanocomposites, it could be due to the nanofillers homogenous dispersion within the chitosan matrix and not exhibited on the film surface (Deng et al. 2020, Kaur et al. 2018). The oxygen content of the neat chitosan film (CH-HA 0%) was 30.44 %, and it increased to 35.62%, 36.57%, 37.55%, and 36.60% in case of CH-HA 1%, CH-HA 3%, CH-HA 5%, and CH-HA 10% respectively. Increased in O elements proclaimed a high ratio of polar groups, increasing in intramolecular bonding either from the chitosan's $-NH_2$ or -OH with -OH from HANPs and increased hydrophilicity of the CH-HA bionanocomposites films. The N element content increased in case of 1% and 3% CH-HA films compared to neat chitosan film but observed decreasing with 5% and 10% CH-HA bionanocomposites film (Table 4.3), suggesting that relatively higher-ratio of $-NH_2$ group of the chitosan molecule exposed outside and led to the inhomogeneous dispersion of HANPs (Kaur et al. 2018, Ren et al. 2017).

The C1s high resolution XPS spectra of bionanocomposites shown in figure 4.5 confirmed the further changes in chemical structure. According to the previous articles, the peaks were assigned to -C (C-H) at (283-286 eV) and -C (O, N) at (285-288 eV) in chitosan (Liu et al. 2018, Maachou et al. 2013, Machado et al. 2020). Here, we report, C1s spectra of CH-HA 0% film, the assigned peaks to -C (C-H) at 284 and -C (O, N) at 285.5 eV respectively, while CH-HA film with reinforced HANPs demonstrated little change in the binding energy of -C (C-H) and -C (O, N). The peaks -C (C-H) shifted at 283.47 and 283.51 and in case of 1% and 10% CH-HA and peaks -C (O, N) shifted to 284.9 and 285.01 for 1% and 10% CH-HA respectively when compared to CH-HA 0% (Fig. 4.5). The observed in shift peak position attributed to the change in its chemical environment after modification. These results confirmed the diverse interaction

between HANPs and chitosan during modification.

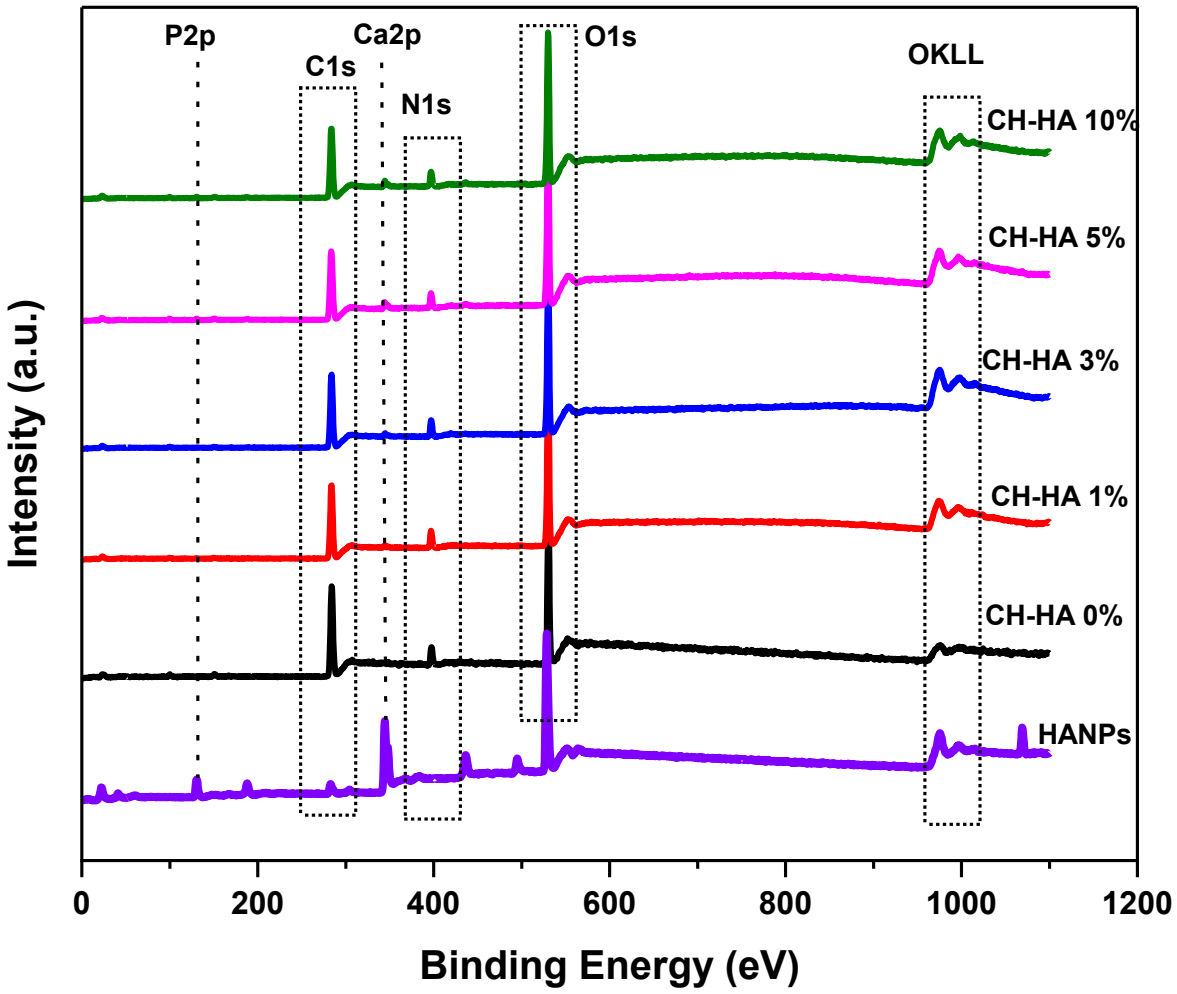

Figure 4.4. XPS survey spectrum of HANPs, and CH-HA bionanocomposites films

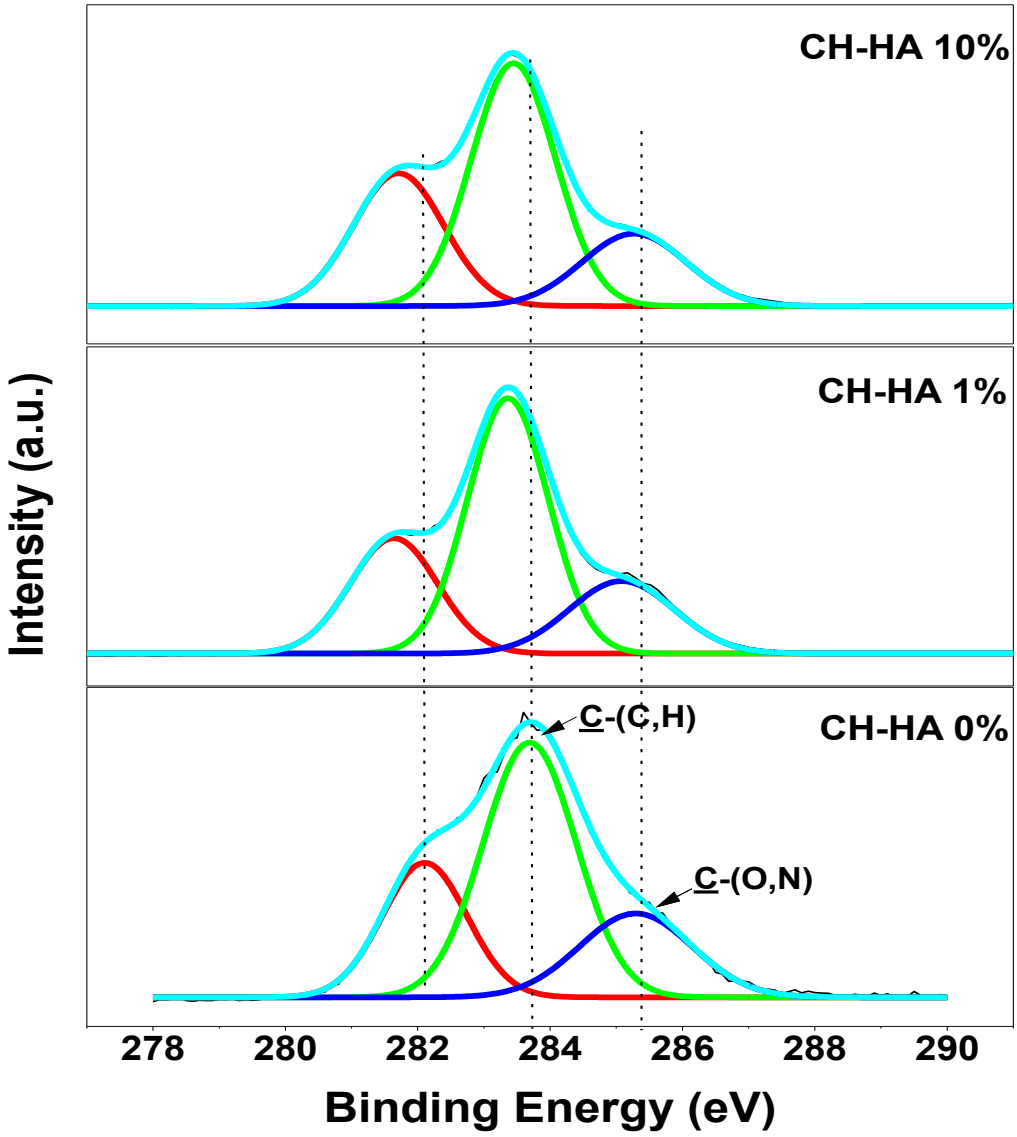

Figure 4.5 XPS high resolution C1s spectrum of 0%,1% and 10% CH-HA bionanocomposites films

Table 4.3 Elemental composition (%) of CH-HA bionanocomposites films

Film samples	O1s	C1s	N1s	Ca 2p
CH-HA 0%	30.44	62.39	5.88	-
CH-HA 1%	36.50	56.48	6.11	-
CH-HA 3%	36.57	56.02	6.25	-
CH-HA 5%	37.55	53.94	5.55	1.16
CH-HA 10%	36.60	54.89	5.69	0.95

4.3.4 Morphology and topography

4.3.4.1 Scanning Electron Microscopy (SEM)

The surface morphology and level of distribution of hydroxyapatite nanoparticles on the chitosan matrix were evaluated by SEM. Figure 6 shows SEM images of synthesized HANPs from eggshell and figure 4.7 exhibits the SEM micrograph of the surface (top view) and the cross-sectional of the 0%, 3% and 10% CH-HA bionanocomposites. The pure chitosan film (CH-HA 0%) exhibited plan smooth surface compared with all the bionanocomposites films with nanoparticles. It can be clearly seen from the images (top view and cross-section) of CH-HA 3 % the nanoparticles were well dispersed in the composite film suggesting exfoliation of hydroxyapatite nanoparticles content in the bionanocomposites while CH-HA 10% showed the HANPs were stacked together, and intercalated structure formed an agglomeration in some area along with some well disperse nanoparticles. SEM results are in good agreement with high mechanical strength of CH-HA bionanocomposites at lower concentration of nanofiller. It is broadly known that good distribution or dispersion of nanofiller into the matrix of polymer enhanced the final properties of nanocomposites (Bourakadi et al. 2019).

4.3.4.2 Transmission Electron Microscopy (TEM)

TEM analyses were done to verify the dispersion of nanoparticles in terms of exfoliation/intercalation. TEM images of HANPs and all the bionanocomposites with and without HANPs nanofiller are displayed in Figure 4.8. The micrograph of CH-HA 1% bionanocomposites film showed well dispersion of nanoparticles due to the exfoliation of HANPs throughout the chitosan matrix. While, in case of 3% HANPs content in the bionanocomposites, the nanofiller were displayed mostly exfoliated with partial intercalated in the chitosan matrix. However, with 5% HANPs, the micrograph has seen mainly exfoliated and intercalated structures, suggesting the sonication time can improve to get good dispersion of the nanoparticles. In the case of CH-HA 10% bionanocomposites film clearly showed phase separation due to larger aggregated region. The magnitude of dispersion is more in 1% and 3% CH-HA films as compared to 5 and 10% CH-HA bionanocomposites. These TEM results in accordance with XRD results, where crystallinity peaks of HANPs have been vanished in the bionanocomposites with lower concentration of nanofiller. A similar finding has been reported by Kaur et al. (Kaur et al. 2018). The average size of rod like nanoparticles were found to be 25-30 nm (diameter) and 40-70 nm in length (using software J).

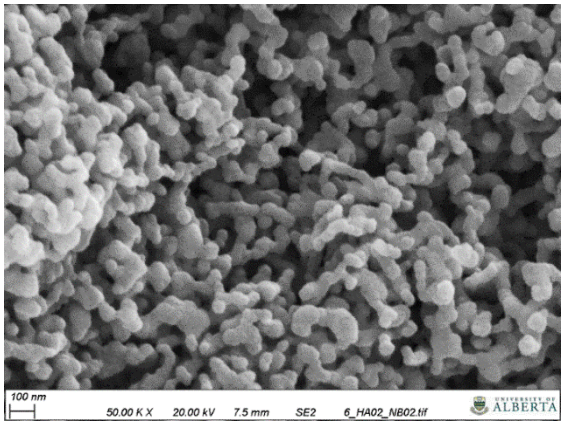

Figure 4.6. SEM image of synthesized HANPs from eggshell

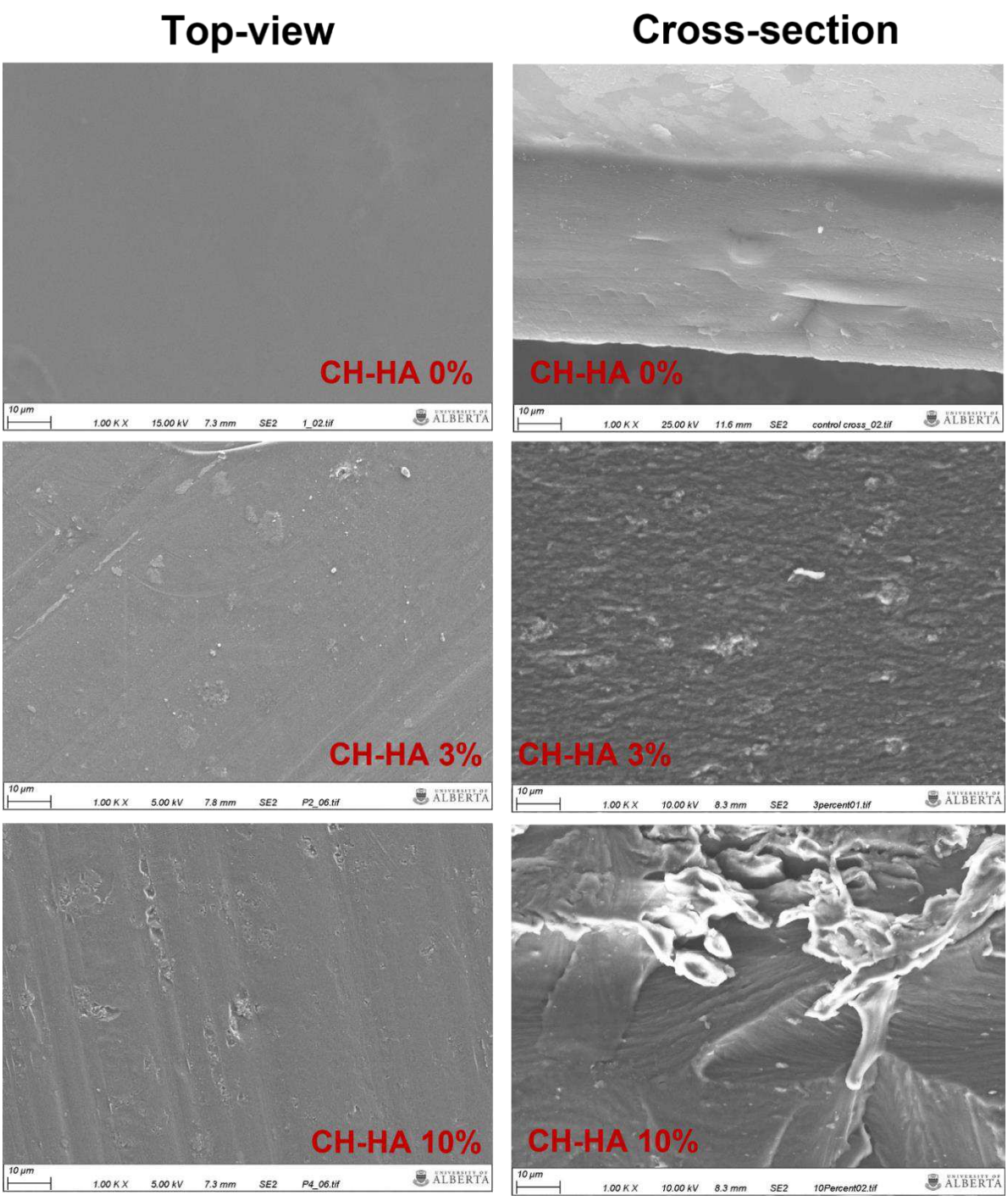

Figure 4.7. SEM images of surface (Top-view) and cross- section micrographs of CH-HA bionanocomposites films

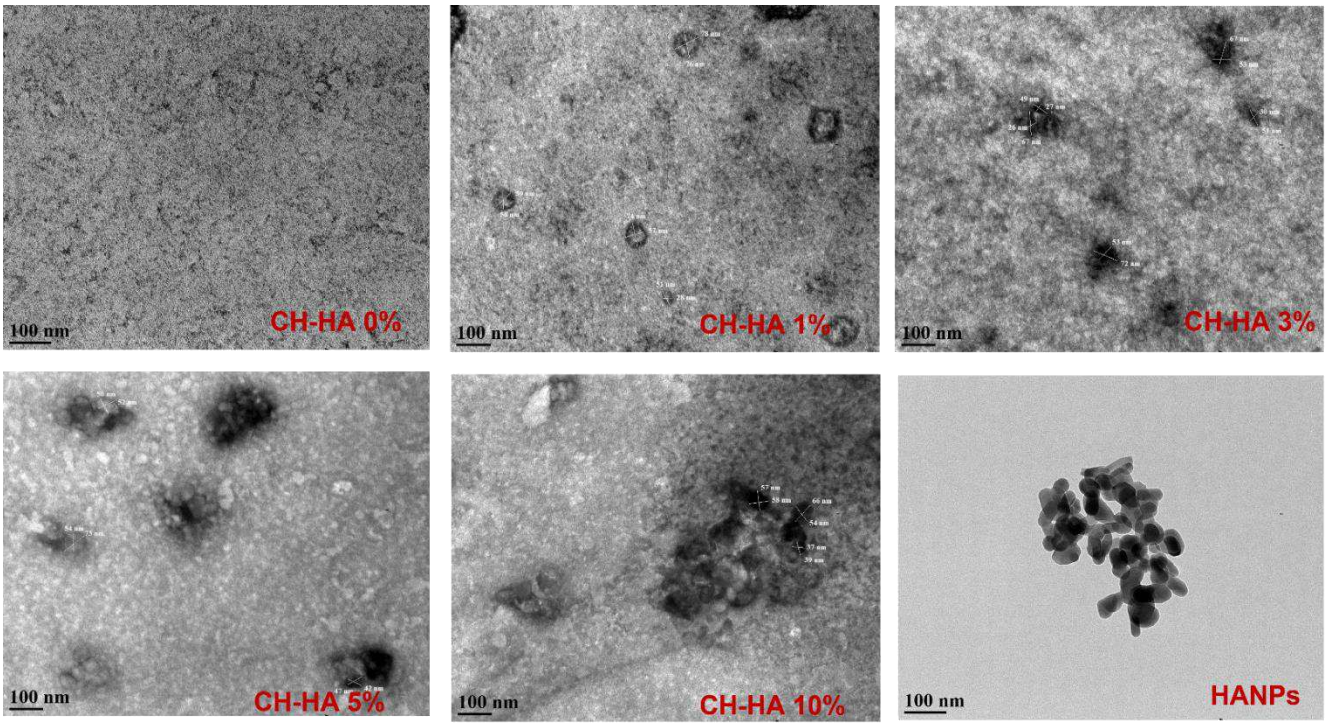

Figure 4.8. TEM micrographs of CH-HA bionanocomposites films reinforced with 0, 1, 3,5 and 10% HANPs and HANPs

4.3.5 Thermal properties

4.3.5.1 Thermogravimetric Analysis (TGA)

TGA analysis was done to observe changes in thermal stability and degradation behavior of all the CH-HA bionanocomposites with and without HANPs. The TGA and DTG (differential thermo-gravimetric analysis) curves of CH-HA bionanocomposites are represented in figure 4.9 (a and b). All the CH-HA composites showed the main three wight loss stages. The first initial weight loss up to 8-9% have seen at 50-130 ℃ because of evaporation of moisture content in its structure (Reddy et al. 2015), the second stage of weight loss observed up to 45-50% at in

between the range of 140 to 400 ^{0}C due to degradation of glycerol and chitosan components (Mohammadi sadati et al. 2022, Riaz et al. 2020, Zima 2018). The major breakdown of chitosan occurs at 140-310 ℃ because of deacetylation and depolymerization of glycosidic linkage in chitosan. The third and final weight loss happened at in between the 400-600 ℃ in temperature range corresponding to the degradation/breakdown of carbonaceous, low molecular gas residue into the char due to oxidation and burning (Bonilla et al. 2018, Yang et al. 2018). It was observed from the TGA data, neat chitosan film (CH-HA 0%) showed the total weight loss of 60% at 374 ℃, while CH-HA 1% and CH-HA 3% exhibited total weight loss of 60% at delayed temperature of 383 ℃ and 404 ℃ respectively. The delayed temperature shown in 1% and 3 % films could be for the stronger interaction of chitosan matrix with nanofillers and led to better thermal stability.

The DTG curve also displayed the three stages of weight loss (Fig. 4.9 (b)) except CH-HA 10%, where first stage moisture loss peak is missing. The first wight loss stage occurred below 100 ℃ for all the CH-HA bionanocomposites films (except CH-HA 10%), due to the mostly evaporation of moisture content, which could be loosely bounded to the plasticizer glycerol and chitosan molecules. In the second stage of weight loss 5% and 10 % films exhibited early weight loss peaks compared to other bionanocomposites films may be due to the weak interaction of HANPs and glycerol with chitosan. While 1% and 3% homogeneous films showed strong interaction of glycerol and chitosan molecules with nanofiller, shown weight loss at higher temperature than that of CH-HA 0%. This proved that lower concentration of 1 and 3% HANPs into chitosan film increased thermal stability. Similar kind of degradation pattern has been reported by other researchers (Grevellec et al. 2001, Kaur et al. 2018). The main third stage showed maximum weight loss due to the degradation of chitosan, where DTG graph appeared delayed peak in case

of CH-HA 1% and 3% bionanocomposites film at 285 ℃ compared with control chitosan films (281 ℃) due to the better dispersion of nanoparticles in the chitosan matrix. These results supported by XRD, FTIR, SEM and TEM analysis.

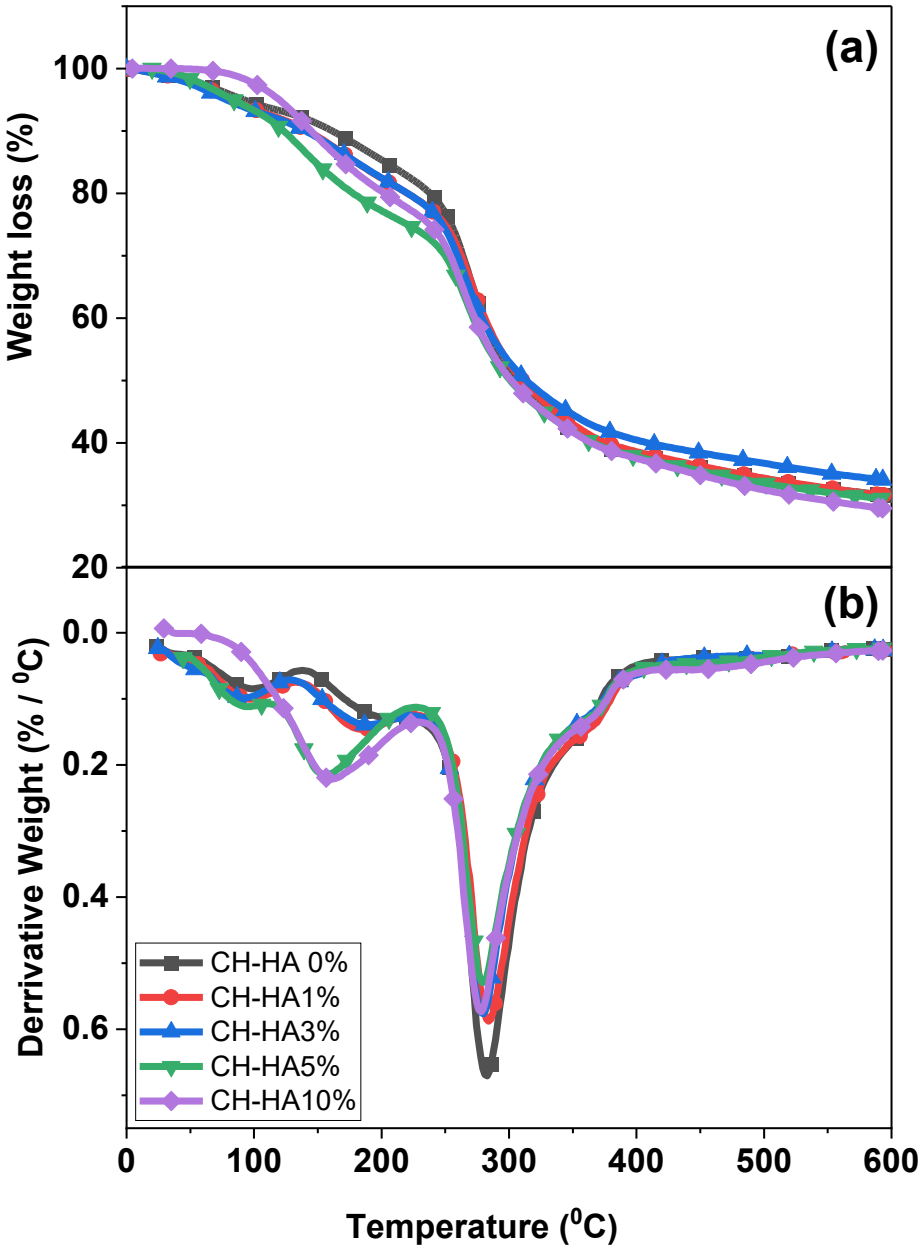

Figure 4.9. (a) TGA and (b) DTG curve of CH-HA bionanocomposites films

4.3.5.2 Differential Scanning Colorimetry (DSC)

The thermal behavior of control chitosan film and its bionanocomposites reinforced with nanofiller HANPs were evaluated using DSC by heating samples from 0 to 350 ℃ and shown in figure 4.10. Control chitosan film exhibited two endothermic peaks at 115 ℃ and 190 ℃ and one exothermic peak at 286 ℃. The first peak at 115 ℃ mainly due to the evaporation of moisture content from chitosan matrix and solvent and second peak at 195 ℃ refers to the melting of the crystalline chitosan structure, and glycerol described as a melting temperature of chitosan (Rao and Johns 2008). The exothermic peak at 286 ℃ due to phase inversion temperature of decomposition of amine unit in chitosan (Ferrero and Periolatto 2012, Kaya et al. 2018). The DSC graph of bionanocomposites reinforced with HANPs, CH-HA 1 % exhibited delayed moisture loss peak at 125 ℃ compared to control chitosan film, as well as all other CH-HA bionanocomposites film. This proved well dispersion of the nanoparticles into the chitosan matrix and due to less polar group available on the surface make the moisture loss difficult (Kaur et al. 2018, Peng et al. 2013). Same trend showed for the crystalline melting temperature (T_m) peaks shift of CH-HA 1% showed delayed at 205 ℃ compared to CH-HA 0% (195 ℃) which could be again better homogeneity of the composite. Similar kind of results observed by Kaur et al. while studying reinforcing effect of inorganic nanoparticles, Montmorillonite (MMT) on Keratin (Kaur et al. 2018).

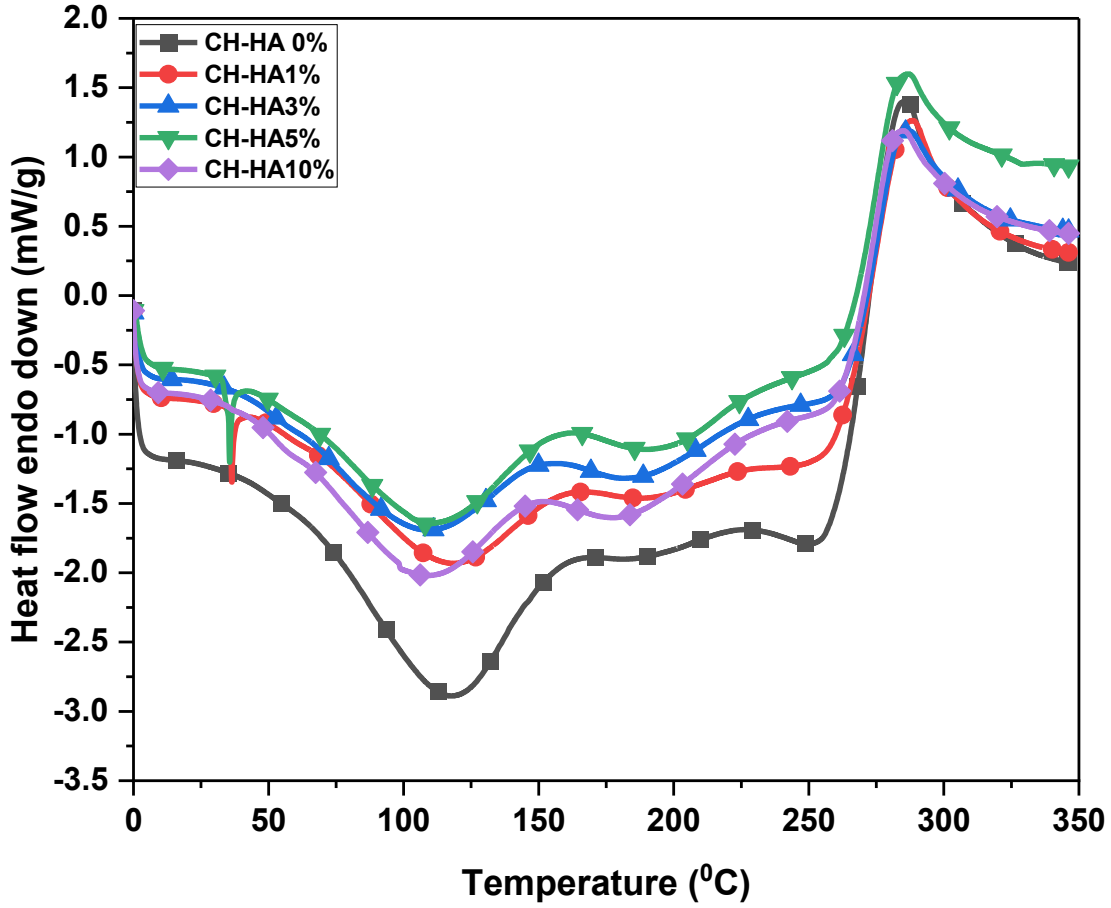

Figure 4.10. DSC curve of CH-HA bionanocomposites films with and without HANPs

4.3.5.3 Dynamic Mechanical Analysis (DMA)

DMA performed to see viscoelastic behavior of all the synthesized bionanocomposites (CH-HA) in terms of changes in storage modulus and damping or tan-delta with change in temperature. Thermal transitions usually occur due to chain mobility of materials/polymers with the temperature change. The glass transition is the most important transition, which is associated with beginning of chain motion, and it is determined from the peak of damping or tan-delta curve. Effect of temperature on the storage modules (E') and tan-delta (tan δ) for all the CH-HA bionanocomposites displayed in figure 4.11 (a) and (b) respectively. Figure 4.11 (a), 0% and 10% CH-HA nanocomposites film showed the highest storage modules (E') at -50 ℃ in all the

composites. With increasing in temperature all bionanocomposites displayed gradual decrease. This gradual decrease in storage modulus in all the composites varies from -40 to 40 °C like synthetic polymers and its characteristics (glassy to rubbery state) related to the thermoplastic material characteristic. CH-HA 0% showed high E' until temperature 114 °C compared to all other bionanocomposites due to its semi crystalline nature. Similar results reported by Noha G. Madian and Noha Mohamed in their work (Madian and Mohamed 2020). However, CH-HA 1 % and 3 % demonstrated high E' above the 115 °C which might be attributed to very stable interaction of chitosan, HANPs and glycerol and similar trend also reported by Kaur et al. (Kaur et al. 2018).

The effect of temperature on tan δ curve observed two main transition peaks for the all the CH-HA bionanocomposites and may be attributed to the weak or strong interaction between plasticizer glycerol, chitosan and nanofiller HANPs. The first peak may be attributed to glycerol-rich region and the second peak could be nanoparticle-rich region. Earlier, similar kind of behavior between glycerol (plasticizer), biopolymers and nanoparticles have been reported (Ullah et al. 2011, Zubair et al. 2019). The glass transition temperature (T_g) for 0%, 1%, 3%, 5% and 10% CH-HA bionanocomposites films were 141, 155, 156, 142 and 135 respectively. In case of CH-HA 1% and 3%, higher (T_g) with broad peaks were observed than the control chitosan film, which could be attributed to better interaction of nanoparticles (hindrance in chitosan chain mobility) into the chitosan matrix and increased the crosslinking ability leading to the better dispersion of HANPs in the composites. However, 5% and 10% CH-HA composites showed lower T_g with narrow peaks displayed poor dispersion of HANPs due to the weak bonding between nanoparticles, chitosan, and glycerol. Literature also supports influence of concentration of nanofillers in the polymer matrix effect the T_g value (Tomaszewska et al. 2021).

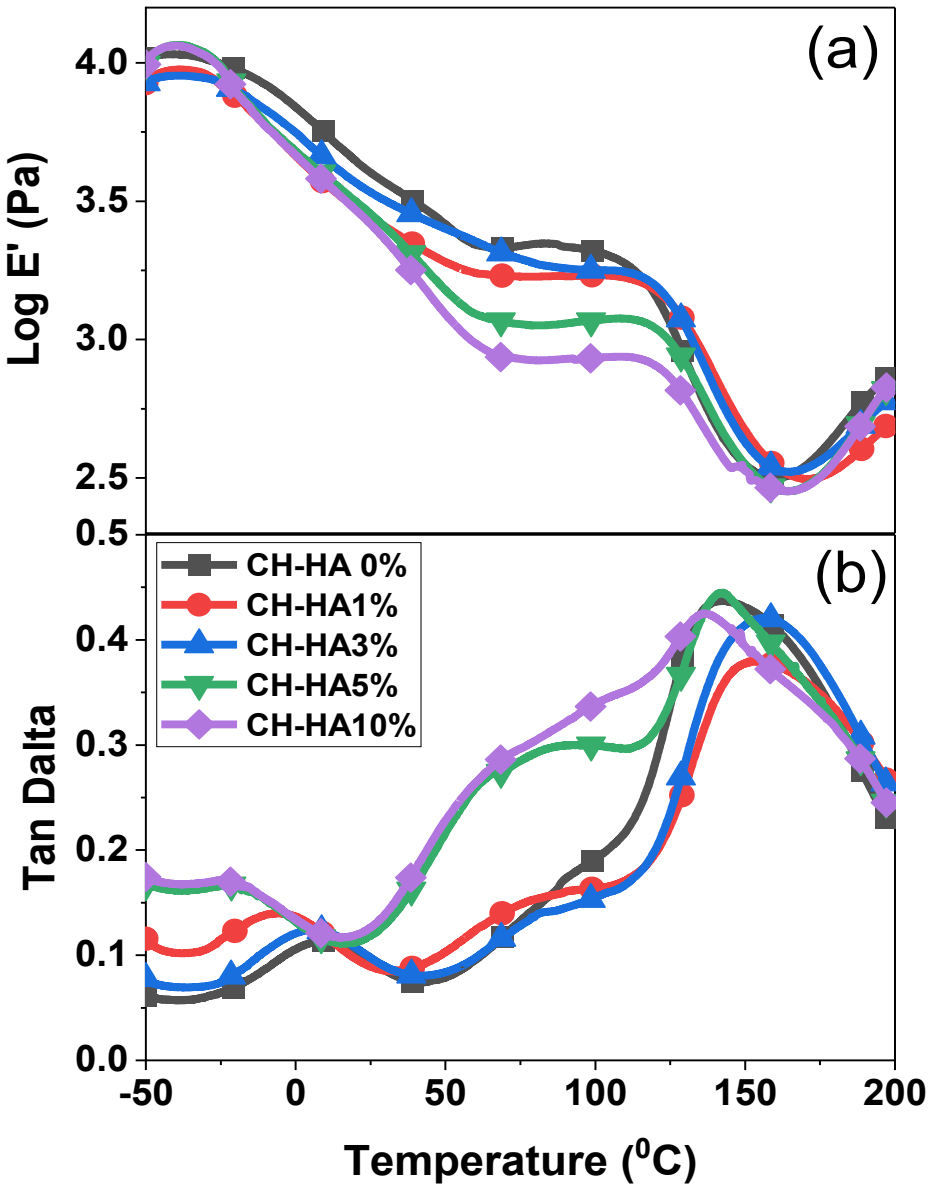

Figure 4.11. DMA curve (a) effect of temperature on log E' and (b) tan delta of CH-HA bionanocomposites films with and without HANPs

4.4 Conclusions

In this work, chitosan-based bionanocomposites reinforced with HANPs were prepared by solvent casting method without any cross-linking agent (glycerol was used as a plasticizer). The results clearly indicated the addition of HANPs showed exceptional mechanical and barrier properties of bionanocomposites film. In the case of film with 3% HANPs content demonstrated highest tensile strength (61.54 % increase compared to neat chitosan film), 1% HANPs content exhibited decrease in WVP (52 %). SEM, TEM and XRD analysis confirmed the 1 and 3 % HANPs content uniformly dispersed (exfoliated to partial intercalated) in the bionanocomposites. However, aggregation is shown at higher concentration (5% and 10%). XPS and FTIR analysis revealed the chemical change occurred due to addition of HANPs. DSC results exhibited improved thermal stability with lower concentration (1%). DMA analysis confirmed the high storage modulus and glass transition showed stable interaction of chitosan, HANPs and glycerol. Overall, the incorporation of HANPs at lower concentration 1% and 3% not only enhanced the thermo-mechanical properties but also showed great enhancement in barrier properties. However, antimicrobial and antioxidant properties of these prepared bionanocomposites need to be determined their claim for as an effective active food packaging.

References

Abdollahi, M., Alboofetileh, M., Rezaei, M. and Behrooz, R. (2013) Comparing physico-mechanical and thermal properties of alginate nanocomposite films reinforced with organic and/or inorganic nanofillers. Food Hydrocolloids 32, 416-424.

Ahari, H., Golestan, L., Anvar, S.A.A., Cacciotti, I., Garavand, F., Rezaei, A., Sani, M.A. and Jafari, S.M. (2022) Bio-nanocomposites as food packaging materials; the main production techniques and analytical parameters. Advances in Colloid and Interface Science 310, 102806.

Aldana, D.S., Villa, E.D., De Dios Hernández, M., Sánchez, G.G., Cruz, Q.R., Gallardo, S.F., Castillo, H.P. and Casarrubias, L.B. (2014) Barrier Properties of Polylactic Acid in Cellulose Based Packages Using Montmorillonite as Filler. Polymers 6(9), 2386-2403.

Ali, A.F., Alrowaili, Z.A., El-Giar, E.M., Ahmed, M.M. and El-Kady, A.M. (2021) Novel green synthesis of hydroxyapatite uniform nanorods via microwave-hydrothermal route using licorice root extract as template. Ceramics International 47(3), 3928-3937.

Apalangya, V., Rangari, V., Jeelani, S., Dankyi, E., Yaya, A. and Darko, S. (2018) Rapid microwave synthesis of needle-liked hydroxyapatite nanoparticles via template directing ball-milled spindle-shaped eggshell particles. Ceramics International 44(6), 7165-7171.

Arikan, E.B. and Ozsoy, H.D. (2015) A review: investigation of bioplastics. Journal of Civil Engineering and Architecture 9(2), 188-192.

Bonilla, J., Poloni, T., Lourenço, R.V. and Sobral, P.J.A. (2018) Antioxidant potential of eugenol and ginger essential oils with gelatin/chitosan films. Food Bioscience 23, 107-114.

Bourakadi, K.E., Merghoub, N., Fardioui, M., Mekhzoum, M.E.M., Kadmiri, I.M., Essassi, E.M., Qaiss, A.e.K. and Bouhfid, R. (2019) Chitosan/polyvinyl alcohol/thiabendazoluim-montmorillonite bio-nanocomposite films: Mechanical, morphological and antimicrobial properties. Composites Part B: Engineering 172, 103-110.

Cui, H., Surendhiran, D., Li, C. and Lin, L. (2020) Biodegradable zein active film containing

chitosan nanoparticle encapsulated with pomegranate peel extract for food packaging. Food Packaging and Shelf Life 24, 100511.

Cunha, C.S., Castro, P.J., Sousa, S.C., Pullar, R.C., Tobaldi, D.M., Piccirillo, C. and Pintado, M.M. (2020) Films of chitosan and natural modified hydroxyapatite as effective UV-protecting, biocompatible and antibacterial wound dressings. International Journal of Biological Macromolecules 159, 1177-1185.

Dash, K.K., Deka, P., Bangar, S.P., Chaudhary, V., Trif, M. and Rusu, A. (2022) Applications of Inorganic Nanoparticles in Food Packaging: A Comprehensive Review. Polymers 14(3), 521.

Deng, L., Li, Y., Zhang, A. and Zhang, H. (2020) Characterization and physical properties of electrospun gelatin nanofibrous films by incorporation of nano-hydroxyapatite. Food Hydrocolloids 103, 105640.

Dong, W., Su, J., Chen, Y., Xu, D., Cheng, L., Mao, L., Gao, Y. and Yuan, F. (2022) Characterization and antioxidant properties of chitosan film incorporated with modified silica nanoparticles as an active food packaging. Food Chem 373, 131414.

Fakhreddin Hosseini, S., Rezaei, M., Zandi, M. and Ghavi, F.F. (2013) Preparation and functional properties of fish gelatin-chitosan blend edible films. Food Chem 136(3-4), 1490-1495.

Ferrero, F. and Periolatto, M. (2012) Antimicrobial finish of textiles by chitosan UV-curing. Journal of nanoscience and nanotechnology 12(6), 4803-4810.

Flauzino Neto, W.P., Silvério, H.A., Dantas, N.O. and Pasquini, D. (2013) Extraction and characterization of cellulose nanocrystals from agro-industrial residue – Soy hulls. Industrial Crops and Products 42, 480-488.

Gasti, T., Dixit, S., Hiremani, V.D., Chougale, R.B., Masti, S.P., Vootla, S.K. and Mudigoudra, B.S. (2022) Chitosan/pullulan based films incorporated with clove essential oil loaded chitosan-ZnO hybrid nanoparticles for active food packaging. Carbohydrate Polymers 277, 118866.

Gholizadeh, B.S., Buazar, F., Hosseini, S.M. and Mousavi, S.M. (2018) Enhanced antibacterial activity, mechanical and physical properties of alginate/hydroxyapatite bionanocomposite film. International Journal of Biological Macromolecules 116, 786-792.

Ghosh, T., Mondal, K., Giri, B.S. and Katiyar, V. (2021) Silk nanodisc based edible chitosan nanocomposite coating for fresh produces: A candidate with superior thermal, hydrophobic, optical, mechanical and food properties. Food Chem 360, 130048.

Goel, V., Luthra, P., Kapur, G.S. and Ramakumar, S.S.V. (2021) Biodegradable/Bio-plastics: Myths and Realities. Journal of Polymers and the Environment 29(10), 3079-3104.

Goh, K.W., Wong, Y.H., Ramesh, S., Chandran, H., Krishnasamy, S., Ramesh, S., Sidhu, A. and Teng, W.D. (2021) Effect of pH on the properties of eggshell-derived hydroxyapatite bioceramic synthesized by wet chemical method assisted by microwave irradiation. Ceramics International 47(7, Part A), 8879-8887.

Grevellec, J., Marquié, C., Ferry, L., Crespy, A. and Vialettes, V. (2001) Processability of Cottonseed Proteins into Biodegradable Materials. Biomacromolecules 2(4), 1104-1109.

Haghighi, H., Licciardello, F., Fava, P., Siesler, H.W. and Pulvirenti, A. (2020) Recent advances on chitosan-based films for sustainable food packaging applications. Food Packaging and Shelf Life 26, 100551.

Husseinsyah, S., Amri, F., Husin, K. and Ismail, H. (2011) Mechanical and thermal properties of chitosan-filled polypropylene composites: The effect of acrylic acid. Journal of Vinyl and Additive Technology 17(2), 125-131.

Indira, J. and Malathi, K.S. (2022) Comparison of template mediated ultrasonic and microwave irradiation method on the synthesis of hydroxyapatite nanoparticles for biomedical applications. Materials Today: Proceedings 51, 1765-1769.

Jakubowska, E., Gierszewska, M., Nowaczyk, J. and Olewnik-Kruszkowska, E. (2020) Physicochemical and storage properties of chitosan-based films plasticized with deep eutectic solvent. Food Hydrocolloids 108, 106007.

Jemli, Y.E., Abdelouahdi, K., Minh, D.P., Barakat, A. and Solhy, A. (2022) Design and Applications of Hydroxyapatite-Based Catalysts, pp. 19-72.

Ji, Y., Yang, X., Ji, Z., Zhu, L., Ma, N., Chen, D., Jia, X., Tang, J. and Cao, Y. (2020) DFT-Calculated IR Spectrum Amide I, II, and III Band Contributions of N-Methylacetamide Fine Components. ACS omega 5(15), 8572-8578.

Kaur, M., Arshad, M. and Ullah, A. (2018) In-Situ Nanoreinforced Green Bionanomaterials from Natural Keratin and Montmorillonite (MMT)/Cellulose Nanocrystals (CNC). ACS Sustainable Chemistry & Engineering 6(2), 1977-1987.

Kaya, M., Khadem, S., Cakmak, Y.S., Mujtaba, M., Ilk, S., Akyuz, L., Salaberria, Asier M., Labidi, J., Abdulqadir, A.H. and Deligöz, E. (2018) Antioxidative and antimicrobial edible chitosan films blended with stem, leaf and seed extracts of Pistacia terebinthus for active food packaging. RSC Advances 8(8), 3941-3950.

Khanzada, B., Mirza, B. and Ullah, A. (2023) Chitosan based bio-nanocomposites packaging films with unique mechanical and barrier properties. Food Packaging and Shelf Life 35, 101016.

Lebreton, L. and Andrady, A. (2019) Future scenarios of global plastic waste generation and disposal. Palgrave Communications 5(1), 6.

Li, L., Iqbal, J., Zhu, Y., Zhang, P., Chen, W., Bhatnagar, A. and Du, Y. (2018) Chitosan/Ag-hydroxyapatite nanocomposite beads as a potential adsorbent for the efficient removal of toxic aquatic pollutants. International Journal of Biological Macromolecules 120, 1752-1759.

Li, S., Mu, B., Zhang, H., Kang, Y. and Wang, A. (2022) Incorporation of silver nanoparticles/curcumin/clay minerals into chitosan film for enhancing mechanical properties, antioxidant and antibacterial activity. International Journal of Biological Macromolecules 223, 779-789.

Liu, Y., Deng, L., Zhang, C., Chen, K., Feng, F. and Zhang, H. (2018) Comparison of ethyl cellulose–gelatin composite films fabricated by electrospinning versus solvent casting. Journal of Applied Polymer Science 135(46), 46824.

Maachou, H., Genet, M.J., Aliouche, D., Dupont-Gillain, C.C. and Rouxhet, P.G. (2013) XPS analysis of chitosan–hydroxyapatite biomaterials: from elements to compounds. Surface and Interface Analysis 45(7), 1088-1097.

Machado, B.R., Facchi, S.P., de Oliveira, A.C., Nunes, C.S., Souza, P.R., Vilsinski, B.H., Popat, K.C., Kipper, M.J., Muniz, E.C. and Martins, A.F. (2020) Bactericidal pectin/chitosan/glycerol films for food pack coatings: A critical viewpoint. International journal of molecular sciences 21(22), 8663.

Madian, N.G. and Mohamed, N. (2020) Enhancement of the dynamic mechanical properties of chitosan thin films by crosslinking with greenly synthesized silver nanoparticles. Journal of Materials Research and Technology 9(6), 12970-12975.

Mincke, S., Asere, T.G., Verheye, I., Folens, K., Bussche, F.V., Lapeire, L., Verbeken, K., Van Der Voort, P., Tessema, D.A. and Fufa, F. (2019) Functionalized chitosan adsorbents allow recovery of palladium and platinum from acidic aqueous solutions. Green Chemistry 21(9), 2295-2306.

Mohammadi sadati, S.M., Shahgholian-Ghahfarrokhi, N., Shahrousvand, E., Mohammadi-Rovshandeh, J. and Shahrousvand, M. (2022) Edible chitosan/cellulose nanofiber nanocomposite films for potential use as food packaging. Materials Technology 37(10), 1276-1288.

Morsy, R., Ali, S.S. and El-Shetehy, M. (2017) Development of hydroxyapatite-chitosan gel sunscreen combating clinical multidrug-resistant bacteria. Journal of Molecular Structure 1143, 251-258.

Müller, C.M.O., Laurindo, J.B. and Yamashita, F. (2011) Effect of nanoclay incorporation method on mechanical and water vapor barrier properties of starch-based films. Industrial Crops and Products 33(3), 605-610.

Nazeer, M.A., Yilgör, E. and Yilgör, I. (2017) Intercalated chitosan/hydroxyapatite nanocomposites: promising materials for bone tissue engineering applications. Carbohydrate Polymers 175, 38-46.

Peng, Y., Wu, Y. and Li, Y. (2013) Development of tea extracts and chitosan composite films for active packaging materials. International Journal of Biological Macromolecules 59, 282-289.

Priyadarshi, R., Roy, S., Ghosh, T., Biswas, D. and Rhim, J.-W. (2021) Antimicrobial nanofillers reinforced biopolymer composite films for active food packaging applications-a review. Sustainable Materials and Technologies, e00353.

Ramji, V. and Vishnuvarthanan, M. (2022) Chitosan Ternary Bio Nanocomposite Films Incorporated with MMT K10 Nanoclay and Spirulina. Silicon 14(3), 1209-1220.

Rao, V. and Johns, J. (2008) Thermal behavior of chitosan/natural rubber latex blends TG and DSC analysis. Journal of Thermal Analysis and Calorimetry 92(3), 801-806.

Reddy, J.P. and Rhim, J.-W. (2014) Characterization of bionanocomposite films prepared with agar and paper-mulberry pulp nanocellulose. Carbohydrate Polymers 110, 480-488.

Reddy, N., Reddy, R. and Jiang, Q. (2015) Crosslinking biopolymers for biomedical applications. Trends in Biotechnology 33(6), 362-369.

Ren, Y., Xu, L., Wang, C., Wang, X., Ding, Z. and Chen, Y. (2017) Effect of dielectric barrier discharge treatment on surface nanostructure and wettability of polylactic acid (PLA) nonwoven fabrics. Applied Surface Science 426, 612-621.

Rhim, J.-W., Hong, S.-I. and Ha, C.-S. (2009) Tensile, water vapor barrier and antimicrobial properties of PLA/nanoclay composite films. LWT-Food Science and Technology 42(2), 612-617.

Rhim, J.-W., Hong, S.-I., Park, H.-M. and Ng, P.K.W. (2006) Preparation and Characterization of Chitosan-Based Nanocomposite Films with Antimicrobial Activity. Journal of Agricultural and Food Chemistry 54(16), 5814-5822.

Rhim, J.W., Lee, S.B. and Hong, S.I. (2011) Preparation and characterization of agar/clay nanocomposite films: the effect of clay type. Journal of food science 76(3), N40-N48.

Riaz, A., Lagnika, C., Luo, H., Dai, Z., Nie, M., Hashim, M.M., Liu, C., Song, J. and Li, D. (2020) Chitosan-based biodegradable active food packaging film containing Chinese chive (Allium tuberosum) root extract for food application. International Journal of Biological Macromolecules 150, 595-604.

Rinaudo, M. (2006) Chitin and chitosan: Properties and applications. Progress in Polymer Science 31(7), 603-632.

Rong, S.Y., Mubarak, N.M. and Tanjung, F.A. (2017) Structure-property relationship of cellulose nanowhiskers reinforced chitosan biocomposite films. Journal of Environmental Chemical Engineering 5(6), 6132-6136.

Shikinaka, K., Nakamura, M. and Otsuka, Y. (2020) Strong UV absorption by nanoparticulated lignin in polymer films with reinforcement of mechanical properties. Polymer 190, 122254.

Spirescu, V.A., Chircov, C., Grumezescu, A.M., Vasile, B.Ș. and Andronescu, E. (2021) Inorganic Nanoparticles and Composite Films for Antimicrobial Therapies. International journal of molecular sciences 22(9), 4595.

Teixeira, S., Rodriguez, M., Pena, P., De Aza, A., De Aza, S., Ferraz, M. and Monteiro, F. (2009) Physical characterization of hydroxyapatite porous scaffolds for tissue engineering. Materials Science and Engineering: C 29(5), 1510-1514.

Thein-Han, W.W. and Misra, R.D. (2009) Biomimetic chitosan-nanohydroxyapatite composite scaffolds for bone tissue engineering. Acta Biomater 5(4), 1182-1197.

Tomaszewska, J., Sterzyński, T., Woźniak-Braszak, A. and Banaszak, M. (2021) Review of Recent Developments of Glass Transition in PVC Nanocomposites. Polymers 13(24), 4336.

Trakoolwannachai, V., Kheolamai, P. and Ummartyotin, S. (2019) Development of hydroxyapatite from eggshell waste and a chitosan-based composite: In vitro behavior of human osteoblast-like cell (Saos-2) cultures. International Journal of Biological Macromolecules 134, 557-564.

Ullah, A., Vasanthan, T., Bressler, D., Elias, A.L. and Wu, J. (2011) Bioplastics from Feather Quill. Biomacromolecules 12(10), 3826-3832.

Ummartyotin, S. and Tangnorawich, B. (2015) Utilization of eggshell waste as raw material for synthesis of hydroxyapatite. Colloid and Polymer Science 293(9), 2477-2483.

Vaia, R.A. and Giannelis, E.P. (2001) Liquid crystal polymer nanocomposites: direct intercalation of thermotropic liquid crystalline polymers into layered silicates. Polymer 42(3), 1281-1285.

Yang, J., Xiong, L., Li, M. and Sun, Q. (2018) Chitosan–Sodium Phytate Films with a Strong Water Barrier and Antimicrobial Properties Produced via One-Step-Consecutive-Stripping and Layer-by-Layer-Casting Technologies. Journal of Agricultural and Food Chemistry 66(24), 6104-6115.

Zhang, X., Liu, D., Jin, T.Z., Chen, W., He, Q., Zou, Z., Zhao, H., Ye, X. and Guo, M. (2021) Preparation and characterization of gellan gum-chitosan polyelectrolyte complex films with the incorporation of thyme essential oil nanoemulsion. Food Hydrocolloids 114, 106570.

Zhou, C., Wang, X., Wang, Y., Song, X., Fang, D. and Ge, S. (2021) The sorption of single- and multi-heavy metals in aqueous solution using enhanced nano-hydroxyapatite assisted with ultrasonic. Journal of Environmental Chemical Engineering 9(3), 105240.

Zima, A. (2018) Hydroxyapatite-chitosan based bioactive hybrid biomaterials with improved mechanical strength. Spectrochimica Acta Part A: Molecular and Biomolecular Spectroscopy 193, 175-184.

Zou, Z., Ismail, B.B., Zhang, X., Yang, Z., Liu, D. and Guo, M. (2023) Improving barrier and antibacterial properties of chitosan composite films by incorporating lignin nanoparticles and acylated soy protein isolate nanogel. Food Hydrocolloids 134, 108091.

Zubair, M., Wu, J. and Ullah, A. (2019) Hybrid bionanocomposites from spent hen proteins. ACS omega 4(2), 3772-3781.

CHAPTER 5. CONCLUSION AND FUTURE RECOMMENDATIONS

The main objective of this study was to prepare HANPs from eggshell biowaste and incorporate them into chitosan biopolymer matrix to explore the potential of these bionanocomposites for food packaging applications. The first study is focused on the synthesis of HANPs through microwave-assisted precipitation and conventional heating methods with and without green plant template i.e., Azadirachta Indica (AI) leaf extract. XRD and FTIR analyses confirmed the existence of pure single-phase HANPs without any impurities using both methods. It was also observed that the crystallinity and crystalline size of the HANPs obtained by the microwave method were slightly lower compared to the conventional heating method. The morphological evaluation of HANPs by SEM clearly indicates that the AI template played an important role in improving the size and shape of HANPs and to obtain uniform distribution with less agglomeration. TEM confirmed the average size of HANP from both methodologies with an average diameter of 25-30 nm and length of 40-60 nm. From EDX spectra, lower Ca/P ratio (1.81) was observed when microwave assisted precipitation method was used compared to conventional heating method which is 1.95.

In the second study, chitosan matrix reinforced by the synthesized HANPs using various concentrations (1 wt% to 10 wt%). Solvent casting method was used to make films without any cross-linking agent (glycerol was used as a plasticizer). Prepared bionanocomposites films were characterized by various analytical techniques for their physiochemical, mechanical, barrier, and thermal stability properties. The addition of HANPs showed exceptional mechanical and barrier properties of bionanocomposites films. Tensile strengths were found to be increased with increasing HANPs concentrations from 1wt% to 3wt% and then decreased at higher concentrations i.e., 5wt% and 10wt% may be due to poor dispersion of nanoparticles in the

chitosan matrix. The highest tensile strength recorded in the film at 3wt% HANPs was 61.54%, compared to the control neat chitosan films. WVP was observed to be decreased at a lower concentration of HANPs (1wt%) i.e., a lower value which was 52% lower than the control neat chitosan film. However, WVP increased with the increase of HANPs nanofiller contents (3wt%, 5wt% and 10wt%) but the highest value was still lower than the neat chitosan film. SEM, TEM and XRD confirmed that 1wt% and 3wt% of HANPs contents were uniformly dispersed on the chitosan matrix in the bionanocomposites. However, aggregation was observed at higher concentrations of HANPs i.e., 5wt% and 10wt%. XPS and FTIR analyses revealed that some chemical changes occurred in all the CH-HA films due to the addition of HANPs. TGA and DSC results exhibited improved thermal stability of bionanocomposites when 1wt% and 3 wt % of HANP was used. In case of the addition of 1wt% of HANPs, bionanocomposites exhibited that crystalline melting temperature was shifted to the higher temperature which could be better homogeneity of the nanoparticles in the matrix compared to other films.

Overall, synthesized HANPs have a great potential to be used as a nanofiller for chitosan-based bionanocomposites to enhance biopolymer's mechanical, barrier, and thermal properties for food packaging applications.

Future recommendation

Synthesis parameters such as temperature, pH and reaction time play an important role improving in shape, size, crystallinity, and Ca/P ratio of HANPs which is important for different applications. HANPs can be synthesized using different temperatures, pH and reaction time to see their effect on HANPs structure, Ca/P ratio and crystallinity.

AI plant extract can be prepared using specific extraction methods like adsorption chromatography or high-performance liquid chromatography (HPLC) to find out more specific

extracts (such as alkaloids or plant organic compounds) in AI.

Detailed study of HANPs growth kinetics can help understand their crystal structure.

Although the synthesized HANPs' elemental analysis was done using EDX for determination of Ca/P ratio, however, XRF can provide more accurate elemental composition and can be done to identify the elemental composition to find out Ca/P ratio which is important for the biomedical application such as tissue engineering, tissue implants etc.

AI extract plays an important role in synthesizing of HANPs by improving their sizes and shapes, however, further antimicrobial properties can be studied for their use in specific applications.

Although, the prepared bionanocomposites can significantly improve the mechanical and barrier properties of the chitosan films. However, the optical, antimicrobial, and antioxidant properties of these films need to be determined to use them efficiently as active packaging.

These bionanocomposites films are claimed to be fully biodegradable. For that purpose, biodegradation study of such materials is needed.

BIBLIOGRAPHY

Abdollahi, M., Alboofetileh, M., Rezaei, M. and Behrooz, R. (2013) Comparing physico-mechanical and thermal properties of alginate nanocomposite films reinforced with organic and/or inorganic nanofillers. Food Hydrocolloids 32, 416-424.

Agalya, P., Suresh Kumar, G., Srinivasan, R., Prabu, K.M., Karunakaran, G., Cholan, S., Kolesnikov, E. and Kim, M. (2021) Hydroxyapatite-based antibacterial bio-nanomaterials: an insight into the synthesis using mussel shell as a calcium source, physicochemical properties, and nanoindentation characteristics. Applied Physics A 127(8), 589.

Agbeboh, N.I., Oladele, I.O., Daramola, O.O., Adediran, A.A., Olasukanmi, O.O. and Tanimola, M.O. (2020) Environmentally sustainable processes for the synthesis of hydroxyapatite. Heliyon 6(4), e03765.

Aguilar, A.E.M., Fagundes, A.P., Macuvele, D.L.P., Cesca, K., Porto, L., Padoin, N., Soares, C. and Riella, H.G. (2021) Green synthesis of nano hydroxyapatite: morphology variation and its effect on cytotoxicity against fibroblast. Materials Letters 284, 129013.

Ahari, H., Golestan, L., Anvar, S.A.A., Cacciotti, I., Garavand, F., Rezaei, A., Sani, M.A. and Jafari, S.M. (2022) Bio-nanocomposites as food packaging materials; the main production techniques and analytical parameters. Advances in Colloid and Interface Science 310, 102806.

Aldana, D.S., Villa, E.D., De Dios Hernández, M., Sánchez, G.G., Cruz, Q.R., Gallardo, S.F., Castillo, H.P. and Casarrubias, L.B. (2014) Barrier Properties of Polylactic Acid in Cellulose Based Packages Using Montmorillonite as Filler. Polymers 6(9), 2386-2403.

Ali, A.F., Alrowaili, Z.A., El-Giar, E.M., Ahmed, M.M. and El-Kady, A.M. (2021) Novel green synthesis of hydroxyapatite uniform nanorods via microwave-hydrothermal route using licorice root extract as template. Ceramics International 47(3), 3928-3937.

Alorku, K., Manoj, M. and Yuan, A. (2020) A plant-mediated synthesis of nanostructured hydroxyapatite for biomedical applications: a review. RSC Advances 10(67), 40923-40939.

Alzohairy, M.A. (2016) Therapeutics Role of Azadirachta indica (Neem) and Their Active Constituents in Diseases Prevention and Treatment. Evid Based Complement Alternat Med 2016, 7382506.

amar Cheba, B. (2020) Chitosan: Properties, modifications and food nanobiotechnology. Procedia Manufacturing 46, 652-658.

Ambaye, T.G., Vaccari, M., Prasad, S., van Hullebusch, E.D. and Rtimi, S. (2022) Preparation and applications of chitosan and cellulose composite materials. Journal of Environmental Management 301, 113850.

Apalangya, V., Rangari, V., Jeelani, S., Dankyi, E., Yaya, A. and Darko, S. (2018) Rapid microwave synthesis of needle-liked hydroxyapatite nanoparticles via template directing ball-milled spindle-shaped eggshell particles. Ceramics International 44(6), 7165-7171.

Arikan, E.B. and Ozsoy, H.D. (2015) A review: investigation of bioplastics. Journal of Civil Engineering and Architecture 9(2), 188-192.

Arora, B., Bhatia, R. and Attri, P. (2018) New Polymer Nanocomposites for Environmental Remediation. Hussain, C.M. and Mishra, A.K. (eds), pp. 699-712, Elsevier.

Ashokan, A., Rajendran, V., Sampath Kumar, T.S. and Jayaraman, G. (2021) Eggshell derived hydroxyapatite microspheres for chromatographic applications by a novel dissolution - precipitation method. Ceramics International 47(13), 18575-18583.

Athinarayanan, J., Periasamy, V.S. and Alshatwi, A.A. (2020) Simultaneous fabrication of carbon nanodots and hydroxyapatite nanoparticles from fish scale for biomedical applications. Materials Science and Engineering: C 117, 111313.

Bonilla, J., Poloni, T., Lourenço, R.V. and Sobral, P.J.A. (2018) Antioxidant potential of eugenol and ginger essential oils with gelatin/chitosan films. Food Bioscience 23, 107-114.

Bose, S. and Saha, S.K. (2003) Synthesis and Characterization of Hydroxyapatite Nanopowders by Emulsion Technique. Chemistry of Materials 15(23), 4464-4469.

Bourakadi, K.E., Merghoub, N., Fardioui, M., Mekhzoum, M.E.M., Kadmiri, I.M., Essassi, E.M., Qaiss, A.e.K. and Bouhfid, R. (2019) Chitosan/polyvinyl alcohol/thiabendazoluim-montmorillonite bio-nanocomposite films: Mechanical, morphological and antimicrobial properties. Composites Part B: Engineering 172, 103-110.

Bouyer, E., Gitzhofer, F. and Boulos, M. (2000) Morphological study of hydroxyapatite nanocrystal suspension. Journal of Materials Science: Materials in Medicine 11(8), 523-531.

Brundavanam, R.K., Jiang, Z.-T., Chapman, P., Le, X.-T., Mondinos, N., Fawcett, D. and Poinern, G.E.J. (2011) Effect of dilute gelatine on the ultrasonic thermally assisted synthesis of nano hydroxyapatite. Ultrasonics sonochemistry 18(3), 697-703.

Bunaciu, A.A., Udriştioiu, E.g. and Aboul-Enein, H.Y. (2015) X-Ray Diffraction: Instrumentation and Applications. Critical Reviews in Analytical Chemistry 45(4), 289-299.

Cao, W., Yan, J., Liu, C., Zhang, J., Wang, H., Gao, X., Yan, H., Niu, B. and Li, W. (2020) Preparation and characterization of catechol-grafted chitosan/gelatin/modified chitosan-AgNP blend films. Carbohydrate Polymers 247, 116643.

Cengiz, B., Gokce, Y., Yildiz, N., Aktas, Z. and Calimli, A. (2008) Synthesis and characterization of hydroxyapatite nanoparticles. Colloids and Surfaces A: Physicochemical and Engineering Aspects 322(1), 29-33.

Chesley, M., Kennard, R., Roozbahani, S., Kim, S.M., Kukk, K. and Mason, M. (2020) One-step hydrothermal synthesis with in situ milling of biologically relevant hydroxyapatite. Materials Science and Engineering: C 113, 110962.

Clarinval, A.-M. and Halleux, J. (2005) Biodegradable polymers for industrial applications, pp. 3-31, Elsevier.

Costescu, A., Pasuk, I., Ungureanu, F., Dinischiotu, A., Costache, M., Huneau, F., Galaup, S., Coustumer, P.L. and Predoi, D. (2010) PHYSICO-CHEMICAL PROPERTIES OF NANO-SIZED HEXAGONAL HYDROXYAPATITE POWDER SYNTHESIZED BY SOL-GEL. Digest Journal of Nanomaterials & Biostructures (DJNB) 5(4).

Cui, H., Surendhiran, D., Li, C. and Lin, L. (2020) Biodegradable zein active film containing chitosan nanoparticle encapsulated with pomegranate peel extract for food packaging. Food Packaging and Shelf Life 24, 100511.

Cunha, C.S., Castro, P.J., Sousa, S.C., Pullar, R.C., Tobaldi, D.M., Piccirillo, C. and Pintado, M.M. (2020) Films of chitosan and natural modified hydroxyapatite as effective UV-protecting, biocompatible and antibacterial wound dressings. International Journal of Biological Macromolecules 159, 1177-1185.

Dasgupta, S., Tarafder, S., Bandyopadhyay, A. and Bose, S. (2013) Effect of grain size on mechanical, surface and biological properties of microwave sintered hydroxyapatite. Materials Science and Engineering: C 33(5), 2846-2854.

Dash, K.K., Deka, P., Bangar, S.P., Chaudhary, V., Trif, M. and Rusu, A. (2022) Applications of Inorganic Nanoparticles in Food Packaging: A Comprehensive Review. Polymers 14(3), 521.

Deng, L., Li, Y., Zhang, A. and Zhang, H. (2020) Characterization and physical properties of electrospun gelatin nanofibrous films by incorporation of nano-hydroxyapatite. Food Hydrocolloids 103, 105640.

Dong, W., Su, J., Chen, Y., Xu, D., Cheng, L., Mao, L., Gao, Y. and Yuan, F. (2022) Characterization and antioxidant properties of chitosan film incorporated with modified silica nanoparticles as an active food packaging. Food Chem 373, 131414.

El-Aidie, S.A.-A.M. (2018) A review on chitosan: ecofriendly multiple potential applications in the food industry. International Journal of Advancement in Life Sciences Research, 1-14.

Emadian, S.M., Onay, T.T. and Demirel, B. (2017) Biodegradation of bioplastics in natural environments. Waste Management 59, 526-536.

Fakhreddin Hosseini, S., Rezaei, M., Zandi, M. and Ghavi, F.F. (2013) Preparation and functional properties of fish gelatin-chitosan blend edible films. Food Chem 136(3-4), 1490-1495.

Fathi, M., Hanifi, A. and Mortazavi, V. (2008) Preparation and bioactivity evaluation of bone-like hydroxyapatite nanopowder. Journal of materials processing technology 202(1-3), 536-542.

Ferrero, F. and Periolatto, M. (2012) Antimicrobial finish of textiles by chitosan UV-curing. Journal of nanoscience and nanotechnology 12(6), 4803-4810.

Fiume, E., Magnaterra, G., Rahdar, A., Verné, E. and Baino, F. (2021) Hydroxyapatite for Biomedical Applications: A Short Overview. Ceramics 4(4), 542-563.

Flauzino Neto, W.P., Silvério, H.A., Dantas, N.O. and Pasquini, D. (2013) Extraction and characterization of cellulose nanocrystals from agro-industrial residue – Soy hulls. Industrial Crops and Products 42, 480-488.

Gan, C.-d., Jia, Y.-b. and Yang, J.-y. (2021) Remediation of fluoride contaminated soil with nano-hydroxyapatite amendment: Response of soil fluoride bioavailability and microbial communities. Journal of Hazardous Materials 405, 124694.

Gasti, T., Dixit, S., Hiremani, V.D., Chougale, R.B., Masti, S.P., Vootla, S.K. and Mudigoudra, B.S. (2022) Chitosan/pullulan based films incorporated with clove essential oil loaded chitosan-ZnO hybrid nanoparticles for active food packaging. Carbohydrate Polymers 277, 118866.

Ghaffar, I., Rashid, M., Akmal, M. and Hussain, A. (2022) Plastics in the environment as potential threat to life: an overview. Environmental Science and Pollution Research 29(38), 56928-56947.

Ghate, P., Prabhu S, D., Murugesan, G., Goveas, L.C., Varadavenkatesan, T., Vinayagam, R., Lan Chi, N.T., Pugazhendhi, A. and Selvaraj, R. (2022) Synthesis of hydroxyapatite nanoparticles using Acacia falcata leaf extract and study of their anti-cancerous activity against cancerous mammalian cell lines. Environmental Research 214, 113917.

Gholizadeh, B.S., Buazar, F., Hosseini, S.M. and Mousavi, S.M. (2018) Enhanced antibacterial activity, mechanical and physical properties of alginate/hydroxyapatite bionanocomposite film. International Journal of Biological Macromolecules 116, 786-792.

Ghosh, T., Mondal, K., Giri, B.S. and Katiyar, V. (2021) Silk nanodisc based edible chitosan nanocomposite coating for fresh produces: A candidate with superior thermal, hydrophobic, optical, mechanical and food properties. Food Chem 360, 130048.

Goel, V., Luthra, P., Kapur, G.S. and Ramakumar, S.S.V. (2021) Biodegradable/Bio-plastics: Myths and Realities. Journal of Polymers and the Environment 29(10), 3079-3104.

Goh, K.W., Wong, Y.H., Ramesh, S., Chandran, H., Krishnasamy, S., Ramesh, S., Sidhu, A. and Teng, W.D. (2021) Effect of pH on the properties of eggshell-derived hydroxyapatite bioceramic synthesized by wet chemical method assisted by microwave irradiation. Ceramics International 47(7, Part A), 8879-8887.

Gomes, G.C., Borghi, F.F., Ospina, R.O., López, E.O., Borges, F.O. and Mello, A. (2017) Nd:YAG (532nm) pulsed laser deposition produces crystalline hydroxyapatite thin coatings at room temperature. Surface and Coatings Technology 329, 174-183.

Gopi, D., Bhuvaneshwari, N., Indira, J. and Kavitha, L. (2013) Synthesis and spectroscopic investigations of hydroxyapatite using a green chelating agent as template. Spectrochimica Acta Part A: Molecular and Biomolecular Spectroscopy 104, 292-299.

Gopi, D., Bhuvaneshwari, N., Kavitha, L. and Ramya, S. (2015) Novel malic acid mediated green route for the synthesis of hydroxyapatite particles and their spectral characterization. Ceramics International 41(2, Part B), 3116-3127.

Gopi, D., Indira, J., Kavitha, L., Kannan, S. and Ferreira, J.M.F. (2010) Spectroscopic characterization of nanohydroxyapatite synthesized by molten salt method. Spectrochimica Acta Part A: Molecular and Biomolecular Spectroscopy 77(2), 545-547.

Gopi, D., Indira, J., Prakash, V.C.A. and Kavitha, L. (2009) Spectroscopic characterization of porous nanohydroxyapatite synthesized by a novel amino acid soft solution freezing method. Spectrochimica Acta Part A: Molecular and Biomolecular Spectroscopy 74(1), 282-284.

Gopi, D., Kanimozhi, K., Bhuvaneshwari, N., Indira, J. and Kavitha, L. (2014) Novel banana peel pectin mediated green route for the synthesis of hydroxyapatite nanoparticles and their

spectral characterization. Spectrochimica Acta Part A: Molecular and Biomolecular Spectroscopy 118, 589-597.

Grevellec, J., Marquié, C., Ferry, L., Crespy, A. and Vialettes, V. (2001) Processability of Cottonseed Proteins into Biodegradable Materials. Biomacromolecules 2(4), 1104-1109.

Grossman, R.F. and Nwabunma, D. (2013) Biopolymer nanocomposites: processing, properties, and applications, John Wiley & Sons.

Guo, X., Yan, H., Zhao, S., Li, Z., Li, Y. and Liang, X. (2013) Effect of calcining temperature on particle size of hydroxyapatite synthesized by solid-state reaction at room temperature. Advanced Powder Technology 24(6), 1034-1038.

Hadi, Z., Hekmat, N. and Soltanolkottabi, F. (2022) Effect of hydroxyapatite on physical, mechanical, and morphological properties of starch-based bio-nanocomposite films. Composites and Advanced Materials 31, 26349833221087755.

Haghighi, H., Licciardello, F., Fava, P., Siesler, H.W. and Pulvirenti, A. (2020) Recent advances on chitosan-based films for sustainable food packaging applications. Food Packaging and Shelf Life 26, 100551.

Haider, A., Haider, S., Han, S.S. and Kang, I.-K. (2017) Recent advances in the synthesis, functionalization and biomedical applications of hydroxyapatite: a review. RSC Advances 7(13), 7442-7458.

Han, J.-K., Song, H.-Y., Saito, F. and Lee, B.-T. (2006) Synthesis of high purity nano-sized hydroxyapatite powder by microwave-hydrothermal method. Materials chemistry and physics 99(2-3), 235-239.

Han, J.H. (2003) Novel Food Packaging Techniques. Ahvenainen, R. (ed), pp. 50-70, Woodhead Publishing.

Han, S.-C., Jiang, N., Sujandi, Burri, D.R., Choi, K.-M., Lee, S.-C. and Park, S.-E. (2007a) Studies in Surface Science and Catalysis. Zhao, D., Qiu, S., Tang, Y. and Yu, C. (eds), pp. 25-

28, Elsevier.

Han, Y., Li, S., Wang, X., Jia, L. and He, J. (2007b) Preparation of hydroxyapatite rod-like crystals by protein precursor method. Materials research bulletin 42(6), 1169-1177.

Harding, K.G., Gounden, T. and Pretorius, S. (2017) “Biodegradable” Plastics: A Myth of Marketing? Procedia Manufacturing 7, 106-110.

Hassan, M.N., Mahmoud, M.M., Abd El-Fattah, A. and Kandil, S. (2016a) Microwave-assisted preparation of Nano-hydroxyapatite for bone substitutes. Ceramics International 42(3), 3725-3744.

Hassan, M.N., Mahmoud, M.M., El-Fattah, A.A. and Kandil, S. (2016b) Microwave-assisted preparation of Nano-hydroxyapatite for bone substitutes. Ceramics International 42(3), 3725-3744.

Herrero, Y.R. and Ullah, A. (2021) Rapid, Metal-Free, Catalytic Conversion of Glycerol to Allyl Monomers and Polymers. ACS Sustainable Chemistry & Engineering 9(28), 9474-9485.

Husseinsyah, S., Amri, F., Husin, K. and Ismail, H. (2011) Mechanical and thermal properties of chitosan-filled polypropylene composites: The effect of acrylic acid. Journal of Vinyl and Additive Technology 17(2), 125-131.

Huysman, S., De Schaepmeester, J., Ragaert, K., Dewulf, J. and De Meester, S. (2017) Performance indicators for a circular economy: A case study on post-industrial plastic waste. Resources, conservation and recycling 120, 46-54.

Indira, J. and Malathi, K.S. (2022) Comparison of template mediated ultrasonic and microwave irradiation method on the synthesis of hydroxyapatite nanoparticles for biomedical applications. Materials Today: Proceedings 51, 1765-1769.

Irwansyah, F.S., Noviyanti, A.R., Eddy, D.R. and Risdiana, R. (2022) Green Template-Mediated Synthesis of Biowaste Nano-Hydroxyapatite: A Systematic Literature Review. Molecules 27(17), 5586.

Jakubowska, E., Gierszewska, M., Nowaczyk, J. and Olewnik-Kruszkowska, E. (2020) Physicochemical and storage properties of chitosan-based films plasticized with deep eutectic solvent. Food Hydrocolloids 108, 106007.

Jayaprakash, N., Vijaya, J.J., Kaviyarasu, K., Kombaiah, K., Kennedy, L.J., Ramalingam, R.J., Munusamy, M.A. and Al-Lohedan, H.A. (2017) Green synthesis of Ag nanoparticles using Tamarind fruit extract for the antibacterial studies. Journal of Photochemistry and Photobiology B: Biology 169, 178-185.

Jemli, Y.E., Abdelouahdi, K., Minh, D.P., Barakat, A. and Solhy, A. (2022) Design and Applications of Hydroxyapatite-Based Catalysts, pp. 19-72.

Ji, Y., Yang, X., Ji, Z., Zhu, L., Ma, N., Chen, D., Jia, X., Tang, J. and Cao, Y. (2020) DFT-Calculated IR Spectrum Amide I, II, and III Band Contributions of N-Methylacetamide Fine Components. ACS omega 5(15), 8572-8578.

Kalaiselvi, V., Mathammal, R., Vijayakumar, S. and Vaseeharan, B. (2018) Microwave assisted green synthesis of Hydroxyapatite nanorods using Moringa oleifera flower extract and its antimicrobial applications. International Journal of Veterinary Science and Medicine 6(2), 286-295.

Kamalanathan, P., Ramesh, S., Bang, L.T., Niakan, A., Tan, C.Y., Purbolaksono, J., Chandran, H. and Teng, W.D. (2014) Synthesis and sintering of hydroxyapatite derived from eggshells as a calcium precursor. Ceramics International 40(10, Part B), 16349-16359.

Karakas, A., Yoruc, A., Gokce, H., Karabulut, A. and Erdogan, D. (2013) Effect of different phosphorus precursors on biomimetic hydroxyapatite powder properties. Acta Physica Polonica A 123(2).

Karakas Aydınoğlu, A., Yoruc, A., Erdogan, D. and Doğan, M. (2012) Effect of different calcium precursors on biomimetic hydroxyapatite powder properties. Acta Physica Polonica A 121(1).

Karunakaran, G., Cho, E.-B., Kumar, G.S., Kolesnikov, E., Karpenkov, D.Y., Gopinathan, J.,

Pillai, M.M., Selvakumar, R., Boobalan, S. and Gorshenkov, M.V. (2019) Sodium dodecyl sulfate mediated microwave synthesis of biocompatible superparamagnetic mesoporous hydroxyapatite nanoparticles using black Chlamys varia seashell as a calcium source for biomedical applications. Ceramics International 45(12), 15143-15155.

Kaur, M., Arshad, M. and Ullah, A. (2018) In-Situ Nanoreinforced Green Bionanomaterials from Natural Keratin and Montmorillonite (MMT)/Cellulose Nanocrystals (CNC). ACS Sustainable Chemistry & Engineering 6(2), 1977-1987.

Kaya, M., Khadem, S., Cakmak, Y.S., Mujtaba, M., Ilk, S., Akyuz, L., Salaberria, Asier M., Labidi, J., Abdulqadir, A.H. and Deligöz, E. (2018) Antioxidative and antimicrobial edible chitosan films blended with stem, leaf and seed extracts of Pistacia terebinthus for active food packaging. RSC Advances 8(8), 3941-3950.

Khanzada, B., Mirza, B. and Ullah, A. (2023) Chitosan based bio-nanocomposites packaging films with unique mechanical and barrier properties. Food Packaging and Shelf Life 35, 101016.

Kong, L., Ma, J. and Boey, F. (2002) Nanosized hydroxyapatite powders derived from coprecipitation process. Journal of materials science 37, 1131-1134.

Kumar, G.S. and Girija, E.K. (2013) Flower-like hydroxyapatite nanostructure obtained from eggshell: A candidate for biomedical applications. Ceramics International 39(7), 8293-8299.

Kumar, G.S., Muthu, D., Karunakaran, G., Karthi, S., Girija, E.K. and Kuznetsov, D. (2018) Curcuma longa tuber extract mediated synthesis of hydroxyapatite nanorods using biowaste as a calcium source for the treatment of bone infections. Journal of Sol-Gel Science and Technology 86(3), 610-616.

Kumar, G.S., Rajendran, S., Karthi, S., Govindan, R., Girija, E.K., Karunakaran, G. and Kuznetsov, D. (2017) Green synthesis and antibacterial activity of hydroxyapatite nanorods for orthopedic applications. MRS Communications 7(2), 183-188.

Kumar, G.S., Sathish, L., Govindan, R. and Girija, E. (2015) Utilization of snail shells to synthesise hydroxyapatite nanorods for orthopedic applications. RSC Advances 5(49), 39544-

39548.

Kumar, G.S., Thamizhavel, A. and Girija, E. (2012) Microwave conversion of eggshells into flower-like hydroxyapatite nanostructure for biomedical applications. Materials Letters 76, 198-200.

Kumta, P.N., Sfeir, C., Lee, D.-H., Olton, D. and Choi, D. (2005) Nanostructured calcium phosphates for biomedical applications: novel synthesis and characterization. Acta Biomaterialia 1(1), 65-83.

Kuswandi, B. (2016) Nanotechnology in food packaging. Nanoscience in food and agriculture 1, 151-183.

Lebreton, L. and Andrady, A. (2019) Future scenarios of global plastic waste generation and disposal. Palgrave Communications 5(1), 6.

Li, B., Guo, B., Fan, H. and Zhang, X. (2008a) Preparation of nano-hydroxyapatite particles with different morphology and their response to highly malignant melanoma cells in vitro. Applied Surface Science 255(2), 357-360.

Li, B. and Webster, T. (2018) Orthopedic Biomaterials, Springer.

Li, H., Zhu, M., Li, L. and Zhou, C. (2008b) Processing of nanocrystalline hydroxyapatite particles via reverse microemulsions. Journal of materials science 43, 384-389.

Li, L., Iqbal, J., Zhu, Y., Zhang, P., Chen, W., Bhatnagar, A. and Du, Y. (2018) Chitosan/Ag-hydroxyapatite nanocomposite beads as a potential adsorbent for the efficient removal of toxic aquatic pollutants. International Journal of Biological Macromolecules 120, 1752-1759.

Li, S., Mu, B., Zhang, H., Kang, Y. and Wang, A. (2022) Incorporation of silver nanoparticles/curcumin/clay minerals into chitosan film for enhancing mechanical properties, antioxidant and antibacterial activity. International Journal of Biological Macromolecules 223, 779-789.

Lin, D.-J., Lin, H.-L., Haung, S.-M., Liu, S.-M. and Chen, W.-C. (2021) Effect of pH on the In Vitro Biocompatibility of Surfactant-Assisted Synthesis and Hydrothermal Precipitation of Rod-Shaped Nano-Hydroxyapatite. Polymers 13(17), 2994.

Liu, Y., Deng, L., Zhang, C., Chen, K., Feng, F. and Zhang, H. (2018) Comparison of ethyl cellulose–gelatin composite films fabricated by electrospinning versus solvent casting. Journal of Applied Polymer Science 135(46), 46824.

Llanos, J.H. and Tadini, C.C. (2018) Preparation and characterization of bio-nanocomposite films based on cassava starch or chitosan, reinforced with montmorillonite or bamboo nanofibers. International Journal of Biological Macromolecules 107, 371-382.

Lu, Y., Dong, W., Ding, J., Wang, W. and Wang, A. (2019) Nanomaterials from Clay Minerals. Wang, A. and Wang, W. (eds), pp. 485-536, Elsevier.

Maachou, H., Genet, M.J., Aliouche, D., Dupont-Gillain, C.C. and Rouxhet, P.G. (2013) XPS analysis of chitosan–hydroxyapatite biomaterials: from elements to compounds. Surface and Interface Analysis 45(7), 1088-1097.

Machado, B.R., Facchi, S.P., de Oliveira, A.C., Nunes, C.S., Souza, P.R., Vilsinski, B.H., Popat, K.C., Kipper, M.J., Muniz, E.C. and Martins, A.F. (2020) Bactericidal pectin/chitosan/glycerol films for food pack coatings: A critical viewpoint. International journal of molecular sciences 21(22), 8663.

Madian, N.G. and Mohamed, N. (2020) Enhancement of the dynamic mechanical properties of chitosan thin films by crosslinking with greenly synthesized silver nanoparticles. Journal of Materials Research and Technology 9(6), 12970-12975.

Mallakpour, S. and Madani, M. (2015) Effect of functionalized TiO2 on mechanical, thermal and swelling properties of chitosan-based nanocomposite films. Polymer-Plastics Technology and Engineering 54(10), 1035-1042.

Malvano, F., Montone, A.M.I., Capparelli, R., Capuano, F. and Albanese, D. (2021) Development of a Novel Active Edible Coating Containing Hydroxyapatite for Food Shelf-life

Extension. Chemical Engineering Transactions 87, 25-30.

Malvano, F., Montone, A.M.I., Capuano, F., Colletti, C., Roveri, N., Albanese, D. and Capparelli, R. (2022) Effects of active alginate edible coating enriched with hydroxyapatite-quercetin complexes during the cold storage of fresh chicken fillets. Food Packaging and Shelf Life 32, 100847.

Markov, G.G. and Ivanov, I.G. (1974) Hydroxyapatite column chromatography in procedures for isolation of purified DNA. Analytical Biochemistry 59(2), 555-563.

Meski, S., Ziani, S. and Khireddine, H. (2010) Removal of Lead Ions by Hydroxyapatite Prepared from the Egg Shell. Journal of Chemical & Engineering Data 55(9), 3923-3928.

Mincke, S., Asere, T.G., Verheye, I., Folens, K., Bussche, F.V., Lapeire, L., Verbeken, K., Van Der Voort, P., Tessema, D.A. and Fufa, F. (2019) Functionalized chitosan adsorbents allow recovery of palladium and platinum from acidic aqueous solutions. Green Chemistry 21(9), 2295-2306.

Mohammadi sadati, S.M., Shahgholian-Ghahfarrokhi, N., Shahrousvand, E., Mohammadi-Rovshandeh, J. and Shahrousvand, M. (2022) Edible chitosan/cellulose nanofiber nanocomposite films for potential use as food packaging. Materials Technology 37(10), 1276-1288.

Morsy, R., Ali, S.S. and El-Shetehy, M. (2017) Development of hydroxyapatite-chitosan gel sunscreen combating clinical multidrug-resistant bacteria. Journal of Molecular Structure 1143, 251-258.

Motelica, L., Ficai, D., Ficai, A., Truşcă, R.-D., Ilie, C.-I., Oprea, O.-C. and Andronescu, E. (2020) Innovative antimicrobial chitosan/ZnO/Ag NPs/citronella essential oil nanocomposite—Potential coating for grapes. Foods 9(12), 1801.

Müller, C.M.O., Laurindo, J.B. and Yamashita, F. (2011) Effect of nanoclay incorporation method on mechanical and water vapor barrier properties of starch-based films. Industrial Crops and Products 33(3), 605-610.

Nazeer, M.A., Yilgör, E. and Yilgör, I. (2017) Intercalated chitosan/hydroxyapatite nanocomposites: promising materials for bone tissue engineering applications. Carbohydrate Polymers 175, 38-46.

Neelakandeswari, N., Sangami, G. and Dharmaraj, N. (2011) Preparation and characterization of nanostructured hydroxyapatite using a biomaterial. Synthesis and Reactivity in Inorganic, Metal-Organic, and Nano-Metal Chemistry 41(5), 513-516.

Negrila, C.C., Predoi, M.V., Iconaru, S.L. and Predoi, D. (2018) Development of Zinc-Doped Hydroxyapatite by Sol-Gel Method for Medical Applications. Molecules 23(11), 2986.

Ofudje, E.A., Adeogun, A.I., Idowu, M.A. and Kareem, S.O. (2019) Synthesis and characterization of Zn-Doped hydroxyapatite: scaffold application, antibacterial and bioactivity studies. Heliyon 5(5).

Ooi, C.Y., Hamdi, M. and Ramesh, S. (2007) Properties of hydroxyapatite produced by annealing of bovine bone. Ceramics International 33(7), 1171-1177.

Othman, S.H. (2014) Bio-nanocomposite Materials for Food Packaging Applications: Types of Biopolymer and Nano-sized Filler. Agriculture and Agricultural Science Procedia 2, 296-303.

Pandey, J.K., Kumar, A.P., Misra, M., Mohanty, A.K., Drzal, L.T. and Palsingh, R. (2005) Recent advances in biodegradable nanocomposites. Journal of nanoscience and nanotechnology 5(4), 497-526.

Pang, Y.X. and Bao, X. (2003) Influence of temperature, ripening time and calcination on the morphology and crystallinity of hydroxyapatite nanoparticles. Journal of the European Ceramic Society 23(10), 1697-1704.

Peng, Y., Wu, Y. and Li, Y. (2013) Development of tea extracts and chitosan composite films for active packaging materials. International Journal of Biological Macromolecules 59, 282-289.

Phatai, P., Futalan, C.M., Kamonwannasit, S. and Khemthong, P. (2019) Structural characterization and antibacterial activity of hydroxyapatite synthesized via sol-gel method using

glutinous rice as a template. Journal of Sol-Gel Science and Technology 89(3), 764-775.

Priyadarshi, R. and Negi, Y.S. (2017) Effect of varying filler concentration on zinc oxide nanoparticle embedded chitosan films as potential food packaging material. Journal of Polymers and the Environment 25, 1087-1098.

Priyadarshi, R. and Rhim, J.-W. (2020) Chitosan-based biodegradable functional films for food packaging applications. Innovative Food Science & Emerging Technologies 62, 102346.

Priyadarshi, R., Roy, S., Ghosh, T., Biswas, D. and Rhim, J.-W. (2021) Antimicrobial nanofillers reinforced biopolymer composite films for active food packaging applications-a review. Sustainable Materials and Technologies, e00353.

Quadros, M., Momin, M. and Verma, G. (2022) Handbook on Synthesis Strategies for Advanced Materials: Volume-II: Processing and Functionalization of Materials. Tyagi, A.K. and Ningthoujam, R.S. (eds), pp. 617-658, Springer Nature Singapore, Singapore.

Rahman, M.M., Netravali, A.N., Tiimob, B.J., Apalangya, V. and Rangari, V.K. (2016) Bio-inspired “green” nanocomposite using hydroxyapatite synthesized from eggshell waste and soy protein. Journal of Applied Polymer Science 133(22).

Rajabi-Zamani, A.H., Behnamghader, A. and Kazemzadeh, A. (2008) Synthesis of nanocrystalline carbonated hydroxyapatite powder via nonalkoxide sol–gel method. Materials Science and Engineering: C 28(8), 1326-1329.

Ramji, V. and Vishnuvarthanan, M. (2022) Chitosan Ternary Bio Nanocomposite Films Incorporated with MMT K10 Nanoclay and Spirulina. Silicon 14(3), 1209-1220.

Rane, K.D. and Hoover, D.G. (1993) Production of chitosan by fungi. Food biotechnology 7(1), 11-33.

Rao, V. and Johns, J. (2008) Thermal behavior of chitosan/natural rubber latex blends TG and DSC analysis. Journal of Thermal Analysis and Calorimetry 92(3), 801-806.

Reddy, J.P. and Rhim, J.-W. (2014) Characterization of bionanocomposite films prepared with agar and paper-mulberry pulp nanocellulose. Carbohydrate Polymers 110, 480-488.

Reddy, M.M., Vivekanandhan, S., Misra, M., Bhatia, S.K. and Mohanty, A.K. (2013) Biobased plastics and bionanocomposites: Current status and future opportunities. Progress in Polymer Science 38(10), 1653-1689.

Reddy, N., Reddy, R. and Jiang, Q. (2015) Crosslinking biopolymers for biomedical applications. Trends in Biotechnology 33(6), 362-369.

Ren, Y., Xu, L., Wang, C., Wang, X., Ding, Z. and Chen, Y. (2017) Effect of dielectric barrier discharge treatment on surface nanostructure and wettability of polylactic acid (PLA) nonwoven fabrics. Applied Surface Science 426, 612-621.

Rhim, J.-W., Hong, S.-I. and Ha, C.-S. (2009) Tensile, water vapor barrier and antimicrobial properties of PLA/nanoclay composite films. LWT-Food Science and Technology 42(2), 612-617.

Rhim, J.-W., Hong, S.-I., Park, H.-M. and Ng, P.K.W. (2006) Preparation and Characterization of Chitosan-Based Nanocomposite Films with Antimicrobial Activity. Journal of Agricultural and Food Chemistry 54(16), 5814-5822.

Rhim, J.-W. and Lee, J.-H. (2004) Effect of $CaCl_2$ Treatment on Mechanical and Moisture Barrier Properties of Sodium Alginate and Soy Protein-based Films. Food Science and Biotechnology 13(6), 728-732.

Rhim, J.-W., Park, H.-M. and Ha, C.-S. (2013) Bio-nanocomposites for food packaging applications. Progress in Polymer Science 38(10), 1629-1652.

Rhim, J.W., Lee, S.B. and Hong, S.I. (2011) Preparation and characterization of agar/clay nanocomposite films: the effect of clay type. Journal of food science 76(3), N40-N48.

Riaz, A., Lagnika, C., Luo, H., Dai, Z., Nie, M., Hashim, M.M., Liu, C., Song, J. and Li, D. (2020) Chitosan-based biodegradable active food packaging film containing Chinese chive

(Allium tuberosum) root extract for food application. International Journal of Biological Macromolecules 150, 595-604.

Rinaudo, M. (2006) Chitin and chitosan: Properties and applications. Progress in Polymer Science 31(7), 603-632.

Rodrigues, C., de Mello, J.M.M., Dalcanton, F., Macuvele, D.L.P., Padoin, N., Fiori, M.A., Soares, C. and Riella, H.G. (2020) Mechanical, thermal and antimicrobial properties of chitosan-based-nanocomposite with potential applications for food packaging. Journal of Polymers and the Environment 28, 1216-1236.

Rodríguez-Lugo, V., Karthik, T., Mendoza-Anaya, D., Rubio-Rosas, E., Villaseñor Cerón, L., Reyes-Valderrama, M. and Salinas-Rodríguez, E. (2018) Wet chemical synthesis of nanocrystalline hydroxyapatite flakes: effect of pH and sintering temperature on structural and morphological properties. Royal Society open science 5(8), 180962.

Rong, S.Y., Mubarak, N.M. and Tanjung, F.A. (2017) Structure-property relationship of cellulose nanowhiskers reinforced chitosan biocomposite films. Journal of Environmental Chemical Engineering 5(6), 6132-6136.

Ruiz-Hitzky, E., Darder, M. and Aranda, P. (2005) Functional biopolymer nanocomposites based on layered solids. Journal of Materials Chemistry 15(35-36), 3650-3662.

Sadat-Shojai, M., Khorasani, M.-T., Dinpanah-Khoshdargi, E. and Jamshidi, A. (2013) Synthesis methods for nanosized hydroxyapatite with diverse structures. Acta Biomaterialia 9(8), 7591-7621.

Sanuja, S., Agalya, A. and Umapathy, M.J. (2015) Synthesis and characterization of zinc oxide–neem oil–chitosan bionanocomposite for food packaging application. International Journal of Biological Macromolecules 74, 76-84.

Sarode, S., Upadhyay, P., Khosa, M.A., Mak, T., Shakir, A., Song, S. and Ullah, A. (2019) Overview of wastewater treatment methods with special focus on biopolymer chitin-chitosan. International Journal of Biological Macromolecules 121, 1086-1100.

Sawada, M., Sridhar, K., Kanda, Y. and Yamanaka, S. (2021) Pure hydroxyapatite synthesis originating from amorphous calcium carbonate. Scientific Reports 11(1), 11546.

Shi, D., Tong, H., Lv, M., Luo, D., Wang, P., Xu, X. and Han, Z. (2021) Optimization of hydrothermal synthesis of hydroxyapatite from chicken eggshell waste for effective adsorption of aqueous Pb(II). Environmental Science and Pollution Research 28(41), 58189-58205.

Shikinaka, K., Nakamura, M. and Otsuka, Y. (2020) Strong UV absorption by nanoparticulated lignin in polymer films with reinforcement of mechanical properties. Polymer 190, 122254.

Silva, A.O., Cunha, R.S., Hotza, D. and Machado, R.A.F. (2021) Chitosan as a matrix of nanocomposites: A review on nanostructures, processes, properties, and applications. Carbohydrate Polymers 272, 118472.

Singh, N., Ogunseitan, O.A., Wong, M.H. and Tang, Y. (2022) Sustainable materials alternative to petrochemical plastics pollution: A review analysis. Sustainable Horizons 2, 100016.

Sinha Ray, S. (2012) Polylactide-Based Bionanocomposites: A Promising Class of Hybrid Materials. Accounts of Chemical Research 45(10), 1710-1720.

Siva Rama Krishna, D., Siddharthan, A., Seshadri, S.K. and Sampath Kumar, T.S. (2007) A novel route for synthesis of nanocrystalline hydroxyapatite from eggshell waste. Journal of Materials Science: Materials in Medicine 18(9), 1735-1743.

Spirescu, V.A., Chircov, C., Grumezescu, A.M., Vasile, B.Ș. and Andronescu, E. (2021) Inorganic Nanoparticles and Composite Films for Antimicrobial Therapies. International journal of molecular sciences 22(9), 4595.

Teixeira, S., Rodriguez, M., Pena, P., De Aza, A., De Aza, S., Ferraz, M. and Monteiro, F. (2009) Physical characterization of hydroxyapatite porous scaffolds for tissue engineering. Materials Science and Engineering: C 29(5), 1510-1514.

Thein-Han, W.W. and Misra, R.D. (2009) Biomimetic chitosan-nanohydroxyapatite composite scaffolds for bone tissue engineering. Acta Biomater 5(4), 1182-1197.

Tomaszewska, J., Sterzyński, T., Woźniak-Braszak, A. and Banaszak, M. (2021) Review of Recent Developments of Glass Transition in PVC Nanocomposites. Polymers 13(24), 4336.

Trakoolwannachai, V., Kheolamai, P. and Ummartyotin, S. (2019) Development of hydroxyapatite from eggshell waste and a chitosan-based composite: In vitro behavior of human osteoblast-like cell (Saos-2) cultures. International Journal of Biological Macromolecules 134, 557-564.

Ullah, A. and Arshad, M. (2017) Remarkably Efficient Microwave-Assisted Cross-Metathesis of Lipids under Solvent-Free Conditions. ChemSusChem 10(10), 2167-2174.

Ullah, A., Vasanthan, T., Bressler, D., Elias, A.L. and Wu, J. (2011) Bioplastics from Feather Quill. Biomacromolecules 12(10), 3826-3832.

Umesh, M., Choudhury, D.D., Shanmugam, S., Ganesan, S., Alsehli, M., Elfasakhany, A. and Pugazhendhi, A. (2021) Eggshells biowaste for hydroxyapatite green synthesis using extract piper betel leaf - Evaluation of antibacterial and antibiofilm activity. Environmental Research 200, 111493.

Ummartyotin, S. and Tangnorawich, B. (2015) Utilization of eggshell waste as raw material for synthesis of hydroxyapatite. Colloid and Polymer Science 293(9), 2477-2483.

Usami, K. and Okamoto, A. (2017) Hydroxyapatite: catalyst for a one-pot pentose formation. Organic & Biomolecular Chemistry 15(42), 8888-8893.

Vaia, R.A. and Giannelis, E.P. (2001) Liquid crystal polymer nanocomposites: direct intercalation of thermotropic liquid crystalline polymers into layered silicates. Polymer 42(3), 1281-1285.

Varadarajan, V., Varsha, M., Vijayasekaran, K. and Shankar, S.V. (2020) Comparative studies of hydroxyapatite (HAp) nanoparticles synthesized by using different green templates. AIP Conference Proceedings 2240(1), 080002.

Viswanath, B. and Ravishankar, N. (2008) Controlled synthesis of plate-shaped hydroxyapatite

and implications for the morphology of the apatite phase in bone. Biomaterials 29(36), 4855-4863.

Wang, P., Li, C., Gong, H., Jiang, X., Wang, H. and Li, K. (2010) Effects of synthesis conditions on the morphology of hydroxyapatite nanoparticles produced by wet chemical process. Powder Technology 203, 315-321.

Wesley, S.J., Raja, P., Raj, A.A. and Tiroutchelvamae, D. (2014) Review on-nanotechnology applications in food packaging and safety. International Journal of Engineering Research 3(11), 645-651.

Wu, S.-C., Hsu, H.-C., Hsu, S.-K., Chang, Y.-C. and Ho, W.-F. (2015) Effects of heat treatment on the synthesis of hydroxyapatite from eggshell powders. Ceramics International 41(9), 10718-10724.

Wu, S.-C., Hsu, H.-C., Hsu, S.-K., Chang, Y.-C. and Ho, W.-F. (2016) Synthesis of hydroxyapatite from eggshell powders through ball milling and heat treatment. Journal of Asian Ceramic Societies 4(1), 85-90.

Yan, D., Lou, Y., Han, Y., Wickramaratne, M.N., Dai, H. and Wang, X. (2018) Controllable synthesis of poly(acrylic acid)-stabilized nano-hydroxyapatite suspension by an ultrasound-assisted precipitation method. Materials Letters 227, 9-12.

Yang, J., Xiong, L., Li, M. and Sun, Q. (2018) Chitosan–Sodium Phytate Films with a Strong Water Barrier and Antimicrobial Properties Produced via One-Step-Consecutive-Stripping and Layer-by-Layer-Casting Technologies. Journal of Agricultural and Food Chemistry 66(24), 6104-6115.

Yao, H.-L., Yang, C., Yang, Q., Hu, X.-Z., Zhang, M.-X., Bai, X.-B., Wang, H.-T. and Chen, Q.-Y. (2020) Structure, mechanical and bioactive properties of nanostructured hydroxyapatite/titania composites prepared by microwave sintering. Materials chemistry and physics 241, 122340.

Ye, F., Guo, H., Zhang, H. and He, X. (2010) Polymeric micelle-templated synthesis of

hydroxyapatite hollow nanoparticles for a drug delivery system. Acta Biomater 6(6), 2212-2218.

Yeon, K.C., Wang, J. and Ng, S.C. (2001) Mechanochemical synthesis of nanocrystalline hydroxyapatite from CaO and CaHPO4. Biomaterials 22(20), 2705-2712.

Zanotto, A., Saladino, M.L., Martino, D.C. and Caponetti, E. (2012) Influence of temperature on calcium hydroxyapatite nanopowders.

Zhan, J., Tseng, Y.H., Chan, J.C. and Mou, C.Y. (2005) Biomimetic formation of hydroxyapatite nanorods by a single-crystal-to-single-crystal transformation. Advanced Functional Materials 15(12), 2005-2010.

Zhang, H. and Darvell, B.W. (2010) Synthesis and characterization of hydroxyapatite whiskers by hydrothermal homogeneous precipitation using acetamide. Acta Biomaterialia 6(8), 3216-3222.

Zhang, X., Liu, D., Jin, T.Z., Chen, W., He, Q., Zou, Z., Zhao, H., Ye, X. and Guo, M. (2021) Preparation and characterization of gellan gum-chitosan polyelectrolyte complex films with the incorporation of thyme essential oil nanoemulsion. Food Hydrocolloids 114, 106570.

Zhang, Y. and Lu, J. (2007) A simple method to tailor spherical nanocrystal hydroxyapatite at low temperature. Journal of Nanoparticle Research 9(4), 589-594.

Zhou, C., Wang, X., Song, X., Wang, Y., Fang, D., Ge, S. and Zhang, R. (2020) Insights into dynamic adsorption of lead by nano-hydroxyapatite prepared with two-stage ultrasound. Chemosphere 253, 126661.

Zhou, C., Wang, X., Wang, Y., Song, X., Fang, D. and Ge, S. (2021) The sorption of single- and multi-heavy metals in aqueous solution using enhanced nano-hydroxyapatite assisted with ultrasonic. Journal of Environmental Chemical Engineering 9(3), 105240.

Zhou, R., Si, S. and Zhang, Q. (2012) Water-dispersible hydroxyapatite nanoparticles synthesized in aqueous solution containing grape seed extract. Applied Surface Science 258(8), 3578-3583.

Zima, A. (2018) Hydroxyapatite-chitosan based bioactive hybrid biomaterials with improved mechanical strength. Spectrochimica Acta Part A: Molecular and Biomolecular Spectroscopy 193, 175-184.

Zou, Z., Ismail, B.B., Zhang, X., Yang, Z., Liu, D. and Guo, M. (2023) Improving barrier and antibacterial properties of chitosan composite films by incorporating lignin nanoparticles and acylated soy protein isolate nanogel. Food Hydrocolloids 134, 108091.

Zubair, M., Wu, J. and Ullah, A. (2019) Hybrid bionanocomposites from spent hen proteins. ACS omega 4(2), 3772-3781.